SEMI-ANNUAL REPORT

NASA GRANT NSG-1288

SUPPLEMENT NO. 1

ANALYSIS OF THE GAS CORE ACTINIDE TRANSMUTATION REACTOR (GCATR)

J. D. Clement and J. H. Rust

NASA Program Manager, F. Hohl

Prepared for the

National Aeronautics and Space Administration

by the

School of Nuclear Engineering
Georgia Institute of Technology
Atlanta, Georgia 30332

September 1, 1977

105

SEMI-ANNUAL REPORT

NASA GRANT NSG-1288

SUPPLEMENT NO. 1

ANALYSIS OF THE GAS CORE ACTINIDE TRANSMUTATION REACTOR (GCATR)

J. D. Clement and J. H. Rust

NASA Program Manager, F. Hohl

Prepared for the

National Aeronautics and Space Administration

by the

School of Nuclear Engineering
Georgia Institute of Technology
Atlanta, Georgia 30332

September 1, 1977

ACKNOWLEDGMENTS

This work was supported by NASA Grant NSG-1288, Supplement No. 1. The authors wish to express their appreciation to the program manager, Dr. Frank Hohl, for helpful suggestions during the performance of the research.

The following graduate students, supported by the grant, made significant contributions to the research project: Bruce Byrne, John Massey, and Pak Tai Wan.

In addition, the NASA research program was also used as a design project for the Nuclear Engineering design course in the academic curriculum. The following graduate students were of great assistance in the research work: Constantine Bratianu, Stanley Chow, Trent Primm, and Scott Revolinski.

TABLE OF CONTENTS

LIST OF TABLES

LIST OF TABLES (Continued)

LIST OF FIGURES

LIST OF FIGURES (Continued)

LIST OF FIGURES (Continued)

ABSTRACT

The work summarized in this report, which was carried out as a part of a NASA sponsored fissioning plasma research program, consisted of design power plant studies for two applications of the plasma core reactor:

(1) As a breeder reactor

(2) As a reactor able to transmute actinides effectively.

In addition to the above applications the reactor produced electrical power with a high efficiency.

A reactor subsystem was designed for each of the two applications. Tables 1 and 2 summarize the reactor design parameters for the breeder and the actinide transmuter, respectively.

For the breeder reactor, neutronics calculations were carried out for a U-233 plasma core with a molten salt breeding blanket. The primary objectives of the overall nuclear design were to design a reactor with a low critical mass (less than a few hundred kilograms U-233) and also a breeding ratio of 1.01. The later objective was a safety precaution to guard against diversion of fissionable material during blanket reprocessing. Since only enough U-233 would be bred in the blanket to replenish the amount depleted in the core, any diversion of U-233 during reprocessing would result in an insufficient amount of fissionable material to replenish the core and the reactor would shut down. Both of the above objectives were met in the final design. It is also possible to design for much higher breeding ratios in the range 1.1-1.2.

The Plasma Core Actinide Transmutation reactor was designed to transmute the nuclear waste from conventional LWR's. Each LWR is loaded with

Table 1. Plasma Core Breeder Reactor Reference Design

Dimensions of Reactor Regions

U^{233} Plasma	- 165 cm O.D.
Helium	- 285 cm O.D.
BeO Moderator	- 325 cm O.D.
Molten Salt*	- 355 cm O.D.
BeO Reflector	- 375 cm O.D.
Fe Pressure Shell	- 415 cm O.D.

Critical Mass	- 26.3 Kg
Breeding Ratio	- 1.0099
Power	- 2000 MWt
Average Thermal Flux in Plasma	- $3.42 \times 10^{15} \frac{\text{neutrons}}{\text{cm}^2 \text{ sec}}$
Reactor Pressure	- 200 atm
Average Temperatures	
U^{233} Plasma	- 25,000°K
Helium	- 3,000°K
Molten Salt	- 1,015°K
Molten Salt Mass Flow Rate	- 542 Kg/sec

*Molten Salt Composition - 71.7% LiF (99.995% Li^7), 16% BeF_2, 12.3% ThF_4

Table 2. Reactor Characteristics of
Plasma Core Actinide Transmutation Reactor

Reference Design:

Geometry: Spherical

Dimensions of reactor regions:

U^{233} plasma	200 cm	thickness
He	120 cm	thickness
Be moderator	17 cm	thickness
*Act. Oxide + Zr + He	0.85 cm	thickness
Be reflector	80-90 cm	thickness

Critical mass = 380 Kg

Mass of actinides = 1.27 metric tonne

Power = 2000 MWt

Avg. thermal flux in plasma = 2.06×10^{15} n/cm^2-sec

Avg. thermal flux in actinides = 1.23×10^{14} n/cm^2-sec

Reactor pressure = 200 atm.

Temp:

U^{233} plasma	25000°K
He	3000°K
Be moderator	1000°K
Act. Oxide + Zr + He	800°K
Be Reflector	400-600°K.

*Actinide Composition: 74 atomic% Np^{237}; 7 atomic% Am^{241}; 14 atomic% Am^{243}
4 atomic% Cm^{244}.

88 metric tonne of uranium (3.3% U^{235}) and operated until a burnup of 33,000 MWD/MTU is reached. The fuel is discharged from the reactor and cooled for 160 days. Next, the spent fuel is reprocessed during which 100% of Np, Am, Cm, and higher actinides are separated from the other components. The concentrations of these actinides are calculated by ORIGEN and tabulated. These actinides are then manufactured as oxides into zirconium clad fuel rods and charged as fuel assemblies in the reflector region of the plasma core actinide transmutation reactor. Results of actinide burnup calculations for an equilibrium plasma core transmuter servicing 27 PWR's show that after 13 cycles the actinide inventory has stabilized to about 2.6 times its initial loading. There are two mechanisms for the removal of actinides:

(1) They are fissioned directly in the plasma core actinide transmuter

(2) They are removed as U or Pu.

The U and Pu can be used in other reactors. In the equilibrium cycle, about 7% of the actinides are directly fissioned away, while about 31% is removed by reprocessing.

Fluid mechanics, heat transfer, and mechanical design considerations for both reactors are described in the report.

Since it is desirable to have the Plasma Core Breeder Reactor (PCBR) be a self-contained unit, generating its own new fuel, an on-line reprocessing system for the molten salt blanket is a necessity. Chapter 8 describes protactinium removal and salt purification processes, calculations of expected flow rates, and equilibrium concentrations of various isotopes present in the system.

In order to achieve maximum effectiveness from the high temperature coolants from either of the two plasma core reactors, it was decided that a ternary power cycle would produce the highest efficiency power plant. The ternary cycle consists of a combination of MHD, gas turbine, and Rankine cycle energy conversion units. Two concepts were investigated — systems with and without a high temperature regenerator in the helium loop.

The achieved objectives of the study were as follows:

(1) Model the nuclear MHD power plant cycle.

(2) Analyze the power output from the three energy conversion units and evaluate plant overall efficiency.

(3) Make a parametric study of the effect of changing operating variables on plant overall performance.

All studies used values for input data according to current commercial technology (i.e. efficiencies for steam cycle components, gas turbine, and compressors) or with current use in MHD research.

The modeling of the MHD cycle consisted of defining a pseudo-Brayton cycle and treating the expansion within the MHD generator in a similar manner as in a gas turbine. In order to analyse the two systems it was necessary to write two computer codes:

(1) NMHD-1 — code to analyze the nuclear MHD power plant without regeneration in the helium loop

(2) NMHD-2 — code to analyze the nuclear MHD power plant with regeneration in the helium loop.

Table 3 lists input parameters for each system.

A study was made of the effect on overall efficiency of varying the reactor coolant outlet temperature from 3000°K to 4000°K for the two

systems. Table 4 lists typical results, showing an overall plant efficiency as large as 70%.

For Nuclear MHD Power Plant with regeneration, the major contribution of the electric power is produced in the top of the power cycle by the MHD subsystem (33.97% - 45.49% from 100% heat produced by the reactor). The power production has been shifted toward the top of the ternary cycle with a positive effect on overall efficiency. This system produces overall efficiencies that are 25-35% higher than actual power plants in use and that are 15-20% higher than the expected coal-fired MHD power plants.

For Nuclear MHD Power Plants without regeneration, the major contribution of electric power is due to the steam turbine subsystem (36.03% - 36.36% from 100% heat produced by the reactor). Due to a significant fraction of the electric power being produced by the steam cycle with a low efficiency (40%), it is desirable to shift the power production toward the top of the cycle to improve the overall efficiency. This can be achieved by reducing the mass flow rate of helium within the inner loop and increasing the pressure ratio of the MHD generator. This system produced overall efficiencies that are 15-20% higher than actual power plants in use and that are 5-10% higher than the expected coal-fired MHD power plant. Due to the relatively low temperatures within the helium loop, this type of power plant could be considered as a first step in a national program of implementation of MHD power plants with a nuclear source.

Table 3. Input Data for NMHD-1 and NMHD-2

Index	NMHD-1		NMHD-2	
1	Boiler Temperature ----	1000°F	Boiler Temperature ----	1000.°F
2	Boiler Pressure -------	1600 psia	Boiler Pressure -------	1600 psia
3	Condenser Pressure ----	1.0 psia	Condenser Pressure ----	1.0 psia
4	Steam Turbine Efficiency	81%	Steam Turbine Efficiency	81%
5	Pump Efficiency -------	80%	Number of Feed Heaters	0,1 or 2
6	Number of Feed Heaters	0,1 or 2	Reactor Temp Difference	200°K
7	Compressor Efficiency -	85%	Compressor Efficiency -	85%
8	MHD Inlet Temp --------	3000°K	MHD Inlet Temp --------	3000°K
9	MHD Inlet Press -------	200 bar	MHD Inlet Press -------	200 bar
10	MHD Pressure Ratio ----	5.0	MHD Pressure Ratio ----	3.0
11	Gas Turbine Pressure Ratio	2.0	Gas Turbine Press. ratio	3.0
12	Feed Heater 1 Pressure	12. psia	Feed Heater 1 press. --	12. psia
13	Feed Heater 2 Pressure -	4. psia	Feed Heater 2 press. --	4.0 psia
14	Bottom Temp Difference -	150°K	Bottom Temp Diff. ----	150°K
15	MHD Inlet Mach No. ----	0.5	MHD Inlet Mach No. ----	0.5
16	Sep Outlet Mach No. ----	0.1	Sep Outlet Mach No. ---	0.1
17	Gas Turbine Inlet Temp -	1500°K	Gas Turbine Inlet Temp	1500°K
18	MHD Efficiency ---------	49%	MHD Efficiency ---------	49%
19	Gas Turbine Efficiency -	85%	Gas Turbine Efficiency	85%
20	Number of Compress Stages	3.0	Number of Compress Stages	3.0

Table 4. Plant Net Overall Efficiencies For MHD Inlet Temperature Variation

MHD Inlet Temperature	3000°K		3250°K		3500°K		3750°K		4000°K	
Q_R	4973.45	100.0%	5138.94	100.00%	5299.94	100.00%	5458.27	100.0%	5693.55	100.0%
W_{MHD}	1689.52	33.97%	1914.65	37.26%	2139.78	40.37%	2139.78	43.44%	2590.04	45.49%
W_{GT}	319.12	6.42%	319.12	6.21%	319.12	6.02%	319.12	5.85%	319.12	5.60%
W_{ST}	1112.20	22.36%	1112.20	21.64%	1112.20	20.99%	1112.20	20.38%	1112.20	19.53%
η_{PLANT}	62.75%		65.11%		67.38%		69.56%		70.62%	

Q_R = REACTOR HEAT RATE

W_{MHD} = MHD NET ELECTRIC POWER: $W_{MHD} = W_{MHD\ OUTPUT} - W_{COMPRESSOR}$

W_{GT} = GAS TURBINE ELECTRIC POWER: $W_{GT} = W_{GT\ OUTPUT} - 2 \times W_{COMPRESSOR}$

W_{ST} = STEAM TURBINE ELECTRIC POWER: $W_{ST} = W_{ST\ OUTPUT} - W_{PUMP}$

$$\eta_{PLANT} = \left(\frac{W_{MHD}}{Q_R} + \frac{W_{GT}}{G_R} + \frac{W_{ST}}{Q_R}\right) \times 100 = \left(\frac{W_{MHD}}{Q_R}\,100\right) + \left(\frac{W_{GT}}{Q_R}\,100\right) + \left(\frac{W_{ST}}{Q_R}\,100\right) \quad [\%]$$

1. INTRODUCTION

As part of its policy of supporting research and development programs which reside on the frontier of power technology, the National Aeronautics and Space Administration has sponsored work in gaseous fueled reactors and plasma research. The original thrust of the NASA sponsored research, aimed toward development of a space propulsion engine, led to two gas-core reactor concepts - the light bulb and the coaxial flow nuclear reactor concepts.[1-10] Although budgetary and policy factors terminated the development of nuclear powered propulsion engines, the concept of a UF_6 fueled gas core reactor was shown to be very attractive for several other applications.

NASA has continued supporting an ongoing fissioning plasma research program consisting of cavity reactor criticality tests, fluid mechanics tests, investigations of uranium optical emission spectra, radiant heat transfer, power plant studies, and related theoretical work.[10-13] These studies have shown that UF_6 fueled reactors can be quite versatile with respect to power, pressure, operating temperature, and the modes of power extraction. Possible power conversion systems include Brayton cycles, Rankine cycles, MHD generators, and thermionic diodes.[12,13,14,17,18] Recent results of research on the pumping of lasers by fission fragment interactions with a laser gas mixture indicate the possibility of the power extraction in the form of coherent light.[10,12] Another potential application of the gas core reactor is its use for nuclear waste disposal by nuclear transmutation (Gas Core Actinide Transmutation Reactor, GCATR).[10,12,19,20]

Recent work sponsored by NASA at Georgia Tech on the Gas Core Breeder Reactor was reported in References 17 and 18. Further work on

the Gas Core Actinide Transmutation Reactor was reported in Refs. 19 and 20.

This semi-annual report summarizes results of work performed from March 1, 1977 to August 31, 1977 and NASA Research Grant NSG-1288. Work was performed in connection with the UF_6 fuel under near "state-of-the art" temperature conditions, and also on the high temperature fissioning-plasma co-axial flow scheme. This report contains results for the application of the high temperature fissioning-plasma core to transmutation and breeding.

Chapters 2 to 5 apply to the plasma core transmutation reactor and Chapters 6 and 7 relate to the breeder. Chapter 8 applies to both the MHD generator, a component in both systems, and Chapter 10 encompasses the system designs for both applications, showing why the fissioning plasma system is so extraordinarily attractive.

REFERENCES FOR CHAPTER 1

1. RAGSDALE, R. G., "To Mars in 30 Days by Gas Core Nuclear Rocket," Astronautics and Aeronautics, 10, 1 (1971).

2. KUHRT, W. A., "Space Propulsion in the Fiscal Year 2001," Fourth Goddard Memorial Symposium, Space Age in the Fiscal Year 2001, American Astronautical Society, Washington, D. C., (1966).

3. THOM, K., and R. T. SCHNEIDER, editors, "Research on Uranium Plasmas and Their Technological Applications," Proceedings of a Symposium, NASA SP-236 , U. S. Government Printing Office, (1971).

4. RAGSDALE, R. G., "2nd Smyposium on Uranium Plasmas: Research and Applications," AIAA (1971).

5. CLEMENT, J. D., and J. R. WILLIAMS, "Gas Core Reactor Technology," Reactor Technology, 13, 3 (1970).

6. THOM, K., "Review of Fission Engine Concepts," J. Spacecraft and Rockets, 9 (1972).

7. THOM, K., and R. T. SCHNEIDER, "Fissioning Uranium Plasmas," Nuclear Data in Science and Technology, 1, 15-38, International Atomic Energy Agency, Vienna, Austria (1973).

8. ROM, F. E., and RAGSDALE, R. G., "Advanced Concepts for Nuclear Rocket Propulsion," NASA SP-20, U. S. Government Printing Office (1969).

9. SCHWENK, F. C., and FRANKLIN, C. E., "Comparison of Closed-and Open-Cycle Systems," Research on Uranium Plasmas and Their Technological Applications, NASA SP-236, 3-13, U. S. Government Printing Office (1971).

10. THOM, K., R. T., SCHNEIDER, and F. C. SCHWENK, "Physics and Potentials of Fissioning Plasmas for Space Power and Propulsion," International Astronautical Federation 25th Congress, Paper No. 74087, Amsterdam (October 1974).

11. WILLIAMS, J. R., J. D. CLEMENT, and J. H. RUST, "Analysis of UF_6 Breeder Reactor Power Plants," Progress Rept. No. 1, NASA-7067, Georgia Institute of Technology, Atlanta, Ga. (November 1974).

12. SCHWENK, F. C., and K. T. THOM, "Gaseous Fuel Nuclear Reactor Research," Paper presented at the Oklahoma State University Conference on Frontiers of Power Technology (October 1974).

13. WILLIAMS, J. R., and J. D. CLEMENT, "Exploratory Study of Several Advanced Nuclear-MHD Power Plant Systems," Final Status Report, NASA Grant NGR-11-002-145, Georgia Institute of Technology, Atlanta, Georgia (March 1973).

14. CLEMENT, J. D., J. H. RUST, and J. R. WILLIAMS, "Analysis of UF_6 Breeder Reactor Power Plants," Semi-annual Report NASA Grant NSG-1168 (October 1975).

15. PATERNOSTER, R., M. J. OHANIAN, R. T. SCHNEIDER, and K. THOM, "Nuclear Waste Disposal Utilizing a Gaseous Core Reactor," Transactions of the American Nuclear Society, 19, 203 (October 1974).

16. WILLIAMS, J. R., J. D. CLEMENT, and J. R. RUST, "The UF_6 Breeder: A solution to the Problems of Nuclear Powers." Presented at the Inter Society Energy Conversion Conference (August 11-15, 1975).

17. CLEMENT, J. D., and J. H. RUST, "Analysis of UF_6 Breeder Reactor Power Plants, Final Report NASA Grant NSG-1168 (February 1976).

18. CLEMENT, J. D., J. H. RUST, and F. HOHL, "UF_6 Breeder Reactor Power Plants for Electric Power Generation," Invited Paper, presented at Third Symposium on Uranium Plasmas, Princeton University, New Jersey (June 1976).

19. RUST, J. H., J. D. CLEMENT, and F. HOHL, "Georgia Tech Research on the Gas Core Actinide Transmutation Reactor (GCATR)," Invited Paper, presented at Third Symposium on Uranium Plasmas, Princeton University, New Jersey (June 1976).

20. CLEMENT, J. D., J. H. RUST, and F. HOHL, "Analysis of the Gas Core Actinide Transmutation Reactor (GCATR)," Final Report, NASA Grant NSG-1288 (February 1977).

2. NUCLEAR ANALYSIS OF THE PLASMA CORE ACTINIDE TRANSMUTATION REACTOR

The objectives of the nuclear analysis of the plasma core actinide transmutation reactor are:

(1) design a reactor system capable of producing power;

(2) design a reactor able to effectively transmute actinides.

The spent fuel discharged from a LWR consists of structural materials, unfissioned uranium, converted plutonium, other actinides, and fission products. The ratio of these components by weight is as follows:

structural	uranium	plutonium	fission products	other actinides
256	1023	9	36	1

Despite the fact that the other actinides is the smallest component, they are very long lived. After 10^5 years, most of the other components will have decayed to stable isotopes, but these actinides will still be radioactive and may be a significant health hazard in the future. This is the rationale for putting these actinides in a reactor to transmute them to short lived fission products.

The transmutation strategy used for the present calculations is shown in Fig. 2.1. The analysis was performed using the cross section code[2] MC^2, the multi-group diffusion code[3] MACH-I, and the isotope depletion code[1] ORIGEN. The flow diagram for the analysis is shown in Fig. 2.2.

Each LWR is loaded with 88 metric tonne of uranium (3.3% U^{235}) and operated until a burnup of 33,000 MWD/MTU is reached. The fuel is discharged from the reactor and cooled for 160 days. Next, the spent fuel is reprocessed during which 100% of Np, Am, Cm, and higher actinides are separated from the other components. The concentrations of these

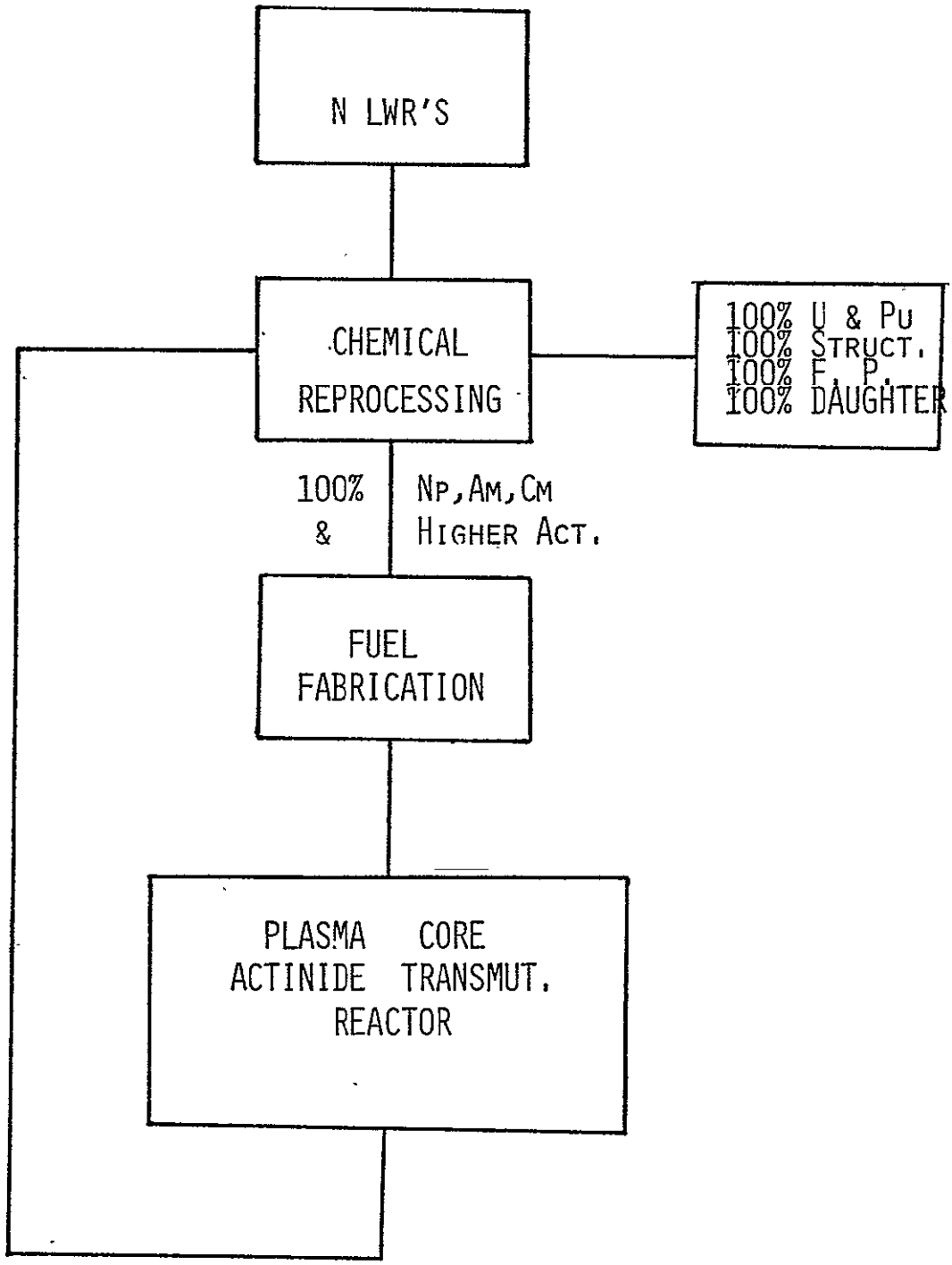

Fig. 2.1 Strategy for actinide transmutation

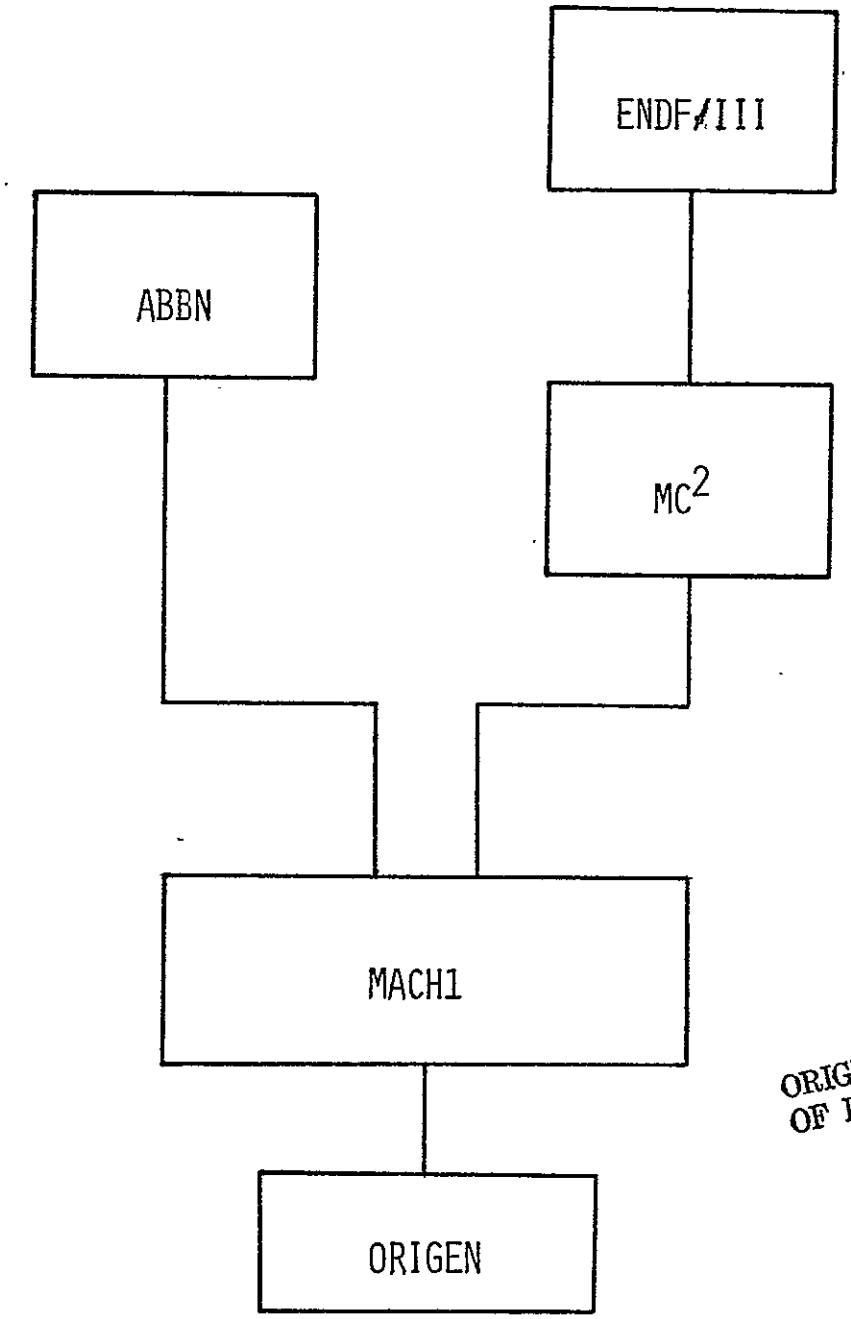

Fig. 2.2 Flowsheet of nuclear analysis computation

actinides are calculated by ORIGEN[1] and are tabulated in Table 2.1. These actinides are then manufactured into fuel rods and charged into the plasma core actinide transmutation reactor.

The basic core configuration is shown in Fig. 2.3.

For simplicity, spherical geometry is used. There are five regions:

(1) Region I consists of the hot fissioning uranium 233 plasma. The bulk temperature is assumed to be around 25,000°K at a pressure of 200 atmospheres. Because of the ionization of the uranium atoms at such temperatures, the U^{233} plasma density is lower than that predicted by the perfect gas law. The equation of state of uranium at such temperatures and pressures is given by Ragsdale.[4]

(2) Region II consists of a helium layer. The bulk temperature is assumed to be at 3,000 K at 200 atm. The perfect gas law is assumed to be valid for helium at these conditions.

(3) Region III consists of a solid liner at 1000 K. For a fast system, stainless steel is chosen as the liner material. For a thermal system, beryllium is used to act as reflector and moderator.

(4) Region IV consists of He cooled, Zr clad actinide fuel rods at 800 K, and 200 atmospheres. The actinides are assumed to be present as oxides. Only the principal actinides, Np-237, Am-241, Am-243 and Cm-244 are included. The other actinides are very small. The concentrations of this region by volume is assumed to be 43% actinide rods, 12% Zr cladding, and 45% He coolant.

(5) Region V consists of a reflector. For a fast system, iron is used; for a thermal system, beryllium is chosen.

Nuclide	Gram-atoms	Kg.
Np237	2.04+4	4.82+3
Np239	3.27-3	7.81-4
Am241	1.93+3	4.65+2
Am242m	3.87+1	9.36+0
Am242	4.65-4	1.12-4
Am243	3.89+3	9.44+2
Cm242	4.50+1	1.09+1
Cm243	3.22+0	7.82-1
Cm244	1.17+3	2.86+2
Cm245	7.89+1	1.93+1
Cm246	9.00+0	2.22+0
Cm247	1.16-1	2.86-2
Cm248	7.78-3	1.93-3
Cm250	4.49-11	1.12-11
Cf249	7.01-5	1.74-5
Cf250	1.28-5	3.20-6
Cf251	6.89-6	1.73-6
Total	2.76+4	6.57+3

Table 2.1

Actinide Concentrations Charged to Plasma Core Actinide Transmutation Reactor

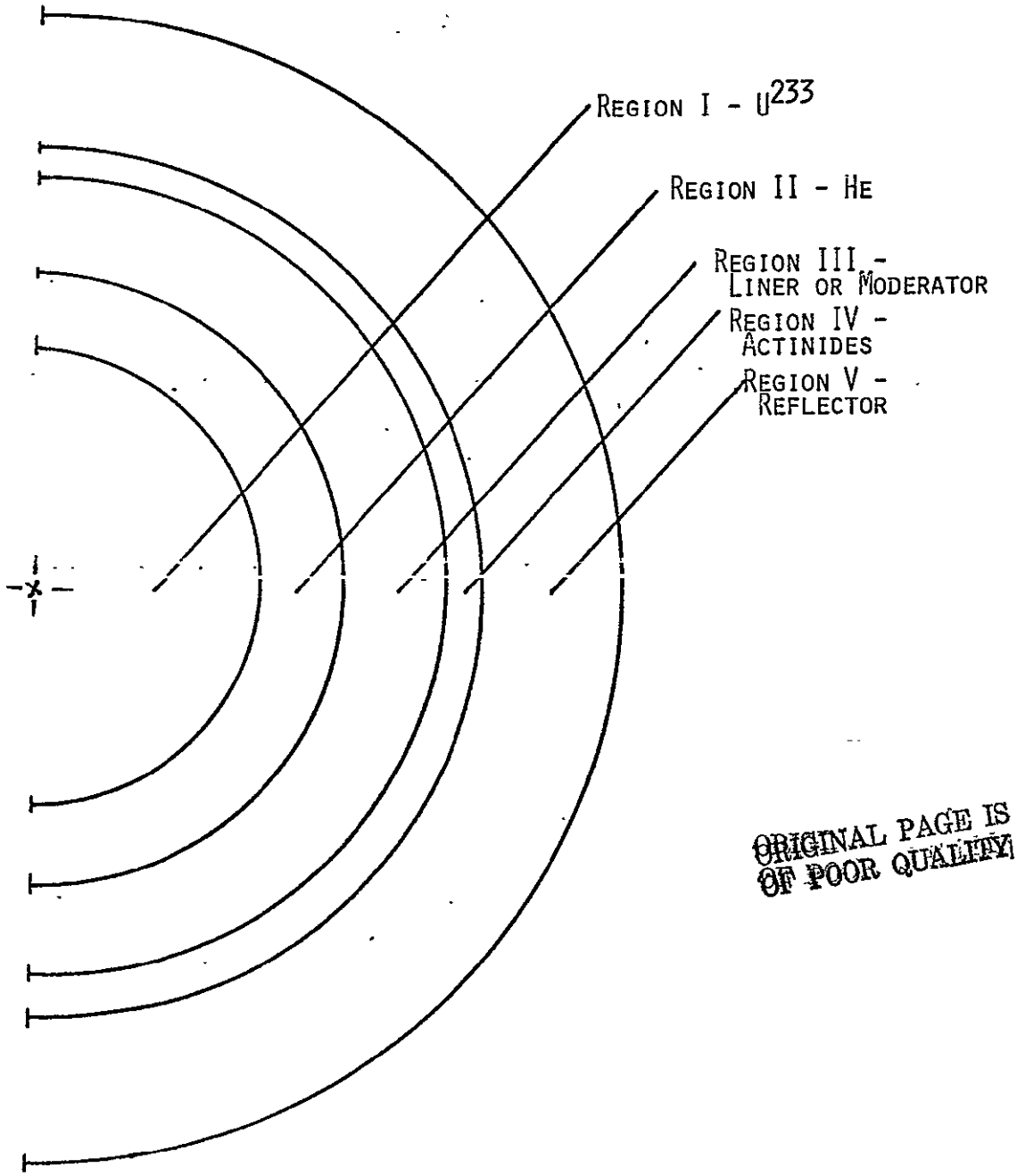

Fig. 2.3 Basic Core Configureation

Both fast and thermal reactors were studied, but the reference design was chosen to be thermal in order to keep the critical mass at a reasonable value. In thermal reactors, beryllium is placed in region III and V.

Table 2.2 summarizes the results obtained for the thermal plasma core reactor.

Table 2.2. Critical Parameters Characterizing Thermal and PCATR

Be thickness	10 cm	13 cm	15 cm	17 cm	20 cm
Critical mass	22000kg	2640kg	562kg	215kg	53kg
Critical radius	778 cm	383 cm	229 cm	166.cm	104 cm
$\overline{E}$ (source)	0.109 kev	2.08 ev	0.37 ev	0.437	0.35 ev
$\ll\sigma_f\gg$ in act. reg.	0.29 b	0.245 b	0.186 b	0.222	0.152 b

He thickness = 25 cm., Act. region thickness = 0.85 cm., Outside Be reflector = 100 cm.

It is observed that increasing the moderation available to core neutrons reduces the critical mass of the plasma core by a factor of 400. However, as the core becomes more thermal, the average fission cross section in the actinide region also decreases.

The dimensions of the reference plasma core actinide transmutation reactor is shown in Table 2.3.

Table 2.3. Reference Plasma Core Actinide Transmutation Reactor

Region No.	Material	Thickness
I	U^{233} (25000°K, 200 atm)	200 cm (375 kg)
II	He (3000 K, 200 atm)	120 cm
III	Be (1000 K)	17 cm
IV	Act. Oxide + Zr + He (800 K, 200 atm)	0.85 cm
V	Be (400 - 600 K)	80-90 cm

Results of actinide burnup calculations for an equilibrium plasma core transmuter are shown in Table 2.4. It is observed that after 13 cycles, the actinide inventory has stabilized to about 2.6 times its initial loading. There are two mechanisms for the removal of actinides: (1) they are fissioned directly in the plasma core actinide transmuter and (2) they are removed as U or Pu. The U and Pu can be used in other reactors. In the equilibrium cycle, about 7% of the actinides are directly fissioned away, while about 31% is removed by reprocessing. This situation is illustrated in Table 2.5.

Table 2.4

Actinide Burnup in Plasma Core Actinide Transmutation Reactor
1100 days of irradiation, 265 days of cooling, 365 days of reprocessing (100% removal of U and Pu, F.P., and Daughters) and fuel fabrication, 27 PWR's serviced (1.27 metric tonnes of actinides charged per cycle). THERM = 0.53648, RES = 1.035, FAST = 4.450, Avg. Thermal Flux = 7.04+12

Batch No.	Cycle No.												
	1	2	3	4	5	6	7	8	9	10	11	12	13
1	1.27	.752	.447	.267	.160	.099	.065	.045	.033	.026	.022	.020	.018
2		1.27	.752	.447	.267	.160	.099	.065	.045	.033	.026	.022	.020
3			1.27	.752	.447	.267	.160	.099	.065	.045	.033	.026	.022
4				1.27	.752	.447	.267	.160	.099	.065	.045	.033	.026
5					1.27	.752	.447	.267	.160	.099	.065	.033	.026
6						1.27	.752	.447	.267	.160	.099	.065	.033
7							1.27	.752	.447	.267	.160	.099	.065
8								1.27	.752	.447	.267	.160	.099
9									1.27	.752	.447	.267	.160
10										1.27	.752	.447	.267
11											1.27	.752	.447
12												1.27	.752
13													1.27
⋮													
Total	1.27	2.02	2.47	2.74	2.90	3.00	3.06	3.11	3.14	3.16	3.19	3.20	3.22

Table 2.5 Actinide Inventory During Equilibrium PCATR Cycle

Beginning of Cycle	3.3MT
Fissioned	- 0.23MT (7%)
Reproc.	- 1.02MT (31%)
End of Cycle	2.05MT
Charge	1.27MT
Beginning of Next Cycle	3.32MT

REFERENCES FOR CHAPTER 2

1. BELL, M. J., "ORIGEN - The ORNL Isotope Generation and Depletion Code," ORNL-4628 (May 1973).

2. TOPPEL, B. J., A. L. RAGO, and D. M. O'SHEA, MC^2 - A Code to Calculate Multigroup Cross Sections," ANL - 7318 (1967).

3. MENELEY, D. A., L. C. KVITEK, and D. M. O'SHEA, "MACH1 - A One-Dimensional Diffusion-Theory Package," ANL - 7223 (June 1966).

4. RAGSDALE, R. G., "Relationship between Engine Parameters and the Fuel Mass Contained in An Open-Cycle Gas Core Reactor," Proceedings of the Symposium on Research on Uranium Plasma and Their Technological Applications, Univ. of Florida (January 1970).

3. FLUID MECHANICS OF PLASMA CAVITY REACTORS

In plasma core reactors (PCR) the gaseous uranium is confined in a somewhat spherical geometry by the hydrodynamic forces exerted by the coolant. The coolant enters radially towards the central uranium plasma, providing both containment and cooling. Due to the nature of processes inherent to PCRs, there are some very interesting fluid dynamic problems. The gaseous uranium metal is not completely confined by the coolant and, therefore, moves slowly through the cavity and is exhausted with the coolant. As the plasma moves through the core it radiates its energy to the coolant, which leaves the reactor in the neighborhood of $3000^{o}K$.

Figure 3.1 shows a schematic of the flow expected to be encountered in a PCR. The advantages and the disadvantages of the PCR all stem from the gaseous state of uranium fuel. By being in the gaseous form the maximum operating temperature is increased by 10 fold over conventional power sources. Also, very small critical masses are possible. One of the main disadvantages is that the fuel moves through the reactor as shown in Fig. 3.1. The amount of fuel that goes through the system is very important. Small core loadings are of no value if the mass flow rate of uranium is excessively high, and if a large piping system is required to be full of expensive fully enriched uranium. Therefore, one of the first goals of any PCR fluid dynamic analysis and design would be a small fuel to coolant flow ratio.

In the late 1960's and early 1970's a considerable amount of work was done with hydrodynamic containment schemes. These consisted of

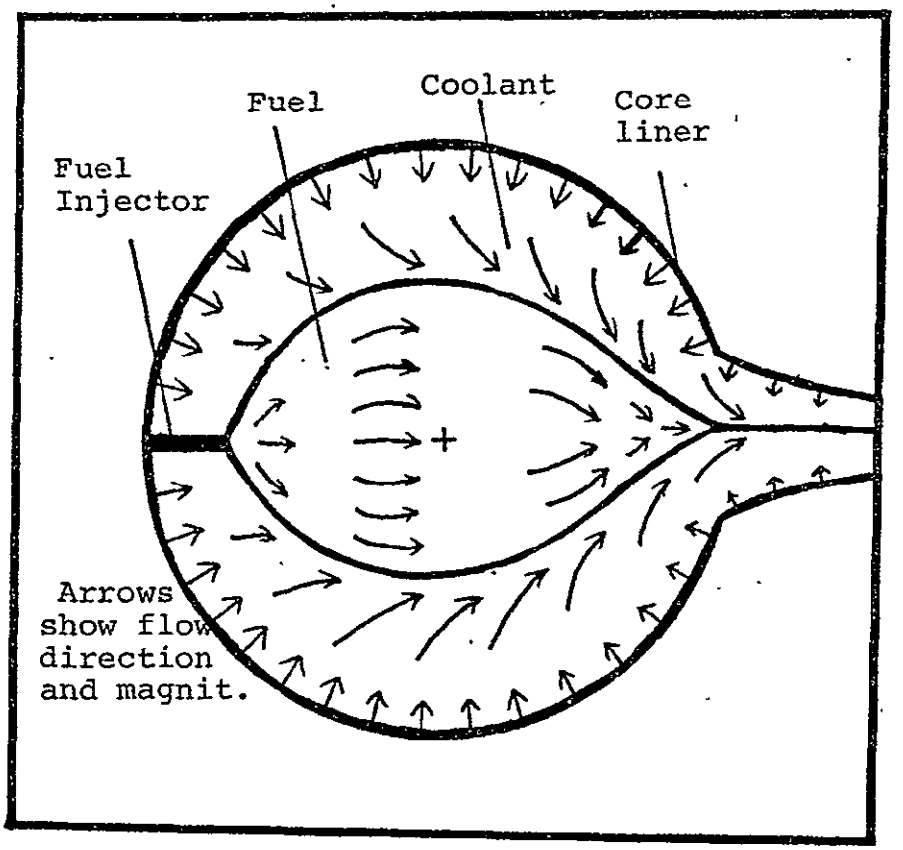

Fig. 3.1 Flow Field of PCR.

rotating cylindrical flows, vortex flows, coaxial flows, and spherical-radial flows. Experiments and analysis were done on all flow arrangements to identify trends and establish parameters important to good confinement and heat transfer. The results of two of these efforts are shown in Fig. 3.2. The data shown are for both cylindrical and spherical coaxial flows. The mass flow ratio ($\dot{m}_{coolant}/\dot{m}_{fuel}$) is shown as a function of the ratio fuel volume/cavity volume. Both graphs show that for a spherical geometry a high mass flow ratio (above 100/1) is obtained only when the volume ratio is less than 0.25. This implies a radius ratio r_{fuel}/r_{total} of less than 0.63. For the reactor core sizes studied in this report the above finding leads to the following conclusions for cavity size:

	CORE I	CORE 20
Fuel Radius	~50 cm	~200 cm
Fuel + coolant radius for $\dot{m}_s/\dot{m}_e = \frac{1}{100}$	~95 cm	~320 cm
for $\frac{\dot{m}_c}{\dot{m}_c} = \frac{1}{1000}$	~109 cm	~430 cm

Reactors of the size listed above would be of about 2000 MW(th) and range from about $\frac{1}{2}$ to 2 times the size of present day PWR pressure vessels.

The exact nature of the flow pattern in the core is unknown at this time. Knowledge of this would require extensive experimentation and analytical work to solve the coupled energy and momentum equations. For this project it is felt that identification of the main design goal

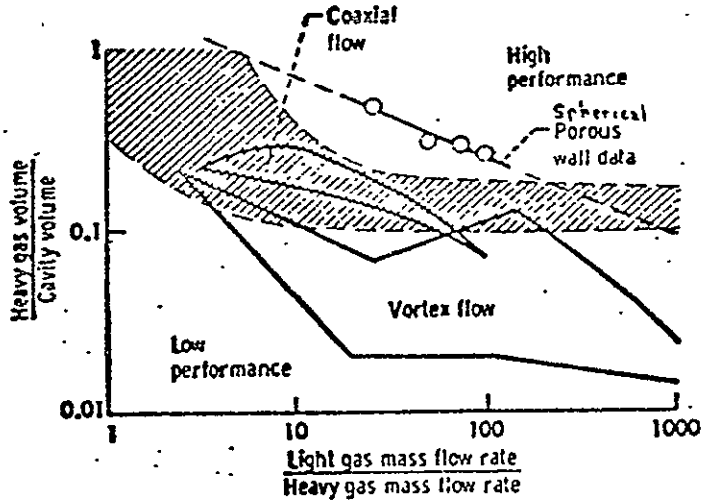

Fig. 3.2(a) Porous Wall Data on Gas Core Performance Map (4)

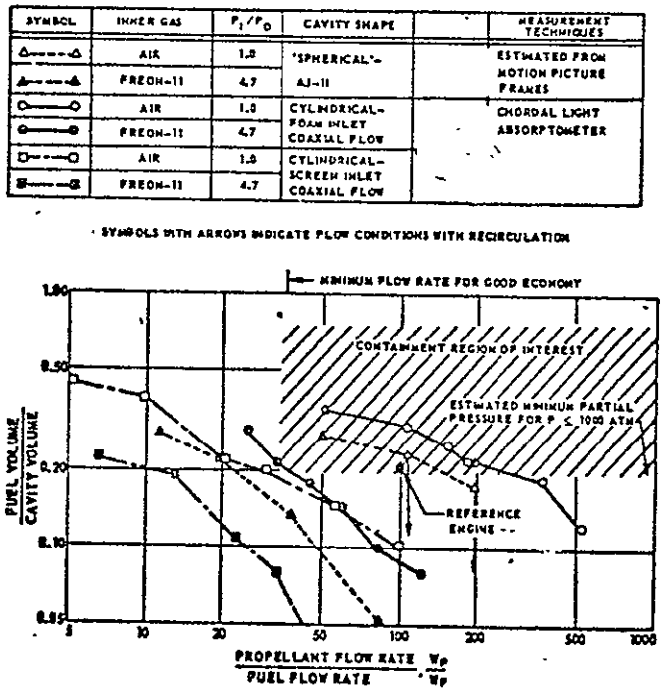

Fig. 3.2(b) Comparison of Coaxial-Flow and Spherical Cavity Containment Results (5)

(low fuel flow rate) and the parameters which control the attainment of this goal is sufficient. The problems of core temperature profiles and wall cooling needs will be discussed in later sections.

For the plasma core reactor the coolant will have to absorb the thermal radiation emitted by the uranium plasma and transfer this energy to a MHD generator, gas turbine, and various heat exchangers. Due to the high operating temperature of the uranium plasma (~25,000°K) and the MHD cycle, the coolant used in the PCR will have to have some additional characteristics above and beyond those of conventional coolants. Table 3.1 shows some of the properties which the PCR working fluid must have. Items 6-7-8 are the "extra" characteristics required by the PCR.

When the PCR was being considered by NASA as a propulsion device, hydrogen was used as the coolant because of its high specific impulse.[1,6,7,8] However, for central station power (on earth, other planets, or a space station) the dangers and chemical reactivity of hydrogen seem to make other choices more attractive. Also, hydrogen is optically transparent to radiation below 1216Å until a temperature of 5000 to 6000 °K is reached. As Fig. 3.3. shows, the emission spectra of uranium plasmas is in the range of 3000 to 8000Å , and hence, hydrogen requires an added submicron sized seed to increase its absorption. Unfortunately, most gases suffer from low absorption in the range of interest and will also require a seed.

Other coolants for central station power plants are listed in Table 3.2. Hydrogen and nitrogen can be discarded immediately because of their high chemical reactivity. Carbon dioxide is good from a thermodynamic and heat transfer point of view, but chemical reactivity and decomposition at high temperatures could cause numerous problems. Helium and other rare gases are good because of their chemical, nuclear, and temperature stability.

Table 3.1 Coolant Properties for the PCR

A. Physical and Nuclear Characteristics

1) Low neutron absorption cross section
2) Low induced radioactivity
3) Good radiation stability
4) Good thermal stability
5) Compatibility with structural and component materials at high temperature
6) Large thermal radiation absorption cross section
7) High electrical conductivity @ $3000^{o}K$
8) Molecular or atomic weight much lower than uranium (to enhance separation)

B. Economic Characteristics

1) Resumable cost
2) Good availability
3) Low pumping or compressing power requirements
4) High thermal conductivity and small viscosities

Table 3.2 Possible Coolants for the PCR

1) Hydrogen
2) Helium
3) Carbon Dioxide
4) Nitrogen

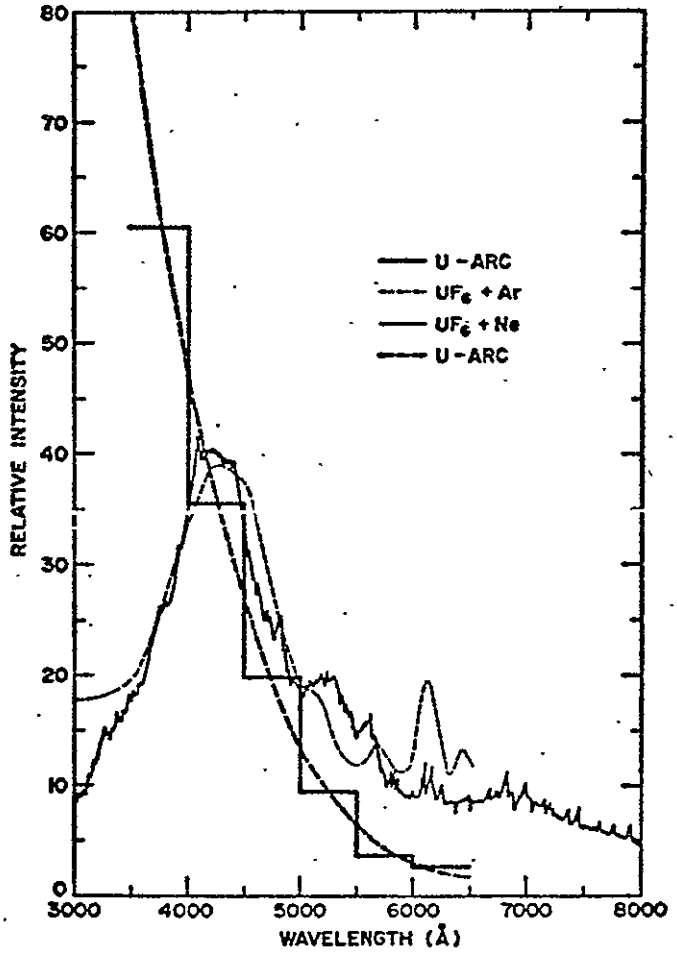

Fig. 3.3 Spectral Distribution of Radiation from Various Uranium Light Sources(10)

These gases also have acceptable thermodynamic and heat transfer properties. Helium, due to its extensive operational experience, low atomic weight and availability is the final choice.

Helium has been shown to readily meet the requirements set forth in Table 3.1 , except for items 6 and 7.[1,9,11] Helium, like other gases, has line absorption being the predominate absorption mechanism; thereby only absorbing a substantial amount of radiation at certain wavelengths. Since the width of these lines is small, the integrated absorption over a range of photon energies would be negligible.[1,6] Exact data for helium absorption in the range emitted by the PCR has not been found. A literature search revealed data only down to 10eV (~124Å). Figure 4 shows data in which helium absorption is compared to that of hydrogen (for which data in the PCR range of interests is available). The data shows that the helium absorption is a little higher than hydrogen in the low energy ranges. Evidence of seeded helium radiation absorption experiments were found, but energy content of the seeded aerosols was reported instead of absorption cross sections.[13] Figure 3.5 shows typical results of these experiments. Here the helium seeded aerosols tend to show a somewhat smaller absorption than hydrogen.

Since no data were found for helium absorption, a few assumptions were made which enabled the study to continue.

1) Since the Lyman Series for helium ranges from 230 to 300Å, it was assumed that discrete absorption would take place in radiation fields of longer wavelength, therefore, necessitating seeding no matter what the absorption coefficient.

2) Since all data found indicated helium absorption

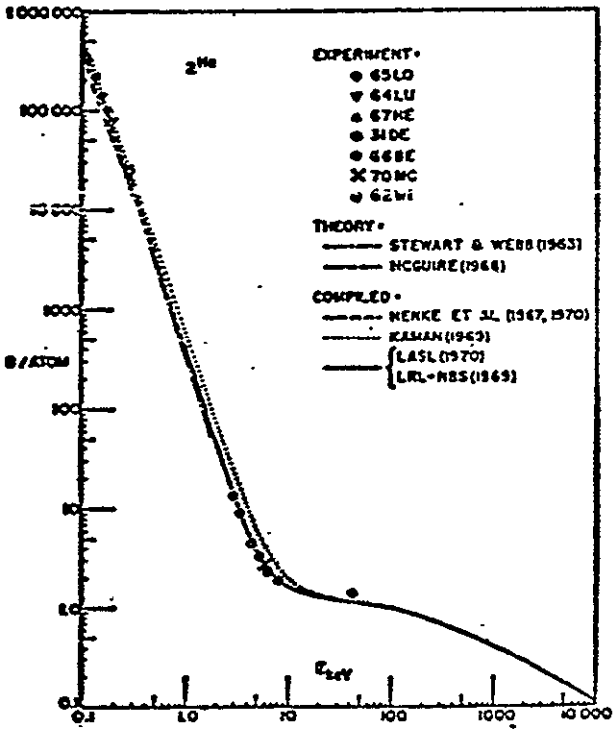

Fig. 3.4 Photon Cross Sections for He and Hydrogen(12)

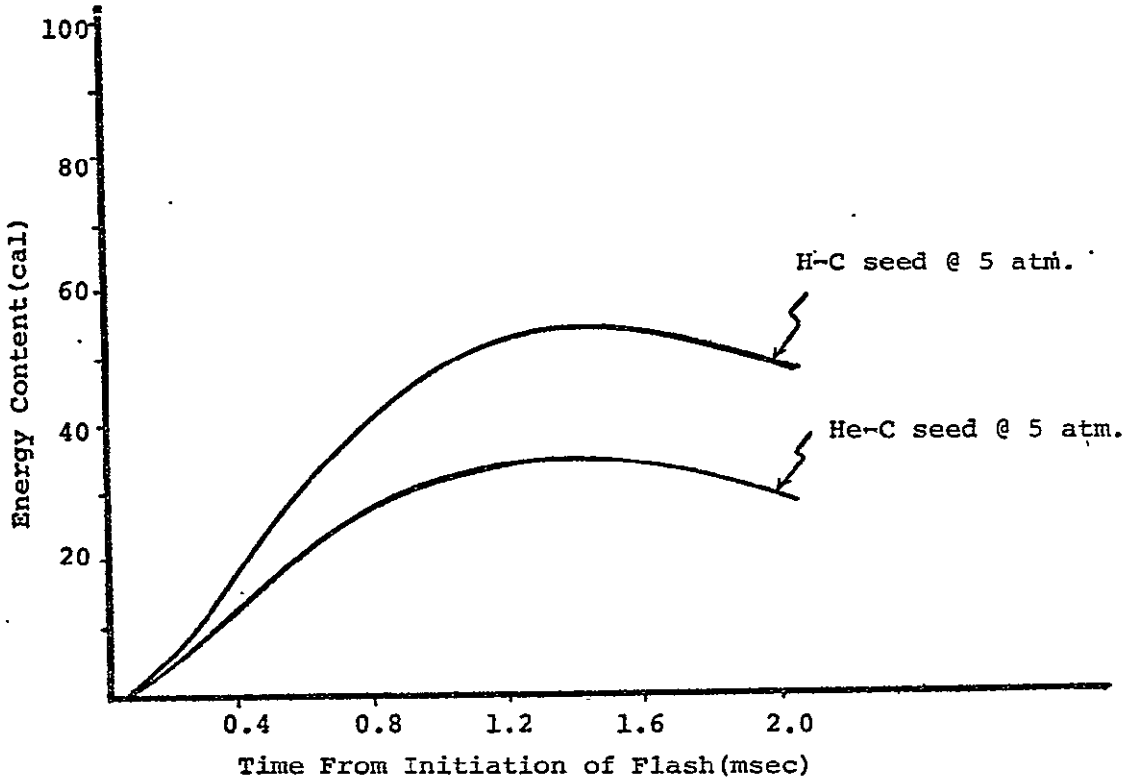

Fig. 3.5 Comparison of H and He Cloud Absorption(13)

of low energy radiation to be "close" to that of hydrogen, and since the absorption in a seeded gas is governed by the seed more so than the gas, data for absorption coefficients in hot seeded hydrogen will be used for this report.

The purpose of seeding the helium is twofold: to increase its absorption coefficient and to make this coefficient as independent of wavelength as possible. Therefore, the first requirement for a seed material is a high, wavelength independent absorption cross section. Secondly, the seed material cannot readily react with the coolant, uranium, or any structural material. Also, the seed should not agglomerate as this causes a decrease in uniformity and decreases the absorption efficiency. These requirements are listed in Table 3.3.

A large amount of work, both theoretical and experimental, has been carried out with seeds of carbon, tungsten, iron, and silicon. Carbon was originally dismissed because of its reactivity with hydrogen, but with helium as the carrier gas this should not be a problem. Figure 3.6 shows a comparison of theoretical absorption coefficients for tungsten, silicon, and carbon at 2000Å as a function of particle size. Figure 3.7 shows the attenuation coefficient of a hydrogen-carbon aerosol at 3450°F.

Table 3.3: Seed Material Requirements

1. Good absorption; independent of wavelength
2. Chemically non-reactive with PCR materials
3. Does not agglomerate easily
4. Compatible with MHD power generation
5. Easily introduced into the helium gas.

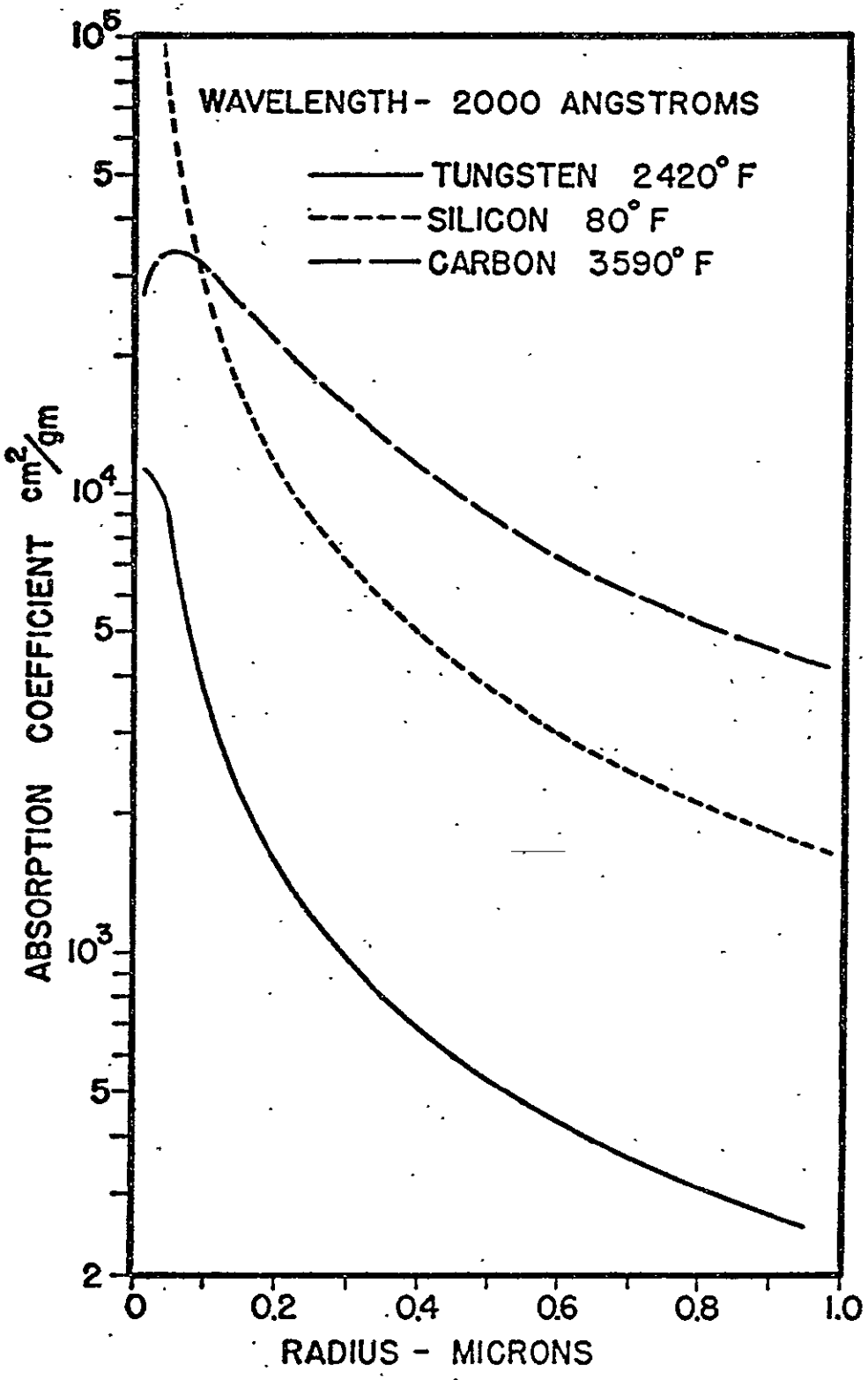

Fig. 3.6 Theoretical Absorption Coefficient of Tungsten, Silicon and Carbon as a Function of Particle Radius

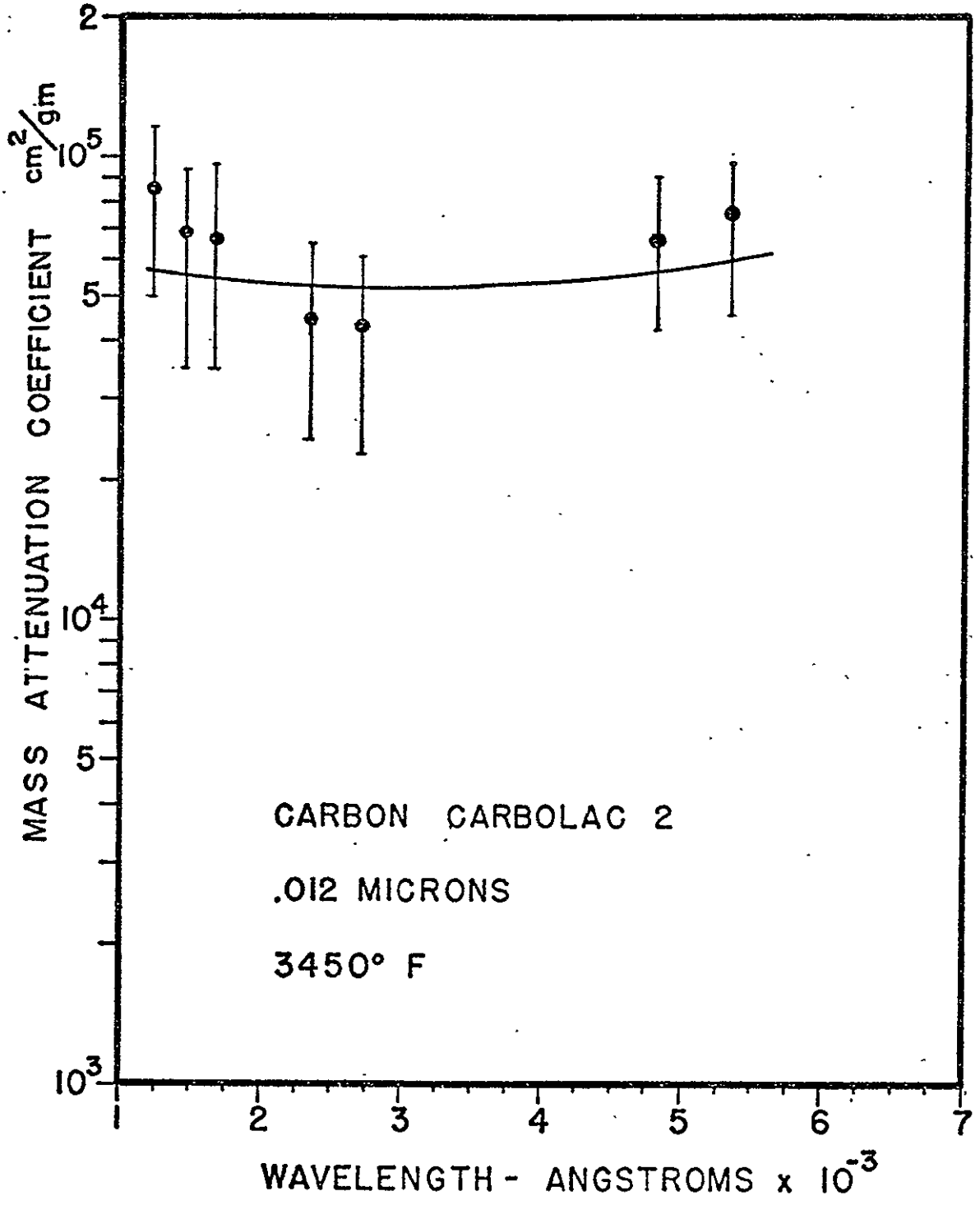

Fig. 3.7 Attenuation Coefficient of Carbon-Hydrogen Aerosol at 3450°F

Comparing this with Fig. 3.8 , which shows the attenuation coefficient for tungsten aerosols at 3000°F, one can see that carbon aerosols have a clear advantage. Also, Fig. 3.7 shows that the carbon seeds produce the required independence with wavelength and have a high overall absorption coefficient, being around $5 \cdot 10^4$ cm^2/gm. For these reasons carbon was chosen as the seed material for use in the PCR.

The overall ability of the gas-seed mixture to attenuate thermal radiation is a function of not only the absorption coefficient of the seed, but also the density of the seed. The density of the seed is in turn limited by the aerosol generator capabilities, the degree of agglomeration, and the particle size.

Aerosol particle densities from 4×10^{-7} to 8×10^{-5} gm/cc have been successfully produced. From this range of particle densities the attenuation parameter $R(cm^{-1})$* can be calculated for various seed-to-coolant density ratios. The results of these calculations are presented in Table 3.4.

The amount of seed needed in the PCR will be determined by the heat loading on the liner wall. Since the core liner will be composed of moderator and structural material, the temperature and heat flux limitations on this component will have to be compatible with the material properties. Beryllium is proposed as the moderating material and stainless steel is for the structural material. Use of these materials will limit the temperature and heat flux to values somewhat close to those of present LMFBR designs (600°K and 2.5 MW/M^2). Figure 3.9 shows the fraction of one core power deposited in the liner. For the two core configurations

*R is the parameter for exponential attenuation of radiation in the formula

$$I/I_o = e^{-Rt}$$ where I is the intensity,

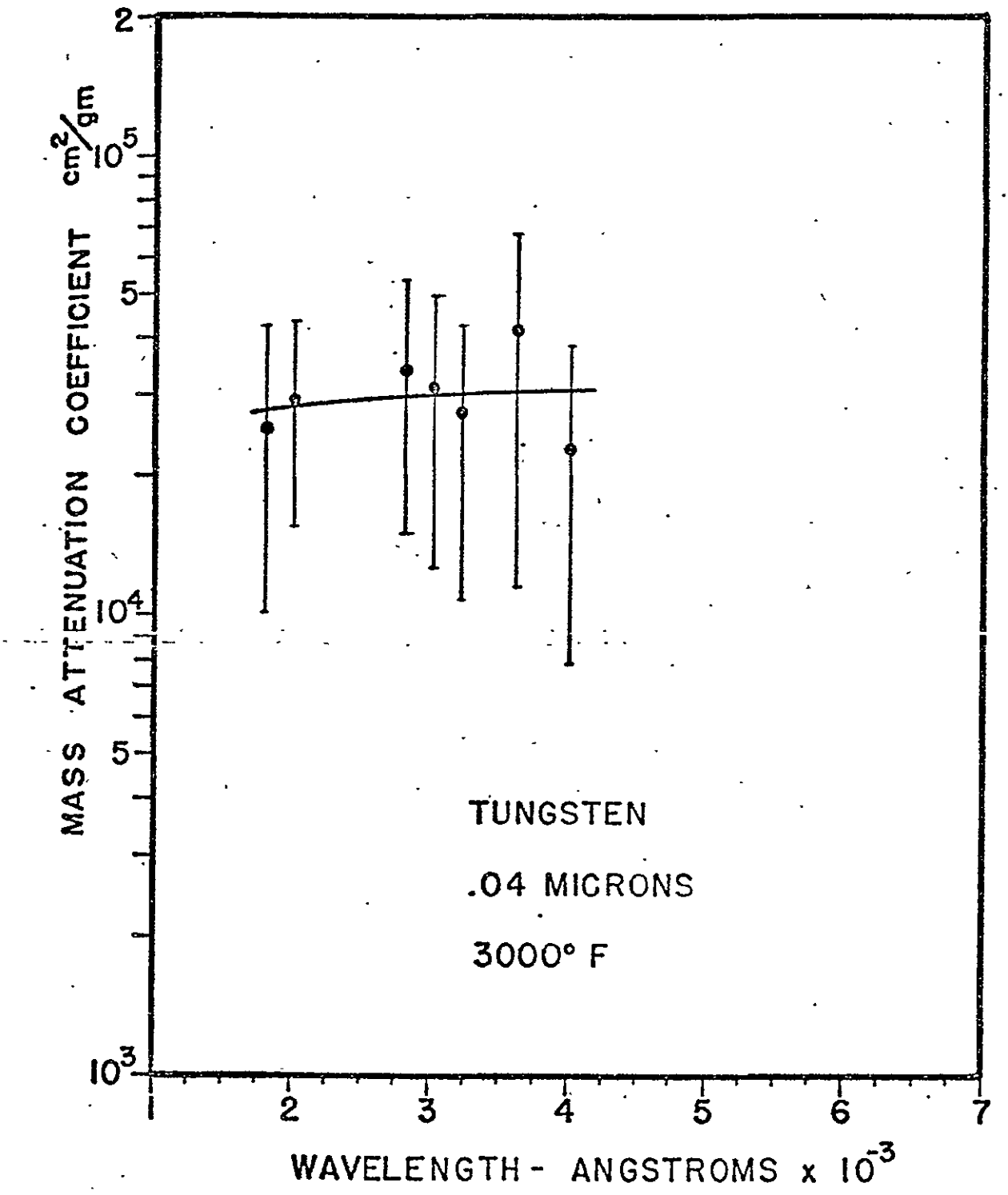

Fig. 3.8 Attenuation Coefficient of Tungsten-Hydrogen Aerosol at 3000°F

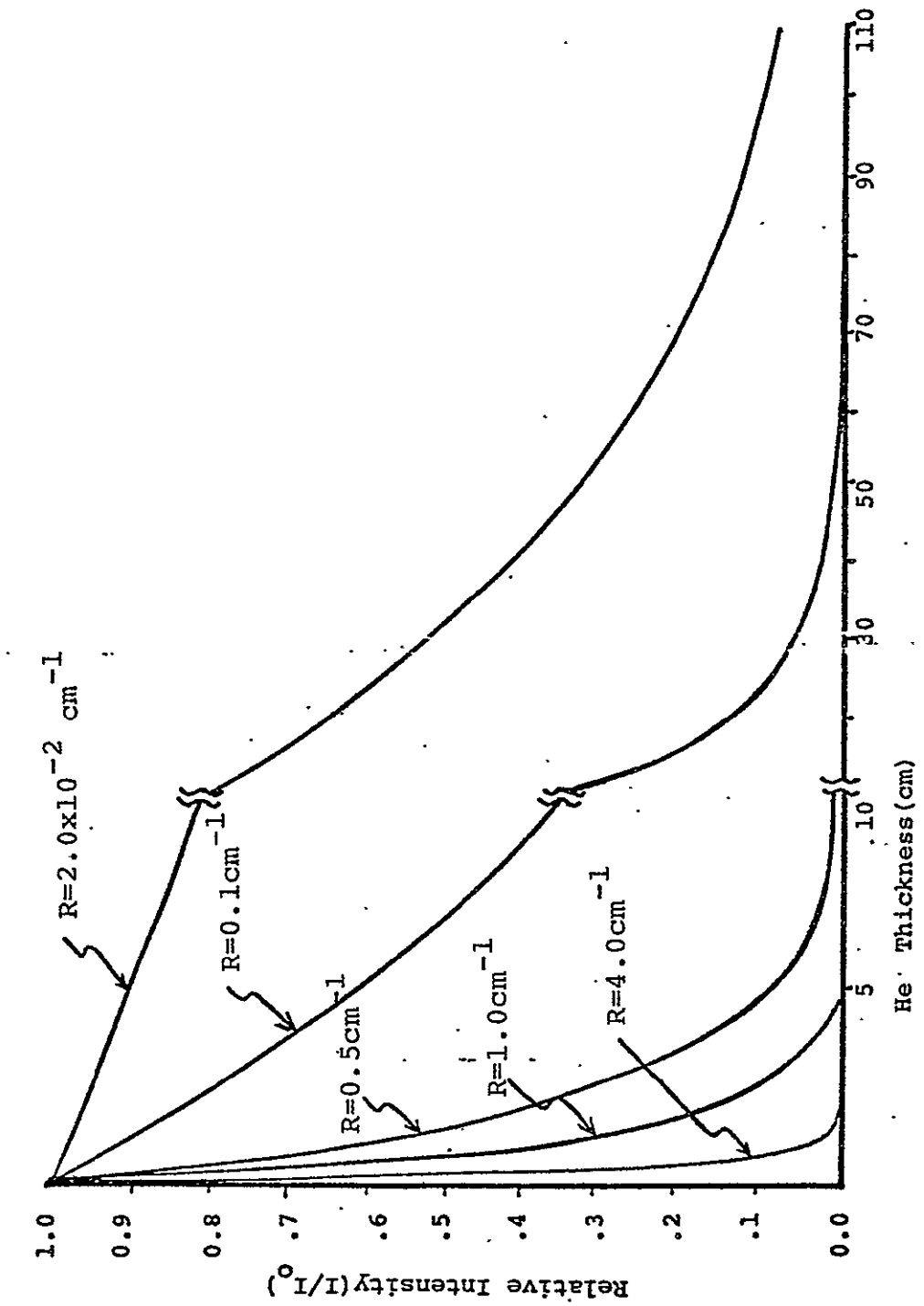

Fig. 3.9 Fraction of Power Deposited in the Core Liner

studied, a value of R from 0.1 to 0.5cm^{-1} would result in a very small heat load on the liner. Table 3.5 summarizes the thermal radiation absorption results for the two cores studied. The fraction of the heat deposited in the liner ranges from negligible to 13.5 MW with a maximum heat flux of 1.07 MW/m^2. This value, although high, is completely within today's technology (the average heat flux in the CRBRP is ~1.27 MW/m^2).[15] To obtain the attenuation shown in Table 3.5 would require particle densities in the range of $2 \cdot 10^{-6}$gm/cc to $1 \cdot 10^{-5}$gm/cc. These are well within current technological capabilities and the resulting particle to carrier densities are low-enough to keep agglomeration to a minimum. Operation in the geometrical and property ranges of Fig. 3.9 should solve the problem of wall heating in the core. The core exhaust nozzle and the MHD duct and its associated piping will still require extensive calculations to determine the cooling required.

Upon absorbing the radiant energy from the uranium plasma, the particle seeds will transfer this energy to the helium coolant. Unlike convential power sources which are limited in the possible ΔT which can be tolerated, the PCR, since it has no structure in the core region proper, can produce any ΔT desired. The desired ΔT can be established by adjusting the mass flow rate of helium. The core inlet temperature is really the only fixed temperature in the entire reactor-power plant system. Since the core liner must be made of a material such as stainless steel and the actinide fuel rods must be clad in zircoloy, the core inlet temperature must be limited to somewhere around 600°K. The outlet temperature may now be adjusted to any desired level for efficient and reliable MHD

Table 3.4 Seed Density Ranges

P particles gm/cc	$\frac{P\ particles}{P\ H_e} \times 100\%$ @1273°K	@3773°K	R cm^{-1}
$4 \cdot 10^{-7}$	0.005%	0.015%	$2 \cdot 10^{-2}$
10^{-6}	0.013%	0.039%	$5 \cdot 10^{-2}$
10^{-5}	0.14%	0.39%	$5 \cdot 10^{-1}$
$5 \cdot 10^{5}$	0.65%	1.94%	2.5
10^{-4}	1.31%	3.87%	5.0

Table 3.5 Seed Absorption Summary

	core radius(cm)	the thickness(cm)	seed period	$R_{cm^{-1}}$	fraction of power in liner	required heat flux to remove liner heat
CORE I	~50 ~50	~50 ~50	0.059% 0.14%	0.1 0.5	13.5 MW $2.8 \cdot 10^{-8}$MW	1.07 MW/m^2 $2.2 \cdot 10^{-9} MW/m^2$
CORE II	~200 ~200	~120 ~220	1.015% 0.015%	0.1 0.1	$1.23 \cdot 10^{-2}$MW $5.6 \cdot 10^{-7}$MW	$1.0 \cdot 10^{-3} MW/m^2$ $4.4 \cdot 10^{-8} MW/m^2$

operation. Figure 3.10 shows the required mass flow rates for a given temperature rise. For efficient MHD operation the reactor exit temperature needs to be in the range of 2500°K to 3500°K, which implies a ΔT of ~1900°K to 2900°K. For this ΔT a mass flow rate of 190 to 130 kg/sec would be required. For the sizes of the reactor cavity studied here this would result in incore velocities of 190 to 1600 cm/sec for a 50 cm radius core and 10 to 100 cm/sec for a 200 cm radius core. For efficient MHD operation an entrance Mach number of 0.5 is also required. For the MHD unit used in this design study, the entrance area is $0.0387m^2$. This implies an area ratio of (A/A^*; where A^* is the critical area size) of 1.524. Working backwards from A_2 to A_1 (see Fig. 3.11) we can find that for a core exit Mach number of 0.1 (low Mach number is needed here to reduce friction and aerodynamic heating of the walls) we need an exit area of $0.175m^2$ (or pipe diameter of 0.472m). This will in turn give us a reactor exit velocity of $4.20 \cdot 10^4$cm/sec. to $2.65 \cdot 10^4$cm/sec.

No attempt has been made to tackle the problem of the details of the flow stability and confinement of the plasma-coolant system. These would be out of the scope of this design project. Attempts have been made to ascertain an "order of magnitude" of the effects and parameters specifically associated with the PCR. Geometry, mass flow and coolant property ranges which would be characteristic of a 2000 MW(th) central power station have been examined. A summary of the fluid mechanical aspects of the PCR design is given in Table 3.6.

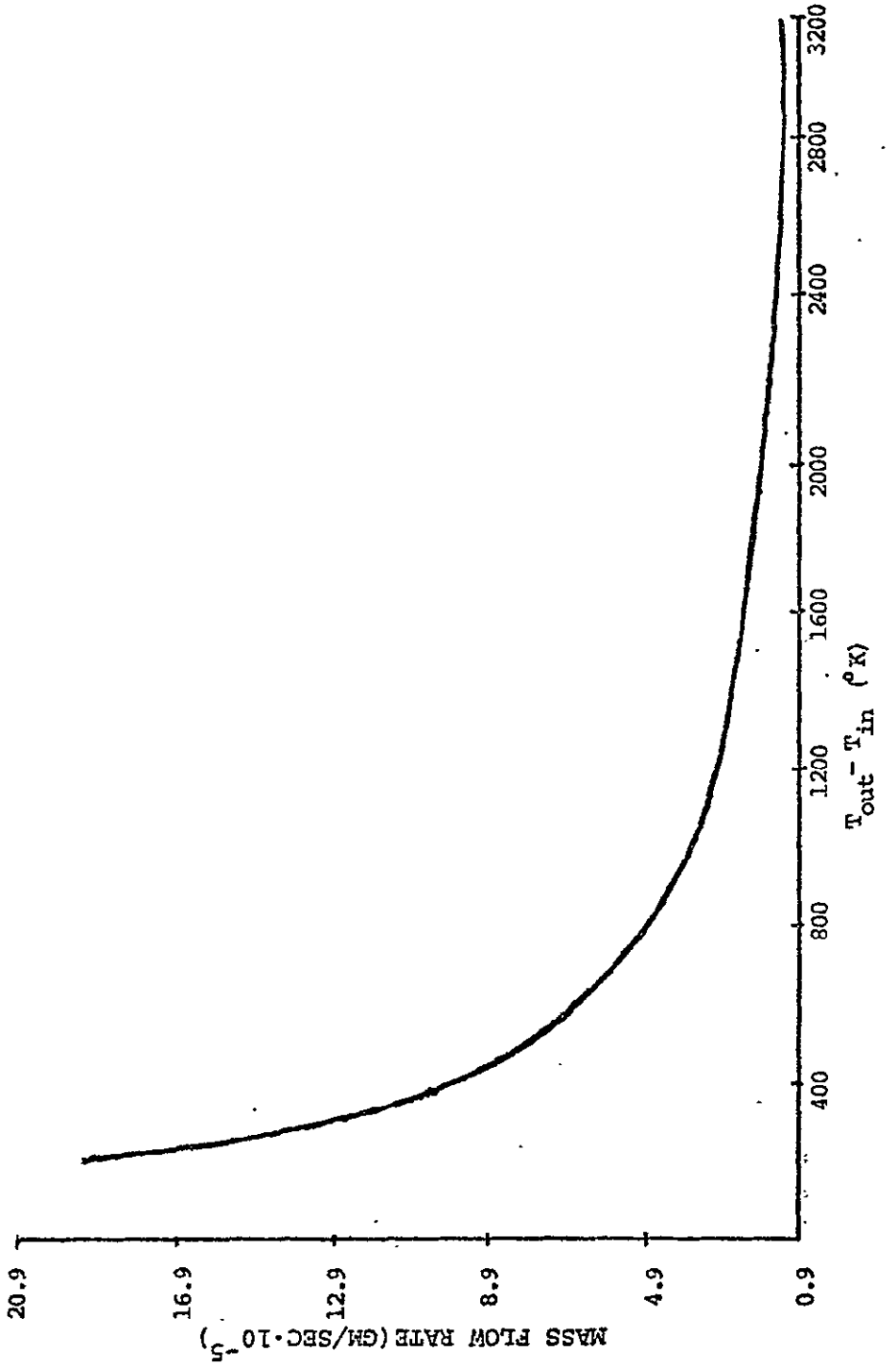

Fig. 3.10 Mass Flow Rate vs Reactor Core Temperature Difference

Table 3.6 Fluid Mechanical Summary

(Item)	(Value) or name
Coolant	Helium
Exit Temp Range	3000 to 3500^{o}K
Fuel to coolant mass flow core	1/100 to 1/1000
Coolant thickness	45 to 220 cm
Plasma radius	50 to 200 cm
Coolant mass flow	120 to 190 kg/sec
Seed material	carbon
Seed size	0.012 microns
Seed density	10^{-6} to 10^{-5} gm/cc
Coolant exit pipe diameter	$2.65 \cdot 10^{4}$ to $4.2 \cdot 10^{4}$

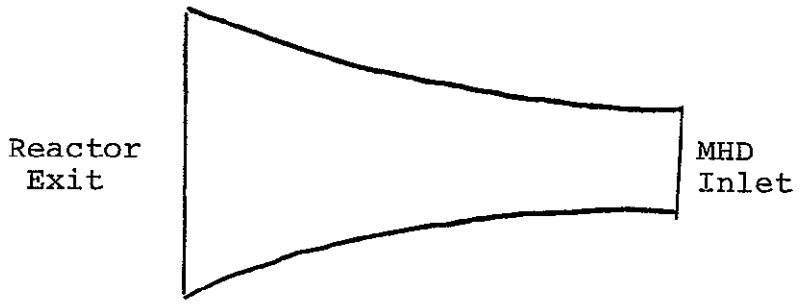

@ A_1 known:
$m_1 = 0.1$
$T_1 = 3000$ K
calculated:
$A_1 = 0.175$ m^2

@ A_2 known:
$A_2 = 0.0387$ m^2
$m_2 = 0.5$
calculated:
$A^* = 0.0254$ m^2

Equation:

$$A/A^* = 1/m[2/(\gamma+1)(1 + (\gamma-1)m^2/2)]^{[(\gamma+1)/2(\gamma-1)]}$$

Fig. 3.11 Area Calculation Technique

REFERENCE FOR CHAPTER 3

1. Moore, F. K. and S. Leibouich, "Self-Confined Rotating Flows for Containment," Research on Uranium Plasmas and their Technological Applications, NASA SP-236, 95, (1966).

2. Mensing, A. E. and J. F. Jaminet, "Experiments on the Containment of Simulated Fuel in Unheated and Heated Vortices," Research on Uranium Plasmas and their Technological Applications, NASA SP-236, 65, (1971)

3. Poutre, H. A., "Estimates of Fuel Containment in a Coaxial Flow Gas Core Nuclear Rocket," Nuclear Technology, 12, 209, (Oct. 1971).

4. Lanzo, C. P., "A Flow Experiment on Curved-Porous Wall Gas-Core Reactor Geometry," Nuclear Applications and Technology, 8, 6 (Jan. 1970).

5. Johnson, B. V. and J. C. Bennett, "Experimental Study of the Effects of Injection Conditions on the Flow in Cylindrical and Spherical Chambers," 2nd Symposium on Uranium Plasmas Research and Applications, Am. Institute of Aeronautic and Astronautics, 204 (Nov. 1971).

6. Meghreblian, R. V., "Gaseous Fission Reactors for Booster Propulsion," American Rocket Society J, 32, 13 (1962).

7. Duke, E. E. and W. J. Houghton, "Gas-Core Nuclear Rocket Engine," Journal of Spacecraft, 4, 12 (1967).

8. Karlheinz, Thom, "Fission Engine Concepts," 2nd Symposium on Uranium Plasmas, Atlanta, Ga. (Nov. 1971).

9. Trauger, D. B., "Operating Experience and Design Trends for Helium Cooled Nuclear Power Reactors," The Helium Soc. Symposium Proceedings, Washington, D. C., 20, (March 1970).

10. Miller, M. H., "Measured Emissivities of Uranium and Tungsten Plasmas," 2nd Symposium on Uranium Plasma: Research and Applications, Atlanta, Ga., 120, (Nov. 1971).

11. Trauger, D. B., Helium Cooled Reactors, USAEC Report TM-2297, Oak Ridge National Lab (1968).

12. Hubbell, J. H., "Photon Cross-section Compilation Activity in the U. S. in the Range 1 KeV to 100 GeV," Journal De Physique C4, C4-14 (Oct. 1971).

13. Birkig, V. C., "Theoretical Absorption in Seeded Gases," Douglas Report DAC 59985, Nasw 1310 (Jan. 1967).

14. Shenoy, A. S., The Attenuation of Radiant Energy in Hot Seeded Hydrogen, Ph.D. Thesis, Georgia Inst. of Tech. School of Nuclear Engineering, (May 1969).

15. Clinch River Preliminary Safety Analysis Report, Project Management Corp., June 1975.

16. Zucrow, M. J. and J. D. Hoffman, Gas Dynamics, 1, 160-241, John Wiley and Sons, Inc., New York (1976).

4. HEAT TRANSFER IN THE PLASMA CORE REACTOR

Plasma core reactors are capable of producing heat at extremely high temperatures for use in rocket propulson, MHD power generation, or process heat applications. Most of the work dealing with heat transfer in a gaseous core reactor has been concerned with reactors used in rockets. Here the uranium plasma heated a hydrogen coolant that was used for propulsion. For central station power production the difference is that helium is used as a coolant and is exhausted through a MHD nozzle. Therefore, previous work on heat transfer of gaseous core reactors can be readily applied to this design study.

The simplest case to analyze is when there is no mixing of the fuel and coolant in the uranium-helium core region.[1] In reality there will be some mixing and some convection effects at the outside surface of the uranium plasma. Therefore, the case analyzed would be a "first estimate" of the temperature distribution in the core.

In this study the steady state temperature profile as a function of radius in a spherical geometry is analyzed. Figure 4.1 shows the geometry and pertinent data. The helium and uranium gases are assumed to be grey gases, which means the radiation absorption coefficient is independent of wavelength. The containment wall is also assumed to be grey so that wall emissivity and reflectivity are independent of wavelength. The approach used is that proposed by Ragsdale and Kascak.[2] In this method the volume heat generation term (q''') is assumed radially dependent and the absorption parameters temperature dependent.

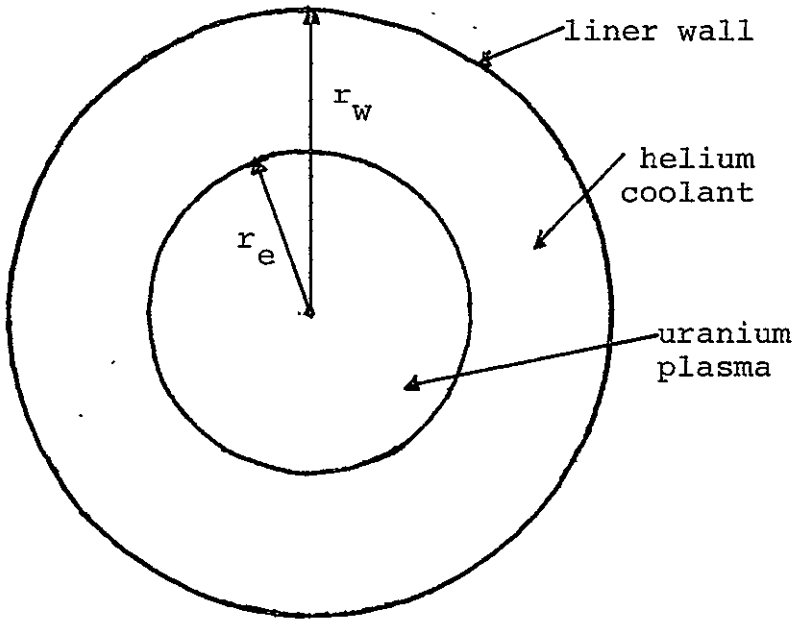

item	value	
r_e	200cm	radius
r_w	320cm	radius
power	2×10^9 watts	reactor power
q''_{edge}	3.98×10^3 watts/cm^2	core edge heat flux
e_w	0.7-0.8	wall emissivity
T_w	800 K	wall temperature
σ	5.7×10^{-12} w/cm°K^4	Stefan-Boltzmann constant

Fig. 4.1 Geometry and Data

If one assumes that the heat flow is basically a diffusion process the heat flux in the core may be expressed by[2]

$$q''(r) = \frac{-4}{3k(T)} \frac{d(\sigma T^4)}{dr} \tag{4.1}$$

where q'' = heat flux

σ = Stefan-Boltzmann constant

T = temperature

r = radius

k = absorption coefficient.

At steady state the heat flux can be related to the volumetric heat generation $q'''(r)$ by

$$q''(r) = \int_0^r q'''(r)\, 4\pi r^2 dr / 4\pi r^2 \ . \tag{4.2}$$

Figure 4.2 shows calculated fission densities for these different PCR radii. If the fission density, and hence the heat generation rate is fitted by a polynominal such as:

$$q'''(r) = \sum_{i=0}^{n} q_i r^i \tag{4.3}$$

then integration of Eq. 4.2 yields

$$q''(r) = \sum_{i=0}^{n} \frac{q_i r^{i+1}}{i+3} \ . \tag{4.4}$$

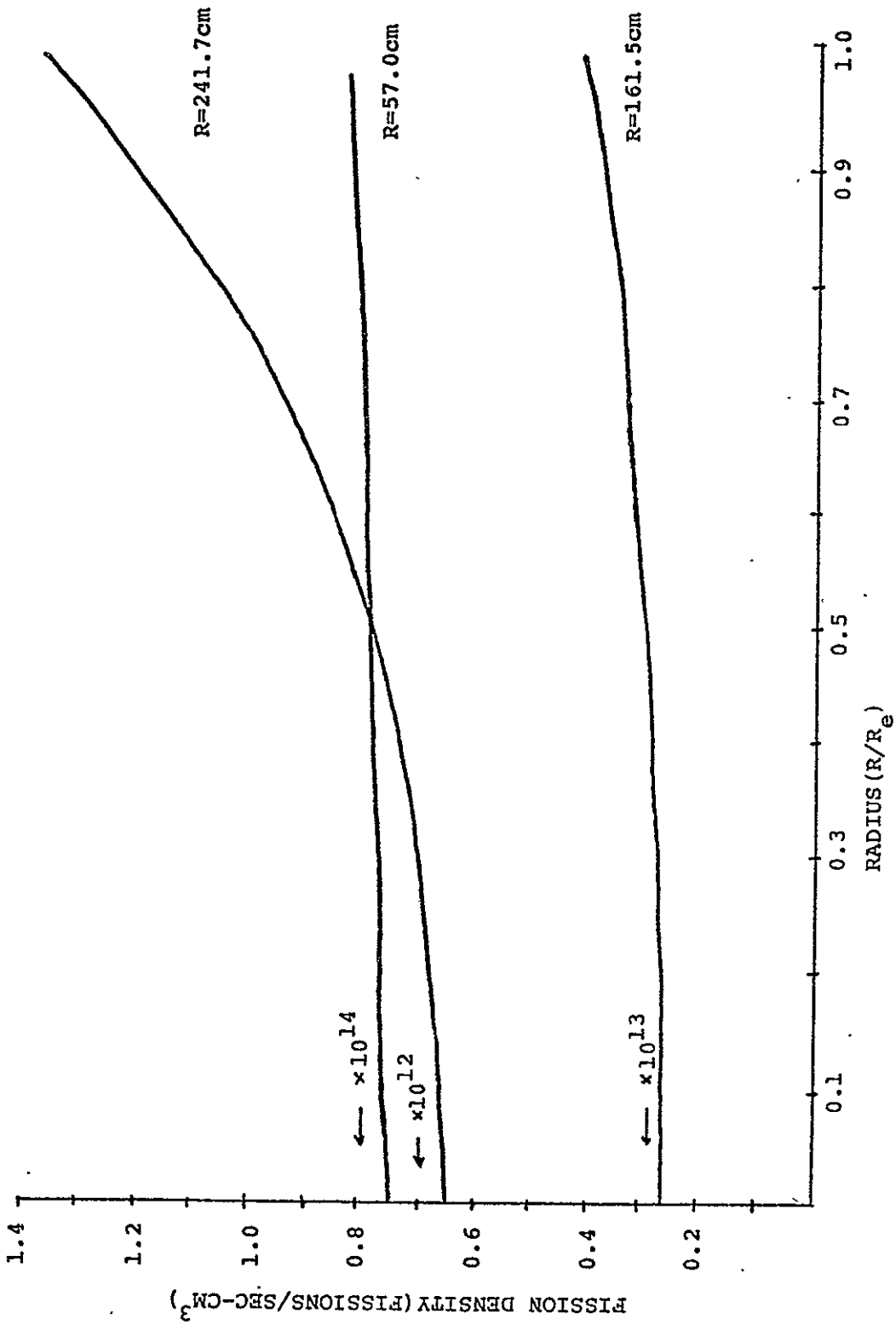

Fig. 4.2 Fission Density vs Radius

Substituting into Eq. 4.1 and rearranging yields

$$\frac{\partial T}{\partial r} = \frac{-3k(T)}{16\sigma T^3} \sum_{i=o}^{n} \frac{q_i \, r^{i+1}}{i+3} \tag{4.5}$$

Equation 4.5 can be solved by numerical techniques with k(T) being supplied via experiment results.

To solve Eq. 4.5 one must also have the boundary conditions for the edge temperature of the reactor (T_e). Unfortunately, this temperature is not known, but because of wall stress and creep limitations the wall temperature (T_w) is known. This temperature will in turn affect the core edge temperature. To get a relationship between T_w and T_e let us first consider a brightness temperature T_b. T_b is defined so that σT_b^4 gives the radiated heat flux at the core edge. T_b is defined by the expression:

$$q_e'' = \sigma F (T_b^4 - T_w^4) \tag{4.6}$$

where $$F = \left[1 + \left(\frac{r_e}{r_o}\right)^2 \left(\frac{1 - \varepsilon_w}{\varepsilon_w}\right)\right]$$

ε_w = emissivity of the wall.

Thus the brightness temperature is found to be:

$$T_b = \left\{\frac{q_e''}{\sigma}\left[1 + \left(\frac{r_e}{r_o}\right)^2 \left(\frac{1 - \varepsilon_w}{\varepsilon_w}\right)\right] + T_w^4\right\}^{1/4} \tag{4.7}$$

where $q''_e = \sum_{i=o}^{n} \frac{q_i \, r_e^{i+1}}{i+3}$ = edge heat flux

To determine the edge temperature from T_b, Ragsdale and Kascak proposed the following relationship:[2]

$$T_e = T_b \left[\frac{1}{2} \left(1 + \frac{3}{2 r_e k(T)} \right) \right]^{1/4} \tag{4.8}$$

Since k(T) is a function of T and, therefore, must be evaluated at T_e, Eq. 4.8 must be solved iteratively. The use of the secant method provides quick convergence.

Once T_e is known T(r) can be solved by any appropriate numerical method. A fourth-order Runga-Kutta program was written and implemented for this purpose. The data for k(T) was input into the program as a polynomial fit to the data shown in Fig. 4.3. The program was checked for accuracy against previous work[1,2] and showed good agreement.

Temperature distributions for the design basis core of 200 to 20 cm in radius were calculated and are shown in Fig. 4.4. The combination of lower temperature (and hence higher absorption coefficient) and a higher fissioning rate at the core edge cause the very rapid temperature increase in the first few centimeters inside the core. This rapid rise could also mean that the core edge temperature has been underestimated; however, the calculations were checked and the values used for T_b and T_e were consistent. These calculations showed that maximum

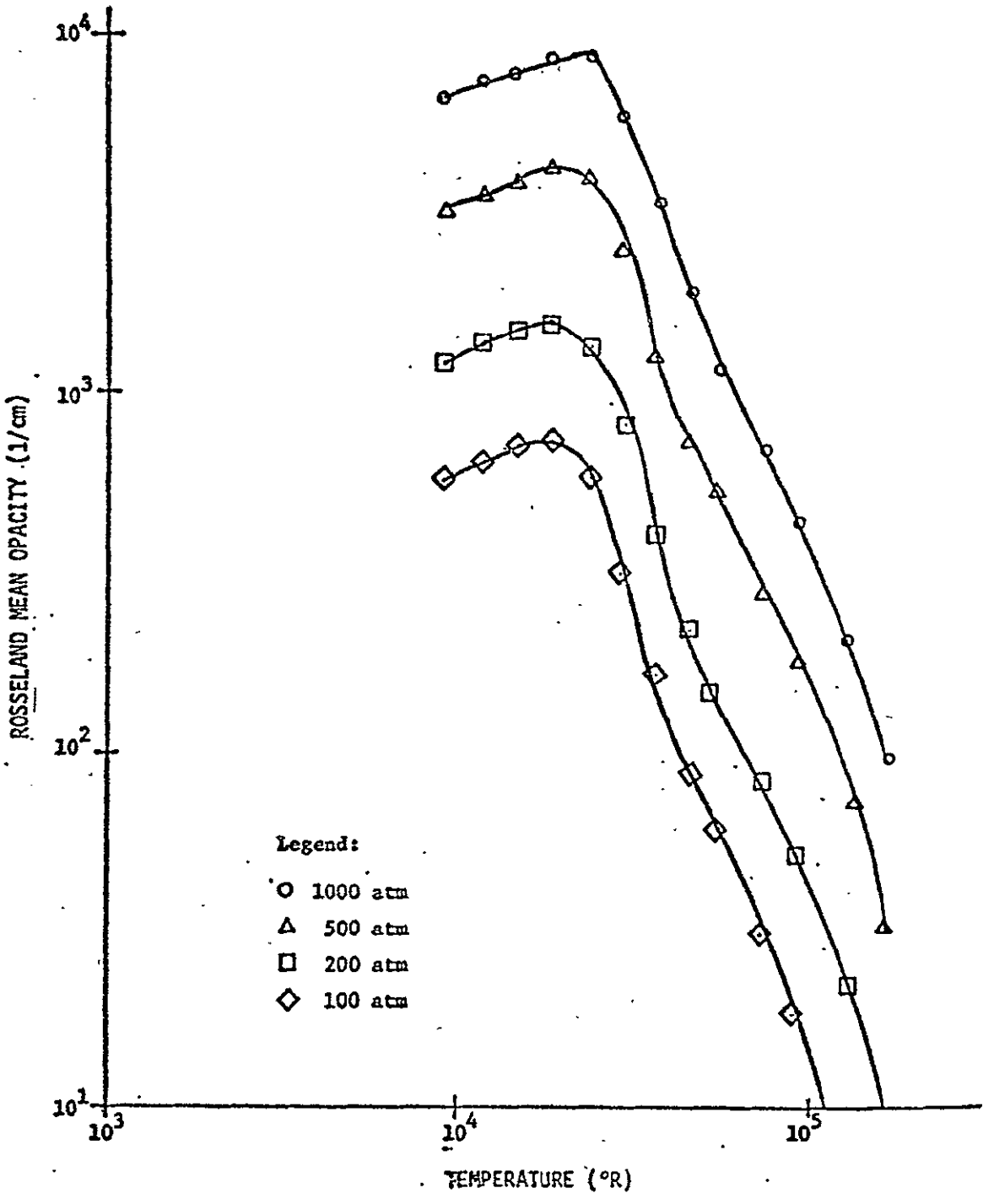

Fig. 4.3 Rosseland Mean Opacity versus Temperature for Uranium.[3]

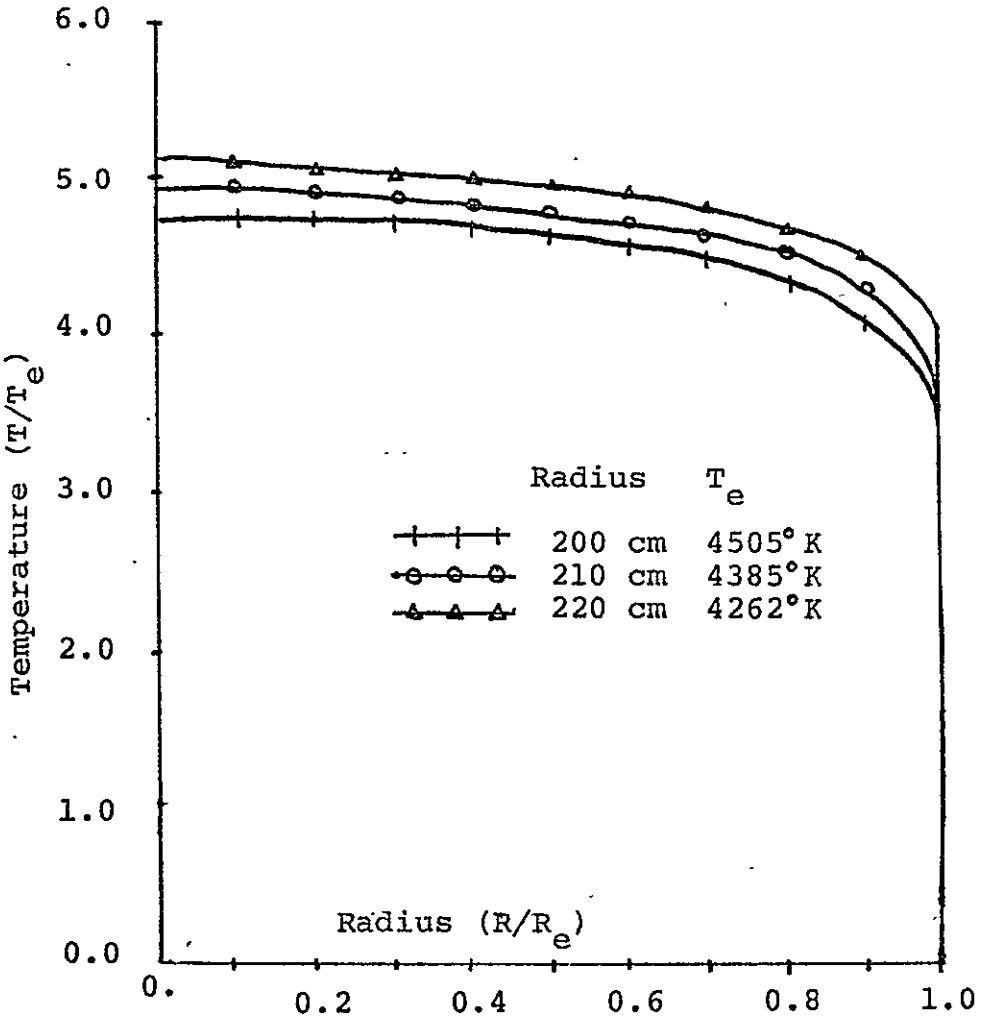

Fig. 4.4 Core Temperature vs Radius

core temperatures ranged from 21,400 to 21,800°K with an average temperature in the neighborhood of 18,500°K.

The transuranium actinides (neptunium, plutonium, americium, curium, etc.) will be introduced into the PCR in the form of zirconium alloy clad rods located just outside the beryllium reflector. The actinides will be in the form of oxides and will be cooled by the helium coolant used in the core. The design constraints for the actinide rods will have to be the same as those used for present day power reactors for safety reasons. These are:

Linear heat rate. . . 500 watts/cm. . . to control amount of stored energy in the fuel.

Maximum clad temperature. . . 500°C. . . to maintain clad strength.

There is a scarcity of thermal-physical property data on the oxides of transplutonium actinides and there is no data on the behavior of mixtures. Their known melting points, are high (~2400°C) and actinide oxide densities are all about the same being ~11 gm/cc.[4] Consequently, since little is known about the actinide oxides, and a sizable fraction of the actinide rods will be uranium oxide, it is assumed that their physical properties are the same as UO_2.[5]

A high burnup rate in the actinide fuel rods is desirable so as to shorten the time required for transforming the actinides by fission. The burnup rate is directly proportional to the volumetric heat generation rate, which is:

$$q'''(r) = \sum_{i=1}^{n} R_i \; \rho_{fission}(r) \qquad (4.9)$$

where

q''' = heat generation rate, watts/cm^3

R_i = energy released per fission (Joules) of ith isotope

$\rho_{fission}$ = fission density of ith isotope, fissions/cm^3-sec.

The value of R_i for the actinides is not known, but it should be close to that of uranium or plutonium (~200MeV/fission). Consequently, the volumetric heat generation for the actinide rods is:

$$q''' = \left(200 \frac{\text{MeV}}{\text{fission}}\right) \cdot \left(\frac{1 \text{ Joule}}{6.242\times10^{12} \text{ MeV}}\right)\left(\bar{\rho}_{fission} \frac{\text{fissions}}{\text{cm}^3 \text{ sec}}\right). \qquad (4.10)$$

For the initial actinide fuel loading into the PCR

$$\bar{\rho}_{fission} = 4.34\times10^{11} \text{ fissions/cm}^3\text{-sec}$$

which gives

$$q''' = 13.90 \text{ watts/cm}^3.$$

This value is considerably lower than the heat rate in present LWRs so the probability of exceeding one of the design limits is very small.

The geometry for the actinide fuel rods was chosen to give a minimum actinide region thickness, as this helped give low critical masses. This also helped keep the flux flat in the actinide region (for even

burn-up), and helped to limit the volume of actinides required to fill the region (at an inner radius of 3.4 meters even a small thickness has quite a large volume). The radius for the fuel rods was set at 0.268 cm with a 0.035 cm thick clad and a gap thickness of 0.015 cm. This gave an overall radius of 0.318 cm (0.25 in. diameter). The rods will be spaced with a 0.142 cm diameter wire wrap with a pitch of 25 cm.

The actinide fuel rods are one meter long and positioned just outside the beryllium liner as shown in Fig. 4.5. Calculations showed, that for the dimensions shown in Fig. 4.5, the neutron flux variation in going from the center of the actinide rods to either end is only 1.0%. Hence, it is a good assumption to assume that the flux and, thus, the power does not change over the rod length. Therefore,

$$q''' \neq f(r,z); \quad q''' = \text{const} = 13.90 \text{ watts/cm}^3.$$

With this value we can now calculate the helium temperature at the exit to the actinide fuel rods. Unfortunately, this is an iterative procedure because the design point temperatures are the core outlet and the actinide inlet. Thus the mass flow rate will have to be varied until the design core outlet temperature is met. The procedure will be:

1) Assume mass flow rate $\dot{m}_1$

2) Calculate $T_{\text{out actinides}} = T_{o_a} = T_{in_a} + \dfrac{\pi r_f^2 \, Hq''' \cdot n}{C_p \dot{m}}$

3) Calculate $T_{\text{out core}} = T_{o_c} = T_{o_a} + \dfrac{P}{C_p \dot{m}}$

4) Check if $T_{o_c} = 3500^{\circ}K$ if not,

redo calculation with new mass flow $\dot{m}_2$.

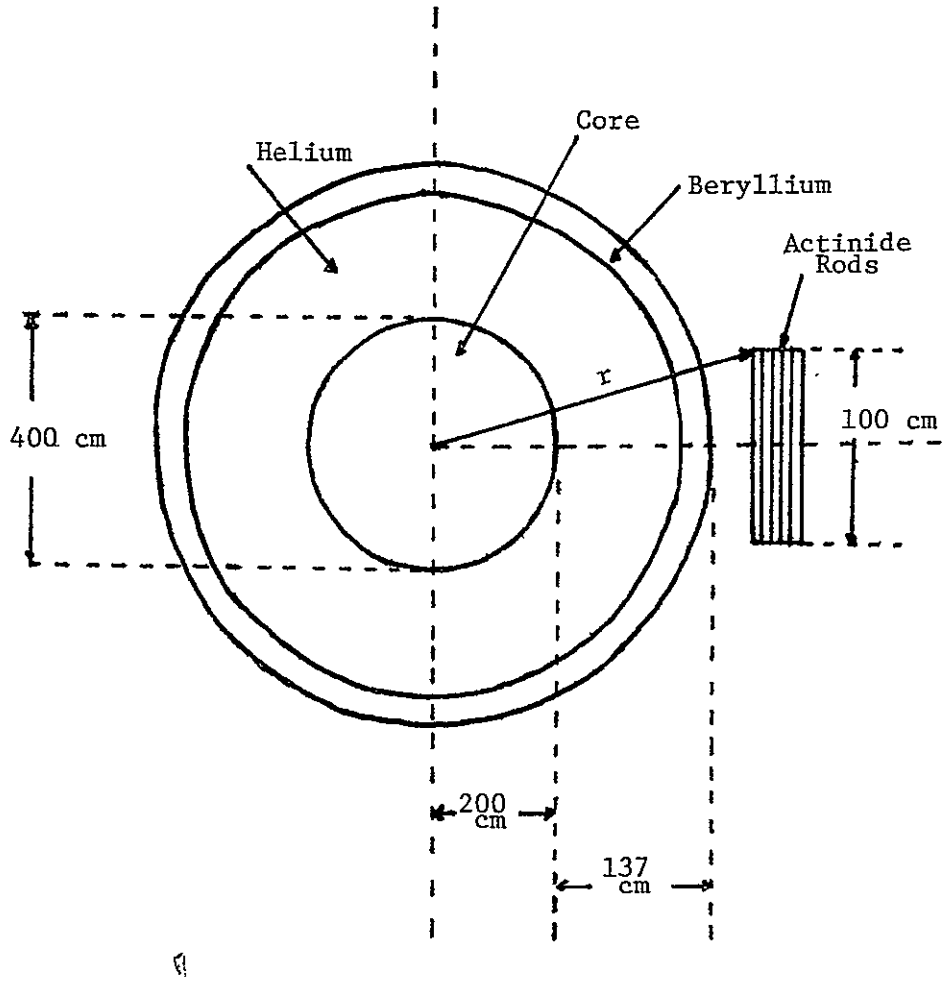

Fig. 4.5 Actinide Location

The above procedure must be done within the design limits set forth and with the following data:

$P = 2000$ MW

$r_f = 0.269$ cm

$H = 100$ cm

n = number of actinide fuel rods:

= 2725 for first fuel loading

$T_{in_a} = 642^{o}K$

$C_{P_{helium}} = 5.20 \frac{J}{gm^{o}K}$

$q''' = 13.9$ watts/cm^3

$r_w = 0.318$ cm

The calculation must also be done taking into account the effects of the uncertainties due to manufacturing tolerances, physical property variations and flow maldistributions. The effects these uncertainities have on the temperature can best be accounted for by applying hot channel/hot spot factors to the computation. Because of the similarity of the actinide rods and the fuel rods of the Clinch River Breeder Reactor the same hot channel/hot spot factors used in its design will be used here.[6] The nuclear hot spot factor for axial variation in the flux will be ignored here due to the arguments given earlier for assuming a flat heat generation rate in the actinide fuel rods. The factors used are:

Coolant	Film	Heat Flux
$F_{\Delta h}$	$F_{\Delta T}$	F_q
1.232	1.168	1.081

Using these factors the actinide fuel rod heat transfer calculations yielded the results shown in Table 4.1. As can be seen the maximum clad temperature turns out to be 647°C (374°C) and is still well within the design limit of 500°C. These calculations are for startup of actinide transmutation. The calculated temperatures at later cycles will probably be higher.

Table 4.1 Actinide Region Thermal Parameters

Maximum CLAD Temperature	646°K
Inlet Helium Temperature	642°K
Outlet Helium Temperature	643.7°K
Mass Flow Rate	134.65 kg/sec
Helium Velocity	5.9×10^4 cm/sec (M = 0.4)

These calculations represent scoping type work and are intended to give "order of magnitude" values for temperatures in each region. A more exact temperature profile for the core region would require detailed information about the flow field inside the uranium plasma and in the helium coolant. Items that were not considered, such as fuel-coolant mixing and the energy of the uranium swept out of the core, need to be analyzed. Also, detailed pressure loss calculations need to be performed for the actinide and core regions. This work, however, is enough to permit a fairly accurate description of the operating conditions inside a PCR. Table 4.2 summarizes design points relevent to the heat transfer analysis of the PCR.

Table 4.2 Heat Transfer Summary

ITEM	VALUE
Actinide Region:	
Helium Inlet Temperature	642°K
Maximum Actinide Temperature	652°K
Maximum Clad Temperature	646°K
Helium Exit Temperature	643.7°K
Core Region:	
Mass Flow Rate	134.65 kg/sec
Helium Exit Temperature	3500°K
Maximum Fuel Temperature	~21,400°K
Exit Helium Velocity	2.85×10^4 cm/sec

REFERENCES FOR CHAPTER 4

1. Rust, J. H. and R. Farr, "Heat Transfer in Gas Core Power Reactors," Exploratory Study of Several Advanced Nuclear MHD Power Plant Systems, Final Status Report, NASA Grant NGR-11-002-145, J. R. Williams and J. D. Clement project directors, 139 (March 1973).

2. Ragsdale, R. G. and A. F. Kascak, "Simple Equations for Calculating Temperature Distribution in Radiating Grey Gases," NASA TN D-5226 (May 1969).

3. Parks, D. E., G. Lane, J. C. Stewart and S. Peyton, "Optical Constants of Uranium Plasma," NASA-CR-72348, GA-8244 (Feb. 1968).

4. Kirk and Othner, Encyclopedia of Chemical Technology, 1, 2nd ed., John Wiley and Sons (1963).

5. Rust, J. H. and J. D. Clement, Analysis of the Gas Core Actinide Transmutation Reactor (GCATR), Annual Report for NASA grant NSG-1288, (Feb. 28, 1977).

6. Cavelli, M. D. and R. A. Markley, "Preliminary Thermal Hydraulic Design and Predicted Performance of the CRBRP Core," 75-HT-71, presented at AIChE-ASME Heat Transfer Conference, San Francisco (Aug. 1975).

5. DESIGN CONSIDERATIONS OF PLASMA CAVITY REACTORS

Figure 5.1 is a schematic of the design base reactor. The relevant dimensions, obtained from the fluid mechanical, nuclear analyses, and thermal-hydraulic analysis are also shown. The reactor is almost 3.40 meters in radius and 7.20 meters in length. Table 5.1 gives the region volumes and components weight.

The beryllium liner, besides serving as the reactor moderator, is also the porous wall and flow director for the helium coolant entrance into the reactor cavity. Beryllium was chosen for the liner because of its exceptional moderating capabilities. The helium temperature in the beryllium liner ranges from 370°C to 400°C which is approximately one-fourth its melting point, so the metal should be able to withstand such a thermal load. There will also be very little pressure difference between the liner inside and outside so the overall stress on the liner should be small. The beryllium metal is encased in a jacket of zirconium alloy and bolted under a small compressive load. Since the thermal expansion of beryllium is greater than zircaloy, at operating temperatures the beryllium should be in even more of a compressive load that should equalize any pressure load on the beryllium. Figure 5.2 shows a detail drawing of the liner.

The actinide fuel rods presented the first real problem in the overall system layout. Since spherical geometry is best from a neutronic and hydrodynamic standpoint for the core, the cylindrical actinide fuel rod did not really "fit" anywhere. It was decided to place the rods just outside the beryllium reflector in a cylindrical annulus region. Each

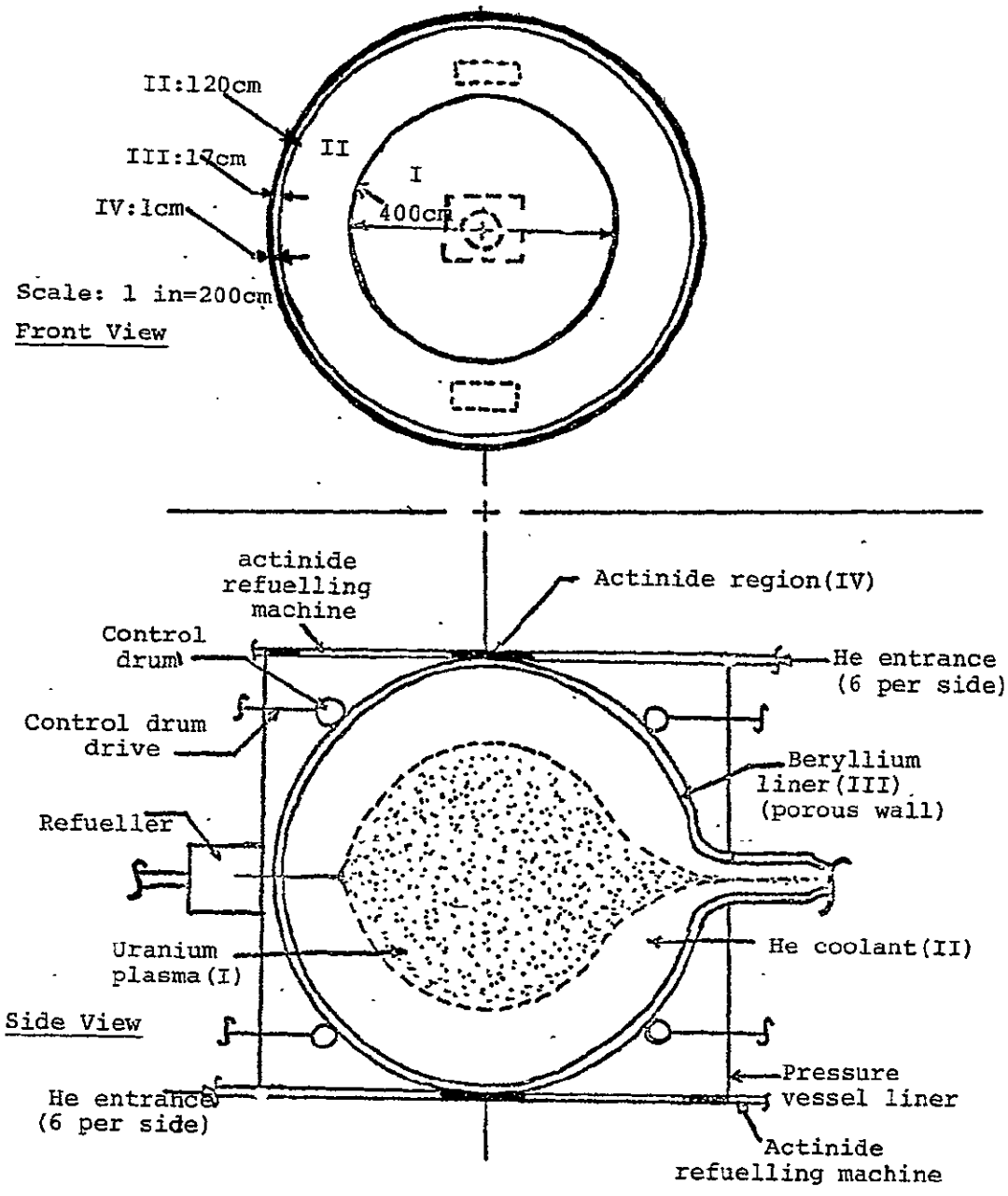

Fig. 5.1 Reactor Schematic

Table 5.1 Volume and Weight of Reactor Components

	Region	Volume	Material Weights
(I)	Uranium plasma	33.51 m^3	~374.0 Kg
(II)	Helium coolant	103.75 m^3	487.0 Kg
(III)	Beryllium liner:	16.0 m^3	29440 Kg
	Zirconium Alloy:	1.29 m^3	8452 Kg
	Helium coolant:	5.73 m^3	26.9 Kg
IV)	Actinide rods:	.0405 m^3	445.43 Kg*
	Zirconium Alloy:	.04126 m^3	270.3 Kg*
	Helium coolant and bond:	.1095 m^3	0.838 Kg*
(V)	Control drums:		
	Cd:	0.000057 m^3	0.493 Kg
	Beryllium Shield:	0.5027 m^3	923.7 Kg
	Zirconium Alloy:	0.1335 m^3	874.6 Kg
(VI)	Helium coolant outside of Beryllium liner and Actinide Region:	101.16 m^3	474.86 Kg

*These are loadings for each year; equilibrium, total region size and weights would be 3 to 4 times these numbers.

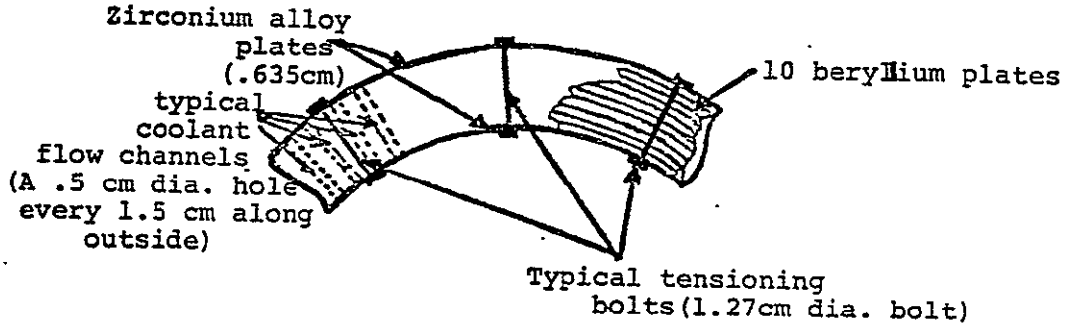

Fig. 5.2 Liner Details

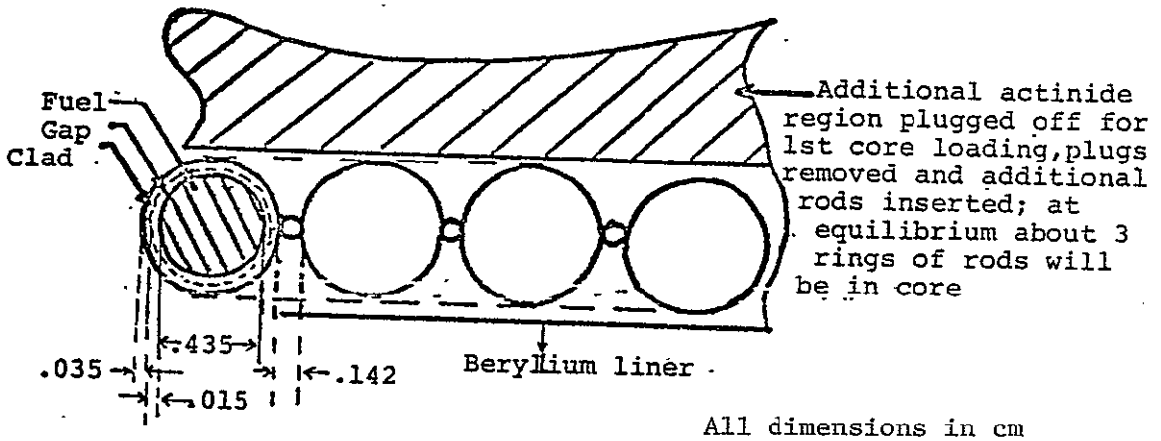

Fig. 5.3 Actinide Fuel Rods

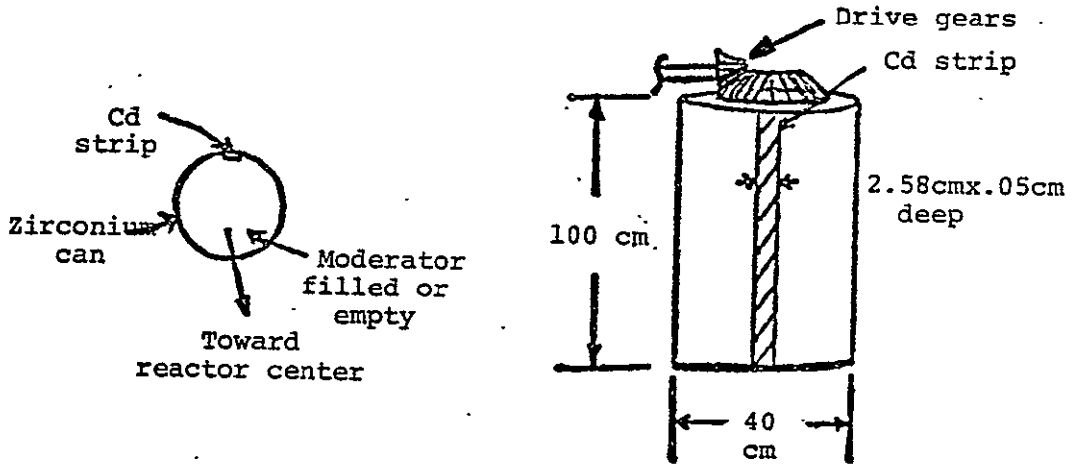

Fig. 5.4 Control Drum Details

rod with its associated clad and wire wrap will require 0.9194 cm width. The rods will be loaded in overlapping annulus regions as more actinides are introduced into the core. The initial charge of actinides should be about 445 Kg of actinide-oxides. This represents the yearly discharge from about 20 PWRs and requires one ring of actinide rods around the core. The equilibrium actinide loading would be about three rings of actinide rods or about 1500 Kg of actinide-oxides. Figure 5.3 shows the detail of the actinide region.

The control drums will be zirconium alloy cylindrical cans filled with beryllium or beryllium oxide with a strip of cadmium on one side. Figure 5.4 shows a typical control drum. These drums will provide the reactivity control needed to assure adequate dynamic control during operation.

A possible reactor layout is shown in Fig. 5.5.

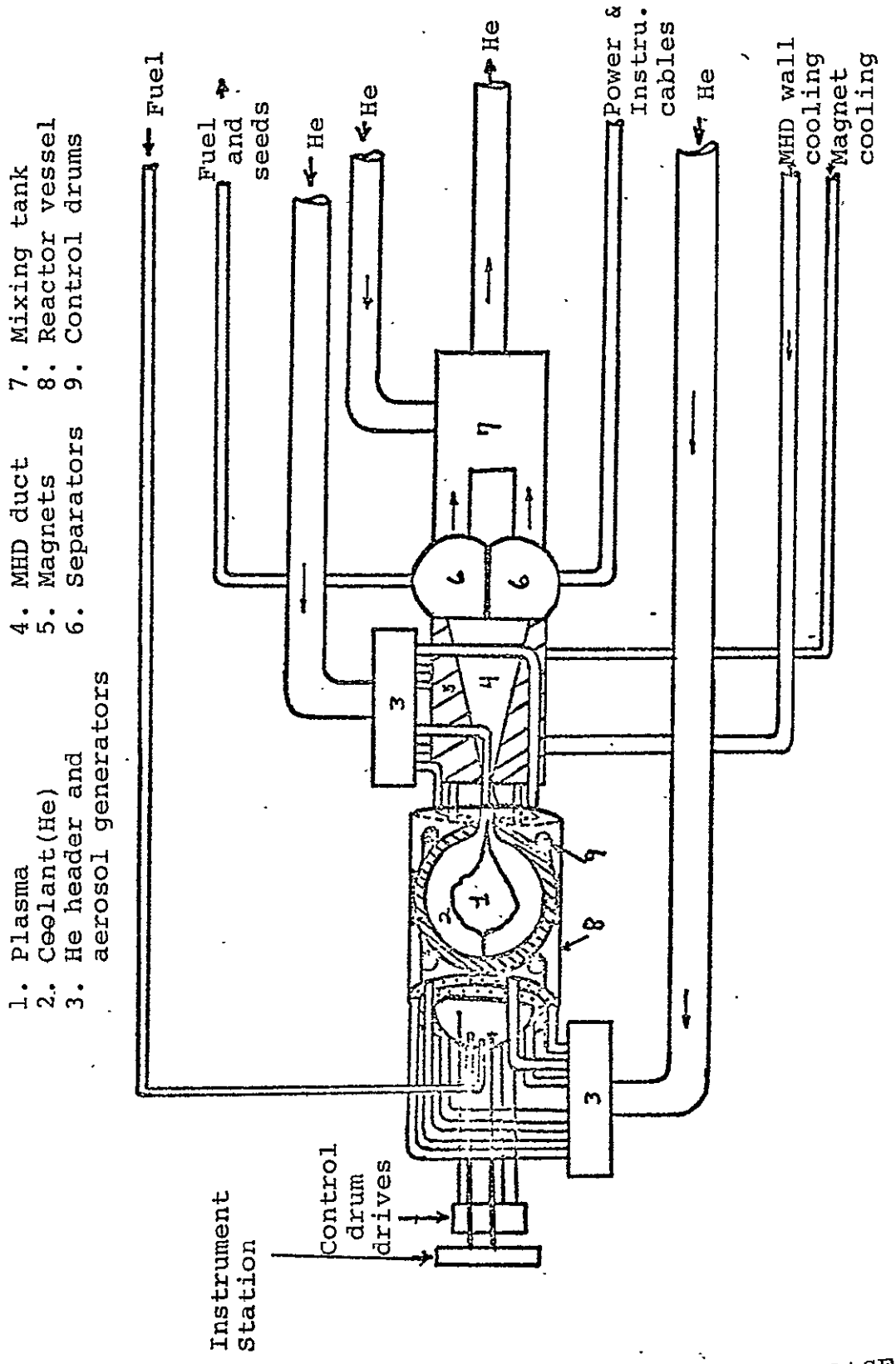

Fig. 5.5 Reactor Layout

REFERENCES FOR CHAPTER 5

1. SESONSKE, Alex, and Samuel GLASSTONE, "Nuclear Reactor Engineering," Van Nostrand Reinhold Company, New York, New York (1967).

2. WHITE, D. W., and J. E. BURKE (Eds.), "The Metal Beryllium," American Society of Metals, (1955).

3. KUNZE, J. F., and J. H. LOFTHOUSE, "Flow and Criticality in the Open Cycle Gas Core," 2nd Symposium on Uranium Plasmas: Research and Applications, 197, Atlanta, Georgia, November (1971).

6. NUCLEAR ANALYSIS-PLASMA CORE BREEDER REACTOR

Neutronics calculations were carried out for a U-233 plasma core with a molten salt breeding blanket. The primary objectives of the overall nuclear design were to design a reactor with a low critical mass (less than a few hundred kilograms U-233) and also a breeding ratio of 1.01. The later objectives was a safety precaution to guard against diversion of fissionable material during blanket reprocessing. Since only enough U-233 would be bred in the blanket to replenish the amount depleted in the core, any diversion of U-233 during reprocessing would result in an insufficient amount of fissionable material to replenish the core and the reactor would shut down. Both of the above objectives were met in the final design.

The Mach-I code[1] was used as the primary computational tool in the nuclear analysis. Mach-I is a one-dimensional diffusion theory code which uses the 26-group ABBN cross section set of Bondarenko, et al.[2] All neutronic calculations were performed by varying the plasma core radius to obtain $K_{eff} = 1.000$ with other dimensions held constant.

Initially, four moderators were analyzed to determine the one most suitable for the final reactor design. The moderators selected were graphite, beryllium, beryllium-oxide, and heavy water. Properties of each of these are listed in Table 6.1.

The geometry used for comparing the moderators is shown in Fig. 6.1. Region I is the core region (U-233 plasma). The pressure is maintained at 200 atmospheres and the average core temperature is 25,000°K.

Table 6.1 Selected Properties of Moderators

Moderator	$\rho(gm/cm^3)$	Atoms or Molecules $/cm^3$	$\Sigma a(cm^{-1})$	$\Sigma s(cm^{-1})$
Graphite	1.60	0.08023×10^{24}	2.728×10^{-4}	0.3851
Be	1.85	0.1236×10^{24}	1.174×10^{-3}	0.8652
BeO	2.96	0.07127×10^{24}	6.771×10^{-4}	0.4846
D_2O	1.105	0.03323×10^{24}	3.323×10^{-5}	0.4519

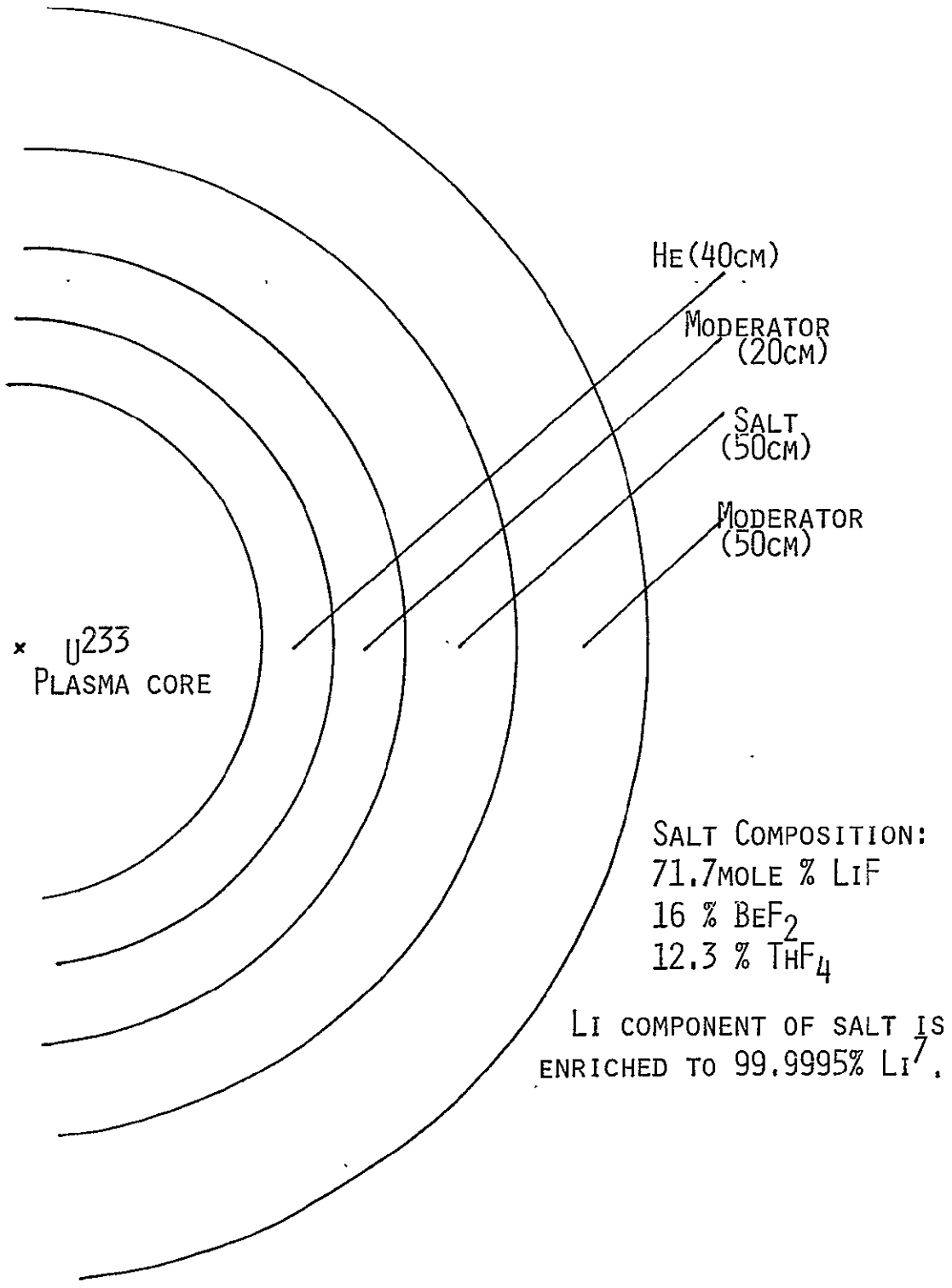

Fig. 6.1 Geometry Used For Moderator Comparison

Region II is the helium region with a pressure of 200 atmospheres and average temperature of 3000°K. This region serves to contain the plasma core as well as remove heat from the plasma core. This region was maintained at a thickness of 40 cm. in these initial calculations. Region III is the moderator region of 20 cm. thickness. This region is necessary to moderate the plasma core sufficiently to attain a small critical mass. Region IV is the molten salt region (50 cm.). The molten salt composition is 71.7 mole % Li F, 16 mole % BeF_2, and 12.3 mole % ThF_4. The Li is enriched to 99.99% in the Li^7 isotope in order to optimize neutron economy. The average temperature in this region is assumed to be 650°C. Region V was another moderator region (50 cm.). This region is necessary to maintain a breeding ratio greater than 1.0.

Results for the moderator comparison are shown in Table 6.2. It is evident from these calculations that either beryllium or beryllium-oxide could be used to meet the two primary objectives of the nuclear design. Beryllium-oxide was selected mainly due to its good thermal properties (m.p. of 2550°C) and also its good moderating and nuclear properties. Metallic beryllium could have been used if sufficient cooling were provided to ensure no melting would occur. All subsequent calculations were performed using BeO as the moderator.

Following the initial calculations to determine the most suitable moderating medium, calculations were performed to determine the effect of salt thickness, inner BeO liner thickness, and outer BeO thickness on critical mass and breeding ratio. These results are presented in Tables 6.3, 6.4 and 6.5. All dimensions except the one being studied remain as shown in Figure 6.1.

Table 6.2 Breeding Ratios and Control Masses for Various Moderators

Moderator	Breeding Ratio	Critical Mass (Kg)
Graphite	1.06	2900
Be	1.12	14
BeO	1.14	17
D_2O	1.13	80

Table 6.3 Effect of Salt Thickness (BeO Moderation)

Salt Thickness	B. R.	Mass (KG)
50 cm.	1.14	17
40 cm.	1.139	16.53
30 cm.	1.130	16.49
20 cm.	1.105	16.33
10 cm.	1.026	14.94

Table 6.4 Effect of Inner Moderator Thickness

Thickness	B. R.	Mass (KG.)
10 cm.	1.143	1250
15 cm.	1.181	50.5
20 cm.	1.140	17
25 cm.	1.086	9.5
30 cm.	1.024	6.7

Table 6.5 Effect of Outer BeO Thickness

Thickness	Critical Mass(KG)	B. R.
50 cm.	17	1.14
40 cm.	17	1.1423
30 cm.	17	1.1420
20 cm.	17	1.1414
10 cm.	17	1.1397
5 cm.	17	1.1376
1 cm.	17	1.1334

The final reactor configuration is shown in Figure 6.2. For this configuration the critical core radius was 82.5 cm. The critical U-233 mass is 26.3 Kg. and the reactor breeding ratio is 1.0099. The helium region is 60 cm. in thickness which gives a $\frac{\text{r-helium}}{\text{r-core}} = 0.727$. This is sufficient for stable plasma confinement.

The final configuration is the only one not feasible. The overall critical mass could be decreased but the molten salt volume would need to be increased to maintain a constant breeding ratio. Table 6.6 summarizes the operating parameters for the plasma core breeder reactor.

Table 6.6 Operating Parameters for Plasma Core Breeding Reactor

1.	Power	2000 MW(th)
2.	Power Density ($^{kw}/\ell$) in Plasma	848.8
3.	Core Volume (cm^3)	2.35×10^6
4.	Core Radius (cm)	82.5
5.	Average Thermal Flux in Plasma ($^{n}/cm^2$-sec)	3.42×10^{15}
6.	Average Fission Density in Plasma ($^{fissions}/cm^3$-sec)	2.63×10^{13}
7.	Critical Mass U-233 (KGS.)	26.36
8.	Reactor Breeding Ratio	1.0099
9.	Peak/Average Fission Density in Plasma	1.126
10.	Fuel Absorption/Fissions in Plasma	1.113

REFERENCES FOR CHAPTER 6

1. MENELEY, D. A., et al., "Mach-I, A One-Dimensional Diffusion Theory Package," ANL-7223, (1966).

2. BONDARENKO, I. I., Ed., Group Constants for Nuclear Reactor Calculations, Consultants Bureau, New York (1964).

7. DESIGN CONSIDERATIONS OF THE BREEDER REACTOR

The material chosen for the pressure vessel was type 347 stainless steel. The pressure vessel is spherical and calculated minimum pressure vessel thicknesses are indicated on Figure 7.1. The designed operating temperature of the pressure vessel is 422°K. The inside radius is 193 cm. with an operating pressure of 200 atm. The minimum wall thickness is then 15.3 cm. and the designed wall thickness is 20 cm.

Figure 7.2 illustrates the helium and molten salt flow paths for the breeder reactor. Approximately 7% of the fission energy appears as energy of the neutrons and gamma rays. This energy, 140 MW, will ultimately be deposited in the reactor moderator, molten salt, and other structural materials. Also, 0.1% of the radiated energy from the plasma core; or 1.86 MW, will be deposited at the BeO wall of the cavity. This heat will be absorbed by the helium passing through the porous wall. The helium cooling the molten salt enters the heat exchanger at 422°K and exits at 649°K.

The molten salt enters the reactor at 920°K (nearly the minimum temperature possible) and is directed by Zircaloy baffles radially inward. The molten salt cools the inner BeO moderator layer and then leaves the reactor at 1110°K. Assuming that the salt absorbs all 140 MW of the heat from the inner layer, the flow rate of the salt will be 542 kg/sec and assuming a 10% pressure loss in the molten salt system, the needed pumping work is 330 KW. Part of the molten salt from the hot leg, 0.332 gm/sec, is diverted to the reprocessing systems. The amount of salt in the reactor is 1.75×10^4 kg and the time spent by the salt in the reactor is 32 sec. There is a 2 cm. gap filled with helium between the molten salt

and the outer BeO moderator layer. This is to insulate the outer moderator and the pressure vessel from the high temperature molten salt.

Zircaloy is used for internal structural materials because of its low neutron absorption. There is a thin Zircaloy layer between the various regions of the reactor. The inner porous liner is a Zircaloy shell filled with BeO, 25% of the volume is passages for the helium coolant.

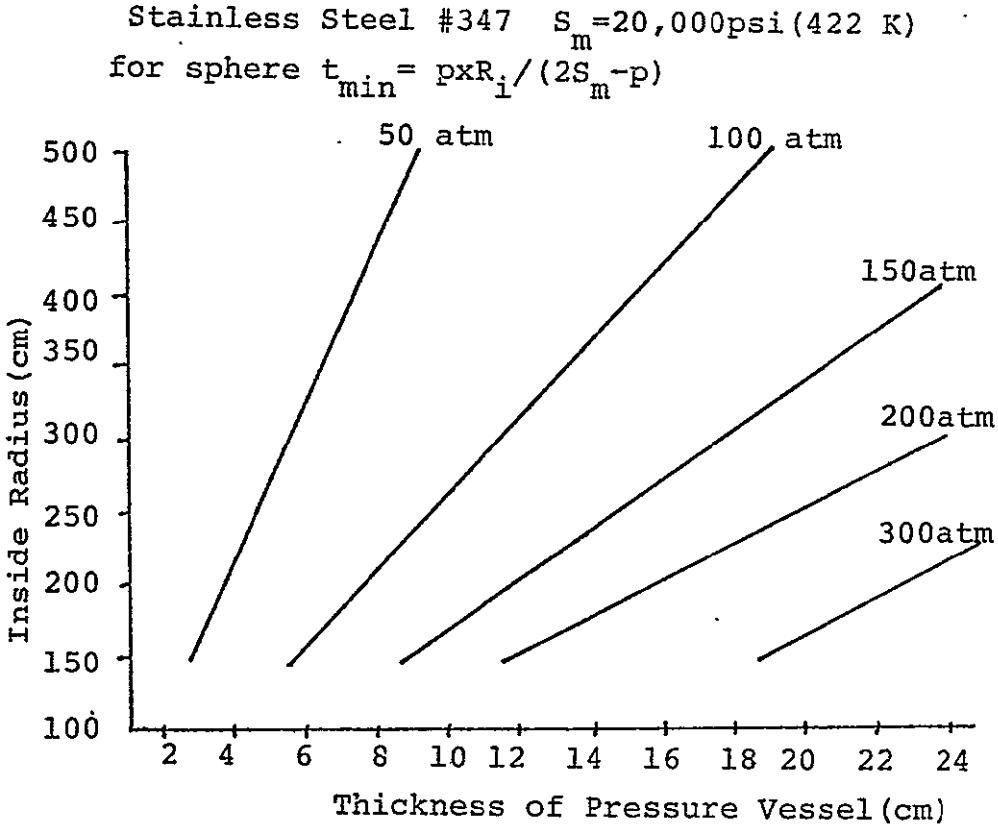

Fig. 7.1 Stainless Steel Pressure Vessel Wall Thickness as a Function of Inside Radius for Various Operating Pressures.

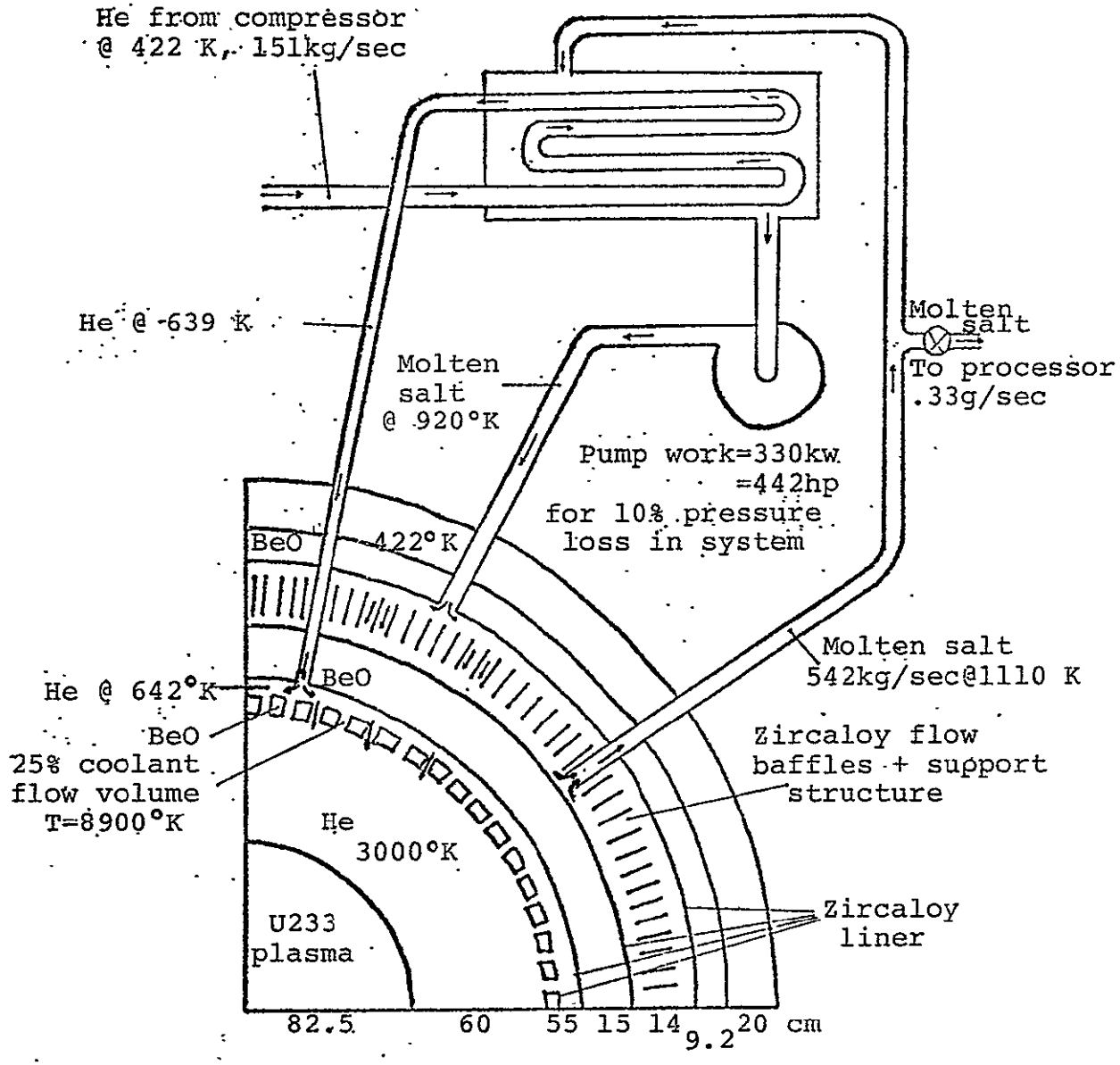

Fig. 7.2 Breeder Reactor Molten Salt Flow Schematic

8. REPROCESSING SYSTEM FOR PLASMA CORE BREEDER REACTOR

Since it is desirable to have the Plasma Core Breeder Reactor (PCBR) be a self-contained unit, generating its own new fuel, an on-line reprocessing system for the molten salt blanket is a necessity. This chapter describes protactinium removal and salt purification processes, calculations of expected flow rates, and equilibrium concentrations of various isotopes present in the system.

The salt used in the blanket is an eutectic mixture composed of LiF, BeF_2, and ThF_4 in the ratios of 72:16:12 mole percent. This particular combination was developed at Oak Ridge National Lab in conjunction with the Molten Salt Breeder Reactor program.

When thorium atoms contained in the salt enter the neutron field around the core, some of the atoms absorb a neutron and transmute to protactinium as shown in Figure 8.1. The protactinium eventually decays to uranium which can then be fed to the core as new fuel. However, as seen in Figure 8.1, Pa^{233} has a substantial cross section (22 barns) and since its half life is 27 days, Pa acts as a poison, siphoning off neutrons which could otherwise irradiate Th atoms. For this reason, it is desirable to remove Pa from the molten salt loop and allow it to decay outside the core.

However, since it is impossible to have a zero protactinium concentration in the molten salt blanket, there will be some uranium present in the core. Some of these atoms will fission and, consequently, there will be some uranium fission products in the molten salt loop. Some of

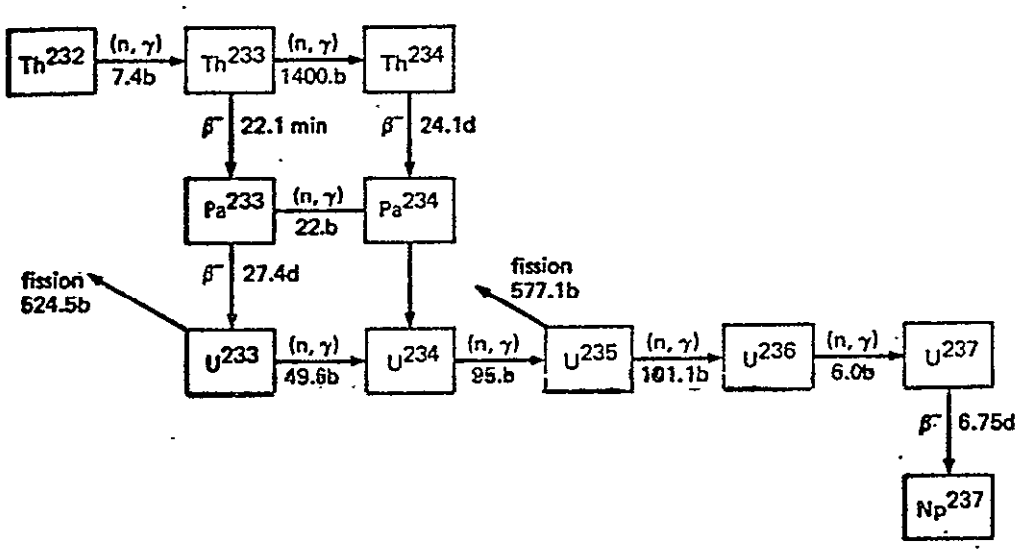

Fig. 8.1 The chain of isotopes created by neutron irradiation of Th232.

these fission products have large cross sections as shown in Table 8.1. Note that Xe and other gaseous fission product poisons are not listed because it is assumed that the blanket can be vented and these gaseous products easily removed. As will be shown later, the necessity of keeping the concentration of fission products at a low level determines the amount of time which the salt can stay in the irradiated blanket region.

In order to achieve the above neutronics goals, a fluorination-reductive extraction system was developed at Oak Ridge National Lab. A description of this process is as follows:[2]

> The fluorination-reductive extraction system for isolating protactinium is shown in its simplest form in Figure 8.2. The salt stream from the reactor first passes through a fluorinator, where most of the uranium is removed by fluorination. Approximately 90% of the salt leaving the fluorinator is fed to an extraction column, where it is countercurrently contacted with a bismuth stream containing lithium and thorium. The uranium is preferentially removed from the salt in the lower extractor, and the protactinium is removed by the upper contactor. A tank through which the bismuth flows is provided for retaining most of the protactinium in the system.
>
> The bismuth stream leaving the lower contactor contains some protactinium as well as the uranium that was not removed in the fluorinator and the uranium that was produced by the decay of protactinium. This stream is contacted with a H_2-HF

Table 8.1 Rare Earth Fission Product Absorption Cross Section

Nd-143	330 barns
La-139	8.9 barns
Eu-153	320 barns

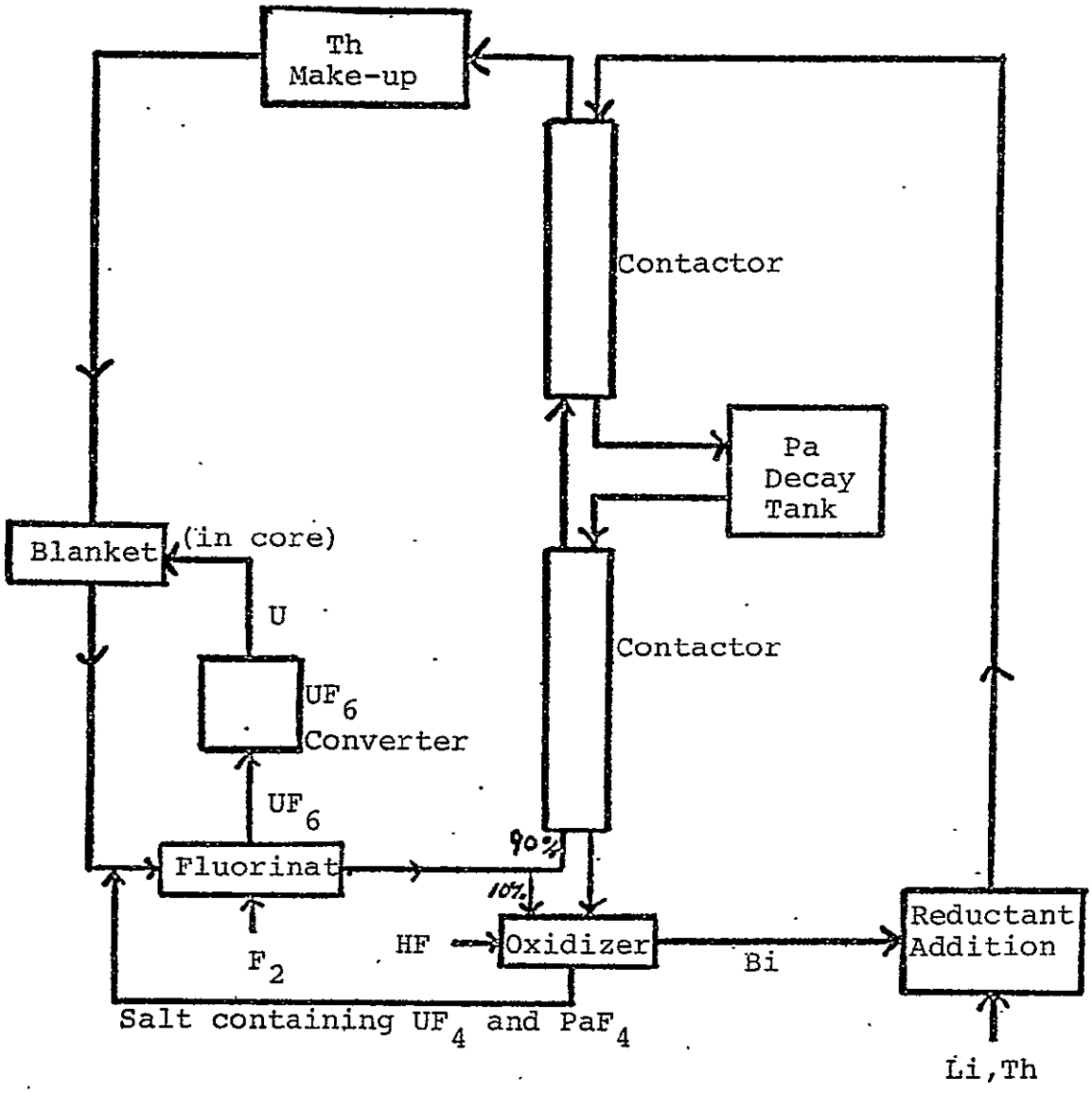

Fig. 8.2 Plasma Core Reactor Reprocessing System

mixture in the presence of approximately 10% of the salt leaving the flourinator in order to transfer the uranium and the protactinium to the salt. The salt stream, containing UF_4 and PaF_4, is then returned to a point upstream of the fluorinator, where most of the uranium is removed. The protactinium passes through the fluorinator and is subsequently extracted into the bismuth. Reductant (Li and Th) is added to the Bi stream leaving the oxidizer, and the resulting stream is returned to the upper contractor. The salt stream leaving the upper contactor is essentially free of uranium and protactinium and would be processed (for removal of any fission product gases and additional thorium added to compensate for that which had been consumed.)

Figure 8.3 describes the UF_6 to U metal conversion process. Unfortunately this is a batch process instead of a continuous flow system as is present in the remainder of the reprocessing set-up. However, there should be no problem providing temporary storage tanks for UF_6.

The UF_6 initially enters a reaction chamber where it is mixed with hydrogen. A reaction is triggered and UF_4 powder and HF gas is produced. The UF_4 is then loaded into a steel "bomb" which has been coated with fused dolomitic lime--lime is one of the few oxides that does not react with molten uranium. The "bomb" is then heated to 565°C where an exothermic reaction takes place and uranium metal solidifies on the bottom of the "bomb". The MgF_2 is removed and U metal of high purity can then be taken from the bottom of the "bomb" and sent to the reactor.[4]

C-2

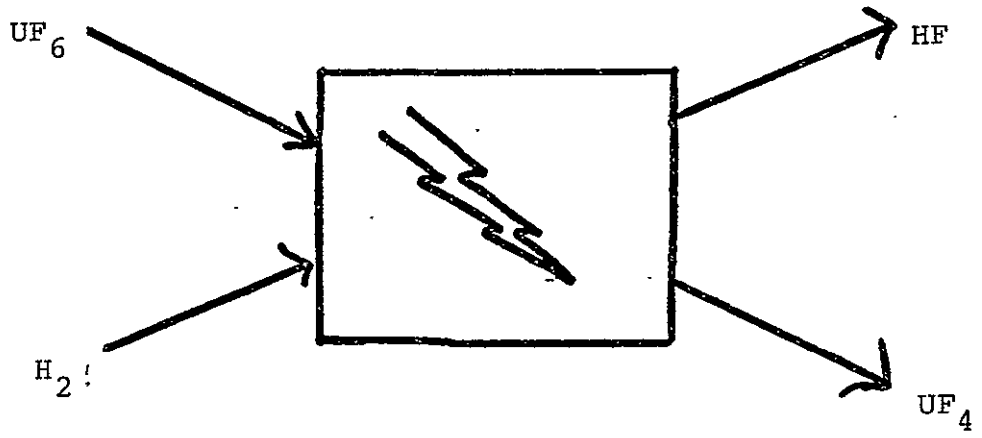

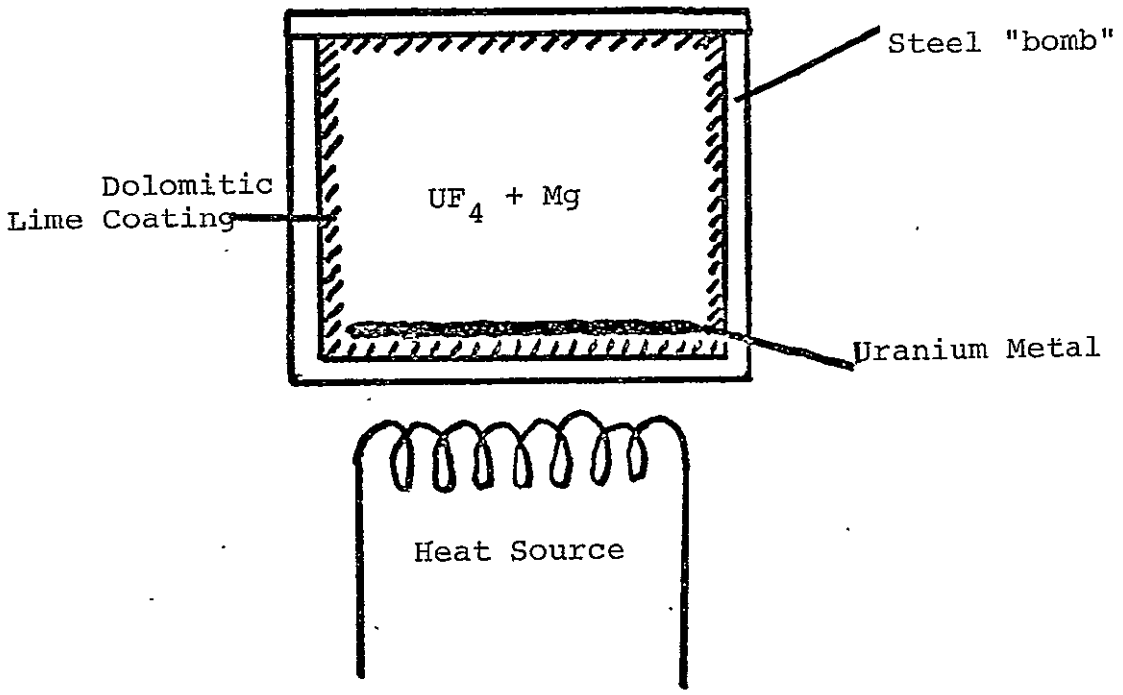

Fig. 8.3 UF_6 to U Metal Batch Process

Given certain constraints on the reprocessing system it is possible to calculate the flow rates which would exist in both the molten salt and bismuth loops. It is also possible to calculate protactinium concentrations throughout the reprocessing system and therefore determine uranium concentrations throughout the system. The constraints which are placed on the reprocessing system are as follows:

1) The protactinium concentration in the molten salt blanket is allowed to reach 95% of the equilibrium value obtained if the salt remained in the active region of the reactor for an infinite amount of time, provided that the concentration of protactinium does not cause parasitic absorption of neutrons by fission products greater than 1% of the absorptions which are due to thorium captures.

2) The volume of the blanket and the flux in the blanket shall be determined by breeding ratio constraints as explained elsewhere in this report.

3) The uranium removal efficiency of the fluorinator and oxidizer is 98%.[4]

4) The operating temperature of the system shall be 640°C (necessary because the salt is a eutectic mixture).[4]

5) The Li concentration in the Bi loop shall be 1%. The Th concentration in the Bi loop shall be held at less than 50% of the solubility of Th in Bi.[5]

6) The Pa distribution coefficient for the contactors, defined as (mole fraction of Pa in Bi at equilibrium)/(mole fraction of Pa in salt at equilibrium), is taken to be 100.[5]

7) The following physics data is assumed:

Neutron Flux	1.0E+14 n/cc-sec.
Volume of Blanket	5.29E+06 cc.
Molar Volume of Salt	0.0598 moles/cc.
Molar Volume of Bi	0.0469 moles/cc.
Pa Absorption Cross section	22 barns
Th Absorption Cross section	7.4 barns
U Absorption Cross section	571.3 barns
U Fission Cross section	524.5 barns
Pa Decay Constant	2.97E-07 sec^{-1}
Concentration of Th in salt	4.32E+21

8) Due to its very short half-life Th^{232} is assumed to transmute directly to Pa^{233} upon being struck with a neutron.

To satisfy assumption 1, we must examine if the Pa concentration in the salt from the output of the blanket will be governed by the rate of fission product captures. To determine the number of fission product captures we must first solve for the Pa and U concentrations. This is done as follows:

$$\frac{d\ Pa}{dt} + \lambda Pa = \sigma_a^{Th}\ \phi\ Th \tag{8.1}$$

where ϕ is the flux, Th is the thorium concentration, and λ the Pa decay constant.

Solving Eq. 8.1 gives

$$Pa = \frac{\sigma_a^{Th}\phi\ Th}{\lambda} - e^{-\lambda t}\left[\frac{\sigma_a^{Th}\phi\ Th}{\lambda} - Pa_o\right] \tag{8.2}$$

The equation for the uranium concentration as a function of time is

$$\frac{dU}{dt} = - \phi \sigma_a^u U + \lambda Pa \tag{8.3}$$

where U is the U-233 concentration.

Solving this equation we have

$$U = U_o e^{-\sigma_a^u \phi t} + \frac{\sigma_a^{Th} Th}{\sigma_a^u} \left(1 - e^{-\sigma^u \phi t}\right) - \lambda \left[\frac{\sigma_a^{Th} \phi\, Th}{\lambda} - Pa_o\right]\left[\frac{e^{-\lambda t} - e^{-\sigma^u \phi t}}{\sigma^u \phi - \lambda}\right] \tag{8.4}$$

If a given atom of material is assumed to spend time T in the blanket, then the number of fissions which occurs during this time is

$$\text{No. of fissions} = \int_o^T \sigma_f^U \phi\, U(t)\, dt \tag{8.5}$$

Evaluating this integral we have

$$\text{No. of fissions} = \sigma_f^u \phi \left[\frac{\sigma_a^{Th} Th}{\sigma_a^u}\left(T - \frac{e^{-\sigma_a^u \phi T} - 1}{\sigma_a^u \phi}\right) - \frac{\lambda}{(\sigma_a^u \phi - \lambda)}\left[\frac{\sigma_a^{Th} \phi Th}{\lambda} - P_{ao}\right]\left[\frac{1 - e^{-\lambda T}}{\lambda} + \frac{e^{-\sigma_a^u \phi T} - 1}{\sigma_a^u \phi}\right]\right] \tag{8.6}$$

and the fission product concentration at the end of a cycle of length T is given by

$$[F.P.] = \left[\int_o^T \sigma\phi\, U(t)\, e^{\sigma_f^u \phi t}\, dt\right] e^{-\sigma_f^u \phi T} \ll \gamma \text{ (No. of fissions)} \tag{8.7}$$

where γ is the probability per fission of getting a particular fission product. Since the fluorinater removes 98% of the uranium in the molten salt on each pass through the system, the entering concentration to the blanket region can be taken as effectively zero.

Solving Eq. 8.7 for a variety of times T, the results, given as $\frac{\Sigma_{Eu}}{\Sigma_{Th}}$ where Σ_{Eu} is the absorption cross section of one of the most troublesome rare earth fission products, Eu^{153}, are shown in Table 8.2. It should be stated that this estimate of the Eu^{153} concentration is high due to the approximation in Eq. 8.7. However, even with this high estimate it can be seen that no fission product removal system is necessary.

To determine the flow rates and concentrations in the system, one must make use of the following mass balance equations.[6] If one refers to the hypothetical exchange column shown in Figure 8.4

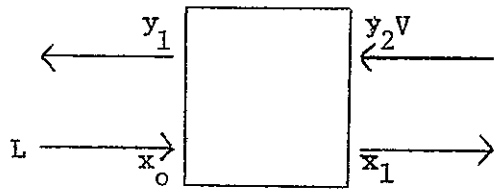

Figure 8.4: Exchange Column Flows

then a material balance yields the following equation:

$$Lx_o + Vy_2 = Lx_1 + Vy_1 \tag{8.8}$$

or

$$L\,(x_o - x_1) = V\,(y_1 - y_2) \tag{8.9}$$

Table 8.2 Protactinium and Europium Concentrations in Blanket

Time in Blanket (days)	Pa Concentration (% of equilibrium)	$\frac{\Sigma_a^{Eu}}{\Sigma_a^{Th}}$ (%)
114	.95	6
45.5	.70	.75
26.1	.50	.165
19.1	.40	.072
10.7	.25	.0135
3.91	.10	$6.9(10^{-4})$

where L and V are flow rates in moles/sec and x and y are concentrations of the transferring material expressed in mole fractions. Now at equilibrium

$$y_1 = K \cdot x_1 \tag{8.10}$$

where K is a constant known as the distribution coefficient. Substituting for x_1 in Equation 8.9 and solving for y_1 we have

$$y_1 = \frac{y_2 + \frac{L}{V} x_o}{\frac{L}{KV} + 1} \tag{8.11}$$

So if we knew the two inlet concentrations and if we can find the flow rates then the outlet concentrations can be calculated.

The value of the flow rates in the Bi and blanket loops must be solved for iteratively. A flow chart of the solution process is shown in Fig. 8.5 and a FORTRAN program written to solve this problem. A value for the Bi flow rate is assumed and for given Pa core concentration, neutron flux, and core volume, the flow rate in the blanket, residence time in the core, and input concentration of Pa to the core can be solved for iteratively.

Now, as referenced above, ORNL report number 4344 gives the distribution coefficient of Pa as a function of time of contact and relative volumes of salt and Bi. Picking a specific distribution coefficient determines the time of contact and the relative volume of the two components. A new value for the Bi flow rate can then be calculated by using the value of the blanket flow rate calculated above. The entire iterative procedure is then repeated with the new Bi flow rate.

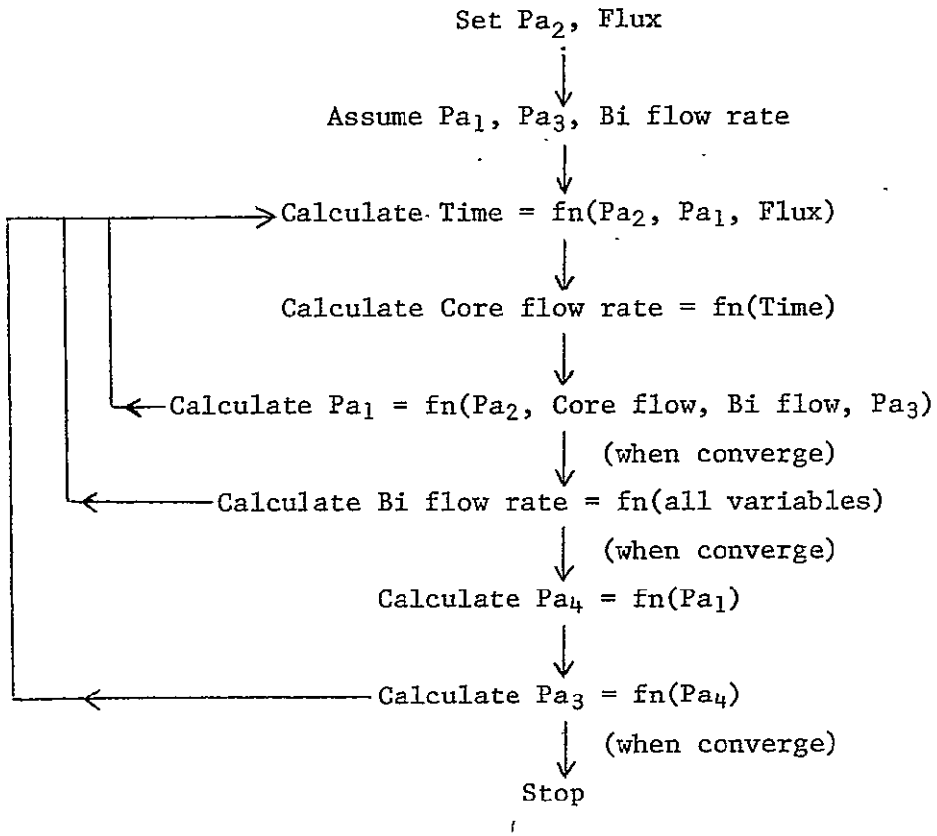

Pa_1 = Core input Pa concentration

Pa_2 = Core output Pa concentration

Pa_3 = Bi loop contactor input Pa concentration

Pa_4 = Bi loop contactor output Pa concentration

Figure 8.5 Flowchart for Calculation of Reprocessing System Flow Rates and Pa Concentration

Once the flow rates have been calculated, the output Pa concentration in the Bi loop from the contactor can then be found from Eq. 8.11 and the input concentration from Eq. 8.9.

It should be noted at this point that if a contactor is composed of several stages with K being the distribution coefficient in each stage, then the procedure described above can be applied to the whole system with the number of stages, N, given by the expression[6]

$$N = \frac{\log \left[\frac{A-1}{A} \left(\frac{y_{n+1} - Kx_o}{y_1 - Kx_o} \right) + \frac{1}{A} \right]}{\log A} \qquad (8.12)$$

where A is the absorption factor and is defined by A = L/(KV). However, for simplicity, this report assumes the contactor to have only one stage.

Performing the calculations described above, the reprocessing system parameters shown in Table 8.3 were calculated.

In conclusion, an on-line, on-site reprocessing system for the Plasma Core Reactor is quite feasible. The technology is available today and the chemical processes involved in uranium separation have been proven in various laboratory experiments at Oak Ridge National Lab as a part of the Molten Salt Breeder program. Only a Pa isolation system is required, no fission product removal system is necessary.

Table 8.3

Summary of Reprocessing Systems Parameters for PCBR

The fission concentration in the blanket per cycle is .333E+18 fissions per cc.

The effective time spent in the core is .655E+01 days.

The flow rate through the core is .691E+00 G-moles/sec.

Input protactinium concentration to the core is .549E+18 atoms per cc.

Output protactinium concentration from the core is .145E+20 atoms per cc.

The flow rate in the Bi loop is .180E+00 G-mole/sec.

The Pa concentration in the Bi loop entering the contactor is .848E+18 atoms per cc.

Output Pa concentration from the contactor is .430E+20 atoms per cc.

The number of stages in the contactor is .100E+01.

REFERENCES FOR CHAPTER 8

1. HENRY, A. F., Nuclear Reactor Analysis, M.I.T. Press, 763, (1975).

2. McNEESE, L. E., "Engineering Development Studies for Molten-Salt Breeder Reactor Processing No. 5," ORNL TM-3140, 15-16, (October 1971).

3. BENEDICT, M., and T. H. PIGFORD, Nuclear Chemical Engineering, McGraw-Hill, 156-158, (1957).

4. McNEESE, L. E., Op. Cit., 18.

5. "Molten Salt Reactor Program Semiannual Progress Report for Period Ending August 31, 1968," ORNL-4344, 292-298, (1969).

6. FOUST, A. S., Principal of Unit Operations, Wiley, 45, 77, (1964).

9. MHD GENERATOR AND SEPARATOR

The plasma core reactor-MHD system was first explored by Colgate and Aamodt in 1957.[1] In 1973, Williams and Clement presented calculations for plasma core reactor-MHD power plants which had efficiencies of 70 percent or more.[2]

The problems associated with the plasma core reactor-MHD system are likely to be severe, but the potential of this system is large enough to warrant serious investigation. The growing program in MHD power generation and the ongoing UF_6 reactor tests at Los Alamos[3] will provide information related to some critical components. However, studies are needed to define the problems unique to plasma core reactor-MHD systems, to offer possible solutions, and to formulate an experimental program if such a program is desired. In view of the growing interests in MHD and plasma core reactor technologies and long lead times in research and development of both space and terrestrial applications, it is both timely and beneficial to initiate such studies.

The analysis of the MHD generator follows that of Ref. 2. The generator is a segmented electrode Faraday generator with cesium seeded helium as the working fluid. Since He does not ionize significantly until 8000°K, even at 1.013 pascals (10^{-4} atmospheres), it may be treated as a perfect gas.[4,5] The relevant gas properties are listed in Table 9.1.

Table 9.1 Gas Properties of Helium

Ratio of Specific Heats, γ	1.6667
Specific Heat at Constant Pressure, Cp	5192 $\frac{J}{Kg^oK}$
Gas Constant	2077 $\frac{J}{Kg^oK}$

The electrical conductivity of the seeded gas is a function of temperature, pressure, and seed mass fraction. Only thermal ionization was considered in this study, although the actual generator includes several non-equilibrium processes due to slow recombination during expansion through the duct (frozen flow), current caused by a motional emf or an electric field, fission fragment, and electromagnetic radiation. The design parameter that is affected directly by the electrical conductivity is the length of the generator. This in turn will influence other parameters as will be subsequently seen.

The generator is a constant velocity generator which is divided into 15 segments to eliminate the Hall current. The state points which are used in the analysis are shown on Fig. 9.1. Note that for a unit mass of helium, a fraction x is diverted to cool the nozzle, a fraction y is diverted to cool the electrodes, and the remaining fraction 1-x-y cools the blanket before entering the reactor cavity.

Given the cavity power, Q_c, and the cavity inlet and exit stagnation temperatures, T_{t_1} and T_{t_2}, respectively, the mass flow rate at the cavity exit is

$$\dot{m}_2 = \frac{Q_c}{H_{t_2} - H_{t_1}} = \frac{Q_c}{Cp(T_{t_2} - T_{t_1})} \tag{9.1}$$

where H_{t_2} and H_{t_1} are stagnation enthalpies at the reactor entrance and exit, respectively.

The static temperature and pressure at the nozzle exit (MHD duct entrance) for an isentropic process are

$$T_3 = \frac{T_{t_2}}{1 + \frac{\gamma-1}{2} M_3^2} \tag{9.2}$$

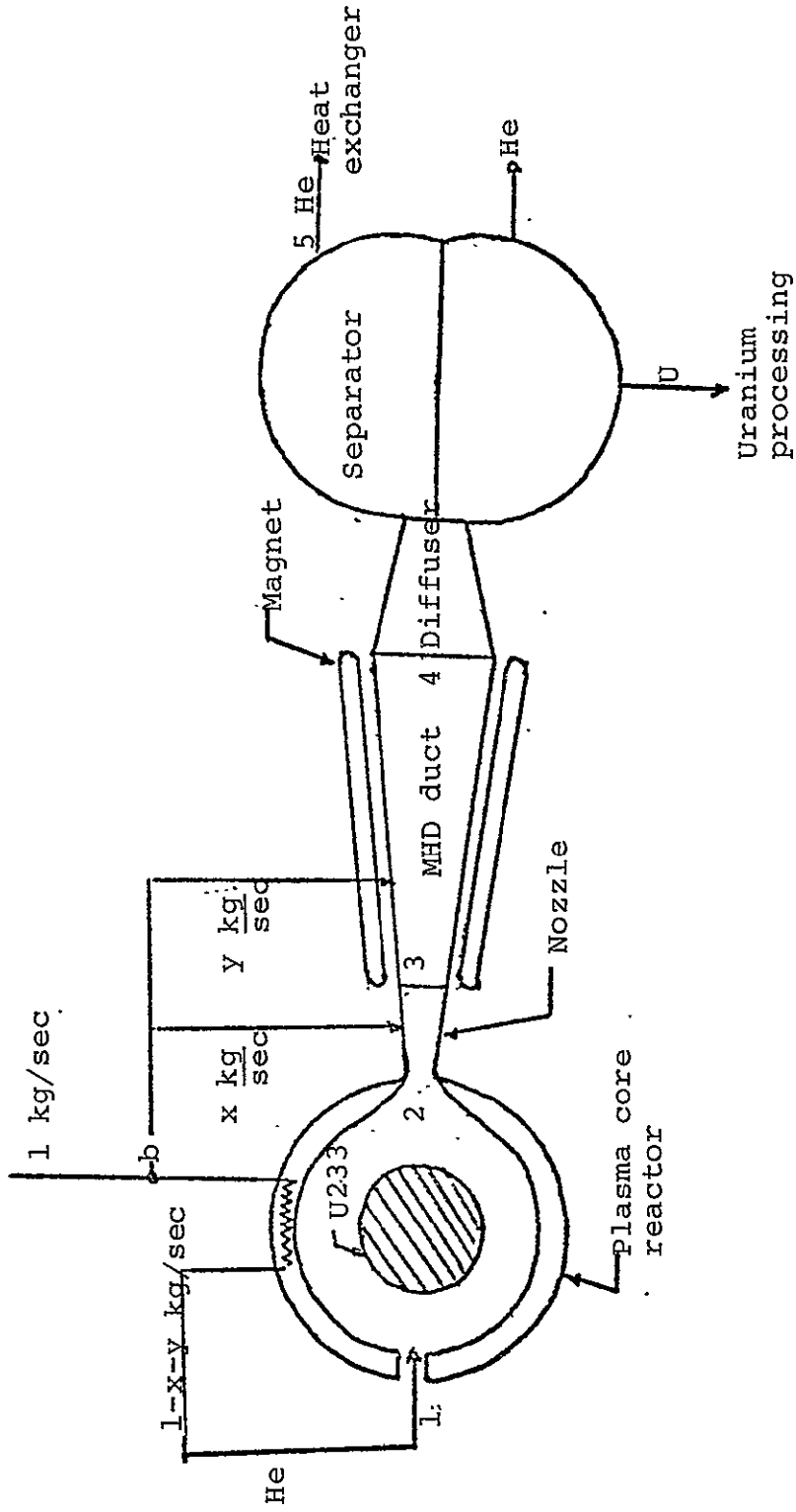

ORIGINAL PAGE IS
OF POOR QUALITY

Fig. 9.1 MHD-Separator System

$$p_3' = \frac{p_{t_2}}{\left[1 + \frac{\gamma-1}{2} M_3^2\right]^{\frac{\gamma}{\gamma-1}}} \tag{9.3}$$

where M_3, the Mach number at the MHD entrance and p_{t_2}, the stagnation pressure at the cavity exit are input quantities.

The helium velocity at the MHD inlet is

$$U_3 = \sqrt{\gamma R T_3'}\, M_3 \tag{9.4}$$

This velocity is constant across the generator. The kinetic energy of the gas is

$$\text{K.E.} = \frac{U_3^2}{2} \tag{9.5}$$

The total enthalpy at the nozzle exit has a component from the cavity and a component due to nozzle cooling

$$H_{t_3} = \frac{(1-x-y)H_{t_2} + x\, H_{t_b}}{1-y} \tag{9.6}$$

The static enthalpy at the MHD inlet is

$$H_3 = H_{t_3} - \text{K.E.} \tag{9.7}$$

The corresponding static pressure and temperature at the MHD inlet are

$$p_3 = p_3' \tag{9.8}$$

$$T_3 = \frac{H_3}{Cp} \tag{9.9}$$

The inlet density of the gas at the MHD inlet is

$$\rho_3 = \frac{p_3}{R\ T_3} \tag{9.10}$$

while the mass flow rate is

$$\dot{m} = \dot{m}_2 \frac{1-y}{1-x-y} \tag{9.11}$$

The MHD inlet area is then

$$A_3 = \frac{\dot{m}_3}{\rho_3\ U_3} \tag{9.12}$$

The pressure ratio for each segment is

$$p_m = \left(\frac{p_3}{p_4}\right)^{\frac{1}{n}} \tag{9.13}$$

where n is the number of segments and $\frac{p_3}{p_4}$, the pressure ratio across the generator are given.

The exit pressure at each segment is

$$p_{m_{i+1}} = \frac{p_{m_i}}{p_m} \quad i = 1,\ldots,n \tag{9.14}$$

with $p_{m_1} = p_3$. The pressure drop for each segment is

$$\Delta p_i = p_{m_{i+1}} - p_{m_i} \qquad i = 1,\ldots,n \tag{9.15}$$

The exit temperature of the i^{th} segment neglecting electrode cooling is

$$T_{m_{i+1}}' = \frac{T_{m_i}'}{p_m \frac{K(\gamma-1)}{\gamma}} \qquad i = 1,\ldots,n \tag{9.16}$$

where K is the MHD loading factor and $T_{m_1}' = T_3$.

The exit enthalpy of each segment with transpirational cooling of the electrode is

$$H_{m_{i+1}} = \frac{H_{m_{i+1}}' \left[1 - y + (i-1)\frac{y}{n}\right] + H_{t_b}\frac{y}{n}}{(1 - y + i\frac{y}{n})} \qquad i = 1,\ldots,n \tag{9.17}$$

with $H_{m_1} = H_{m_1}' = H_3$. The exit temperature at each segment is then

$$T_{m_{i+1}} = \frac{H_{m_{i+1}}}{Cp} \qquad i = 1,\ldots,n \tag{9.18}$$

with $T_{m_1} = T_3$. To find the average conductivity in each segment, σ_i, requires the average temperature and pressure in each segment given by

$$\overline{T}_{m_i} = \frac{T_{m_{i+1}} + T_{m_i}}{2} \tag{9.19}$$

$$\overline{p}_{m_i} = \frac{p_{m_{i+1}} + p_{m_i}}{2} \tag{9.20}$$

The length of each segment is given by

$$\Delta L_i = \frac{|\Delta p_i|}{B^2 U_3 \sigma_i (1-K)} \tag{9.21}$$

where B is the magnetic flux density and is an input quantity.

The density corresponding to T_{m_i} and p_{m_i} is

$$\rho_{m_i} = \frac{p_{m_i}}{RT_{m_i}} \qquad i = 1,\ldots,n \tag{9.22}$$

which is used to determine the inlet area of each segment

$$A_{I_i} = \frac{\dot{m}_3 + \frac{y}{n}\frac{\dot{m}_3\ (i-1)}{1-y}}{U_3\ \rho_{m_i}} \qquad i = 1,\ldots,n \tag{9.23}$$

The exit area of each segment is

$$A_{E_i} = \frac{A_{I_i}}{p_m\ K \frac{(\gamma-1)}{\gamma}\ -1} \qquad i = 1,\ldots,n \tag{9.24}$$

The generator length is

$$L = \sum_{i=1}^{n} \Delta L_i \tag{9.25}$$

$p_4 = p_{m_{n+1}}$ and $T_4 = T_{m_{n+1}}$ so that the MHD exit enthalpy is

$$H_4 = Cp\ T_4 \tag{9.26}$$

The stagnation enthalpy at the MHD exit is

$$H_{t_4} = H_4 + \frac{U_3^2}{2} \tag{9.27}$$

The MHD exit Mach number is

$$M_4 = \frac{U_3}{\sqrt{\gamma R T_4}} \tag{9.28}$$

After leaving the MHD duct, the Mach number of helium is reduced to 0.1 by a diffuser before entering the separators. The temperature and pressure at the separator exit are

$$T_5 = T_4 \frac{(1 + \frac{\gamma-1}{2} M_4^2)}{(1 + \frac{\gamma-1}{2} M_5^2)} \tag{9.29}$$

$$P_5 = P_4 \left[\frac{(1 + \frac{\gamma-1}{2} M_4^2)}{(1 + \frac{\gamma-1}{2} M_5^2)} \right]^{\frac{\gamma}{\gamma-1}} \tag{9.30}$$

Assuming no losses, the thermal energy in the MHD generator is equal to the electric power produced.

$$Q_{MHD} = \dot{m}_2 (H_{t_2} + \frac{x}{1-x-y} H_{t_b} + \frac{y}{1-x-y} H_{t_b} - \frac{1}{1-x-y} H_4) \tag{9.31}$$

Since two separators are used, the flow rate into each separator is

$$\dot{m}_{s_{in}} = \frac{1}{1-y} \frac{\dot{m}_g}{2} \tag{9.32}$$

The gas velocity at the separator exit is

$$U_5 = \sqrt{\gamma R T_5} M_5 \tag{9.33}$$

The helium density at the inlet or exit of each separator is

$$\rho_5 = \frac{p_5}{R T_5} \tag{9.34}$$

The inlet area of each separator is

$$A_{in} = \frac{\dot{m}_{in}}{\rho_5 U_5} \tag{9.35}$$

The separator has two exits connected with two turbine-compressor units. The exit area is

$$A_{ex} = \frac{\dot{m}_{ex}}{\rho_5 U_5} \tag{9.36}$$

where

$$\dot{m}_{ex} = \frac{\dot{m}_{in}}{2} \tag{9.37}$$

A computer program was developed for the MHD generator and separator. A baseline case was established and is summarized in Table 9.2. The assumed magnetic flux density of 18.0 Teslas is very high compared to fields of normal MHD generators but is within superconducting magnet technology. This large value was due to four constraints on

Table 9.2 MHD Reference Design

Core Power = 2000 MWt

MHD Electric Power = 1022 MWe

Reactor Exit Temperature = 3500°K

Cavity Pressure = 2.027×10^7 Pascals (200 ATM.)

MHD Pressure Ratio = 3.0

MHD Exit Temperature = 2273°K

MHD Inlet Mach Number = 0.500

MHD Exit Mach Number = 0.596

Helium Gas Velocity in MHD Duct = 1672 M/sec.

Load Factor = 0.8

Magnetic Flux Density = 18.0 Teslas

MHD Length = 3.47 M

Length/Diameter = 10.75

MHD Inlet Diameter = 0.222 M

MHD Exit Diameter = 0.323 M

CS Seed Fraction = 0.015

Number of Electrode Segments = 15

Conductivity in First Segment = 206 MHOS/M

Conductivity in Last Segment = 7.1 MHOS/M

the generator. First, a reasonable length had to be found. A large pressure ratio would result in excessive lengths (greater than 10 meters). The length of the generator was a strong function of the pressure ratio (Fig. 9.2). This effect was due to the strong variation of electrical conductivity with temperature. At low exit temperatures (less than 2000^{o}K), corresponding to a large pressure ratio, the conductivity decreases by several orders of magnitude from its value at the MHD inlet resulting in a very long generator.

Even more important was the length to diameter ratio of the generator as a function of the MHD pressure ratio (Fig. 9.2). For inert gas generators, L/D is about 10 to insure a well behaved boundary layer. This value may be conservative but was taken as a constraint on the system. Figure 9.3 shows that the magnetic flux density is also a strong function of the MHD pressure ratio for a L/D of 10.

However, the MHD pressure ratio cannot be taken to be too low; otherwise, very little power is extracted. It is desirable to convert as much of the thermal energy in the fluid in the MHD duct as this leads to a higher plant efficiency. It was desired to extract 1000 MWe or more from the plant at high plant efficiencies. This factor plus the constraints on length and L/D led to the values in Table 9.2.

The magnetic field may be considered too high. In this case, the MHD pressure ratio can be dropped which lowers the magnetic field requirements (Fig. 9.3), but decreases the electrical power output (Fig. 9.4). Another alternative is to keep the electric output constant, but increase the core power and decrease the pressure ratio. Again the magnetic field requirement is lower, but the efficiency of the plant

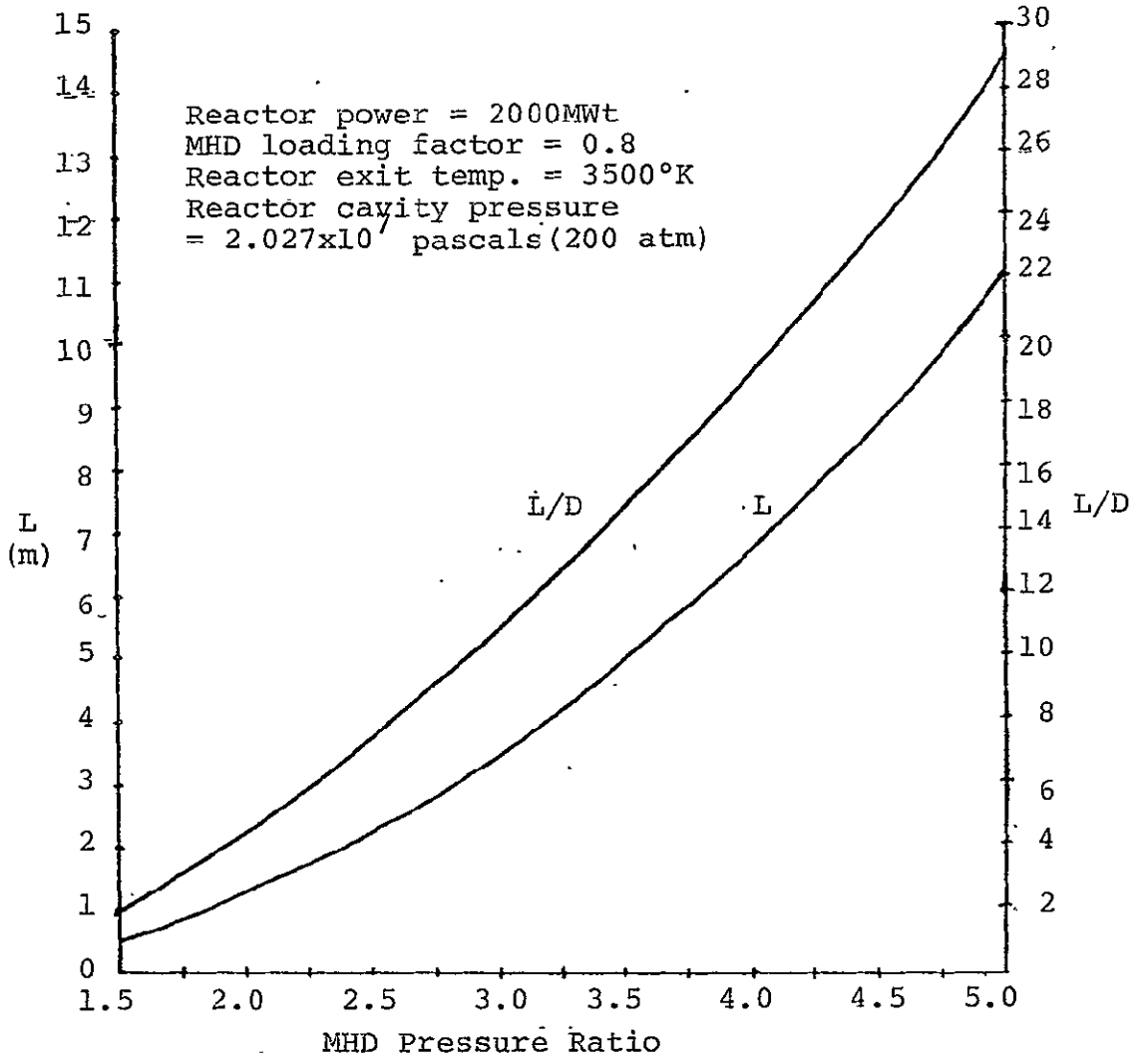

Fig. 9.2 Length and Length-to-Diameter Ratio Versus MHD Pressure Ratio

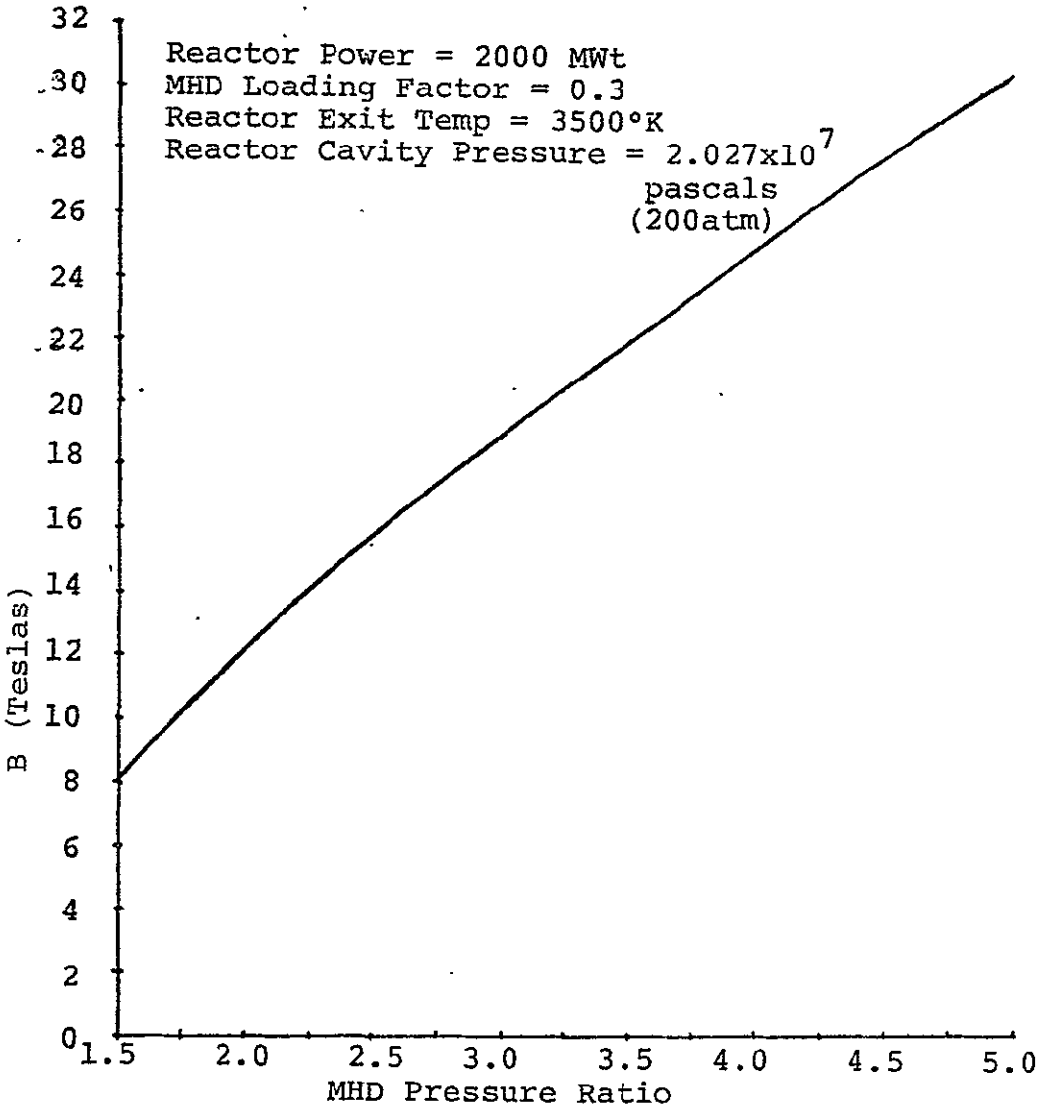

Fig. 9.3 Magnetic Flux Density Versus MHD Pressure Ratio for L/D = 10

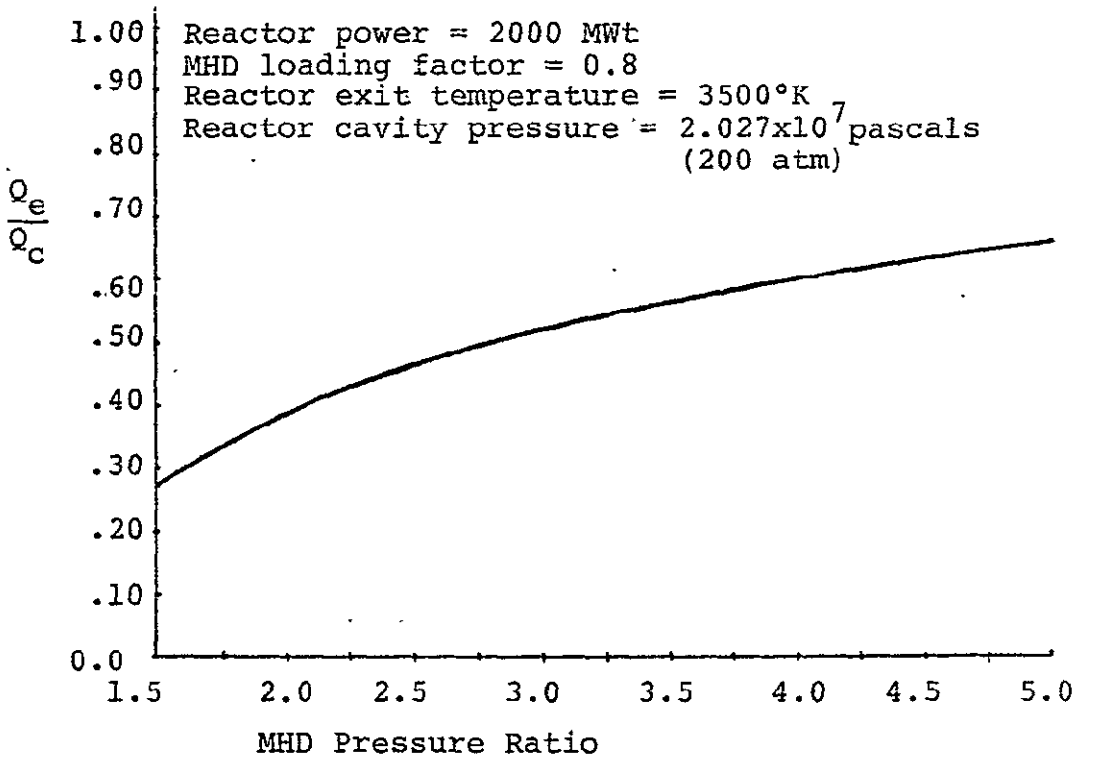

Fig. 9.4 MHD Electric Output Normalized to Cavity Power Versus MHD Pressure Ratio

decreases. The selection of a proper power level depends on economic factors such as capital and fuel costs which is beyond the scope of this study.

In addition, operating at lower cavity pressures would result in an increase in electrical conductivity as large pressures inhibits ionization. However, 200 atmospheres was chosen as the cavity pressure to insure low critical masses for the breeder and actinide transmutation reactor concepts. No optimization of pressure was performed for the combined reactor-MHD system.

The constraints of electric power output, length, length-to-diameter ratio, and cavity pressure lead to a MHD generator with a large magnetic field but is within the technology of superconducting magnets.

An optimization study is needed on cavity power and cavity pressure to obtain a better MHD generator. Also, a two temperature model is needed for the calculation of the electrical conductivity to account for non-equilibrium processes.

The main question of the MHD generator that will have to be answered or solved concerns the flow of uranium through the duct. The fission fragments may enhance ionization in the channel but may also cause serious problems. Some of the problems are:

a) Shielding the superconducting magnet from neutrons and gammas. This should not be too much of a technical problem but may be an economic one. Research on fusion reactors should provide some information in this area,

b) Radiation damage to the electrodes over a prolong period of time. Not much is known in this area and it should be given attention,

c) Condensation of uranium droplets may short out the electrodes. This is probably the most important concern of this type of system and it deserves considerable research.

REFERENCES FOR CHAPTER 9

1. COLGATE, S. A. and A. L. AAMODT, "Plasma Reactor Promises Direct Electric Power," Nucleonics (August 1957).

2. WILLIAMS, J. R. and J. D. CLEMENT, "Exploratory Study of Several Advanced Nuclear - MHD Power Plant Systems," Final Status Report, NASA Grant NGR-11-002-145, Georgia Institute of Technology, (March, 1973).

3. THOM, K., R. J. SCHNEIDER, and F. C. SCHWENK, "Physics and Potentials of Fissioning Plasmas for Space Power and Propulsion," International Astronautical Federation XXVth Congress, Amsterdam, September 30 - October 5, 1974.

4. LICK, W. J. and H. W. EMMONS, Thermodynamic Properties of Helium to 50,000°K, Harvard University Press, (1962).

5. LICK, W. J. and H. W. EMMONS, Transport Properties of Helium from 200 to 50,000°K, Harvard University Press, (1965).

10. POWER PLANT SYSTEMS

In order to achieve maximum effectiveness from the high temperature coolants from plasma core reactors, it was decided that a ternary power cycle would produce the highest efficiency power plant. The ternary cycle consists of a combination of MHD, gas turbine, and Rankine cycle energy conversion units. Two concepts were considered — systems with and without a high temperature regenerator in the helium loop.

The objectives of the study were as follows:

1. Model the nuclear MHD power plant cycle.
2. Analyze the power output from the three energy conversion units and evaluate plant overall efficiency.
3. Make a parametric study of the effect of changing operating variables on plant overall performance.

The components of the propsed systems are shown in Figs. 10.1 and 10.2. For both systems the heat source is a high temperature reactor with a uranium plasma core (UPC). Helium is used to cool the core and is the working fluid for the MHD generator and gas turbine. Helium enters the MHD generator and expands from state 1 to state 2. After the MHD channel it passes through a diffuser and enters the separator where the uranium is separated from the helium. Because of its high temperature at the exit of the separator, the helium needs to be cooled. This process takes place in a mixing tank (MT) where high temperature helium is mixed with helium coming from compressor (C1) in Fig. 10.1. At point 4 the cooled helium enters the gas turbine. After expansion, helium passes through heat exchangers (HE1) and (HE2) where heat is transferred to the steam cycle. Helium is then compressed in the first stage (C1) and

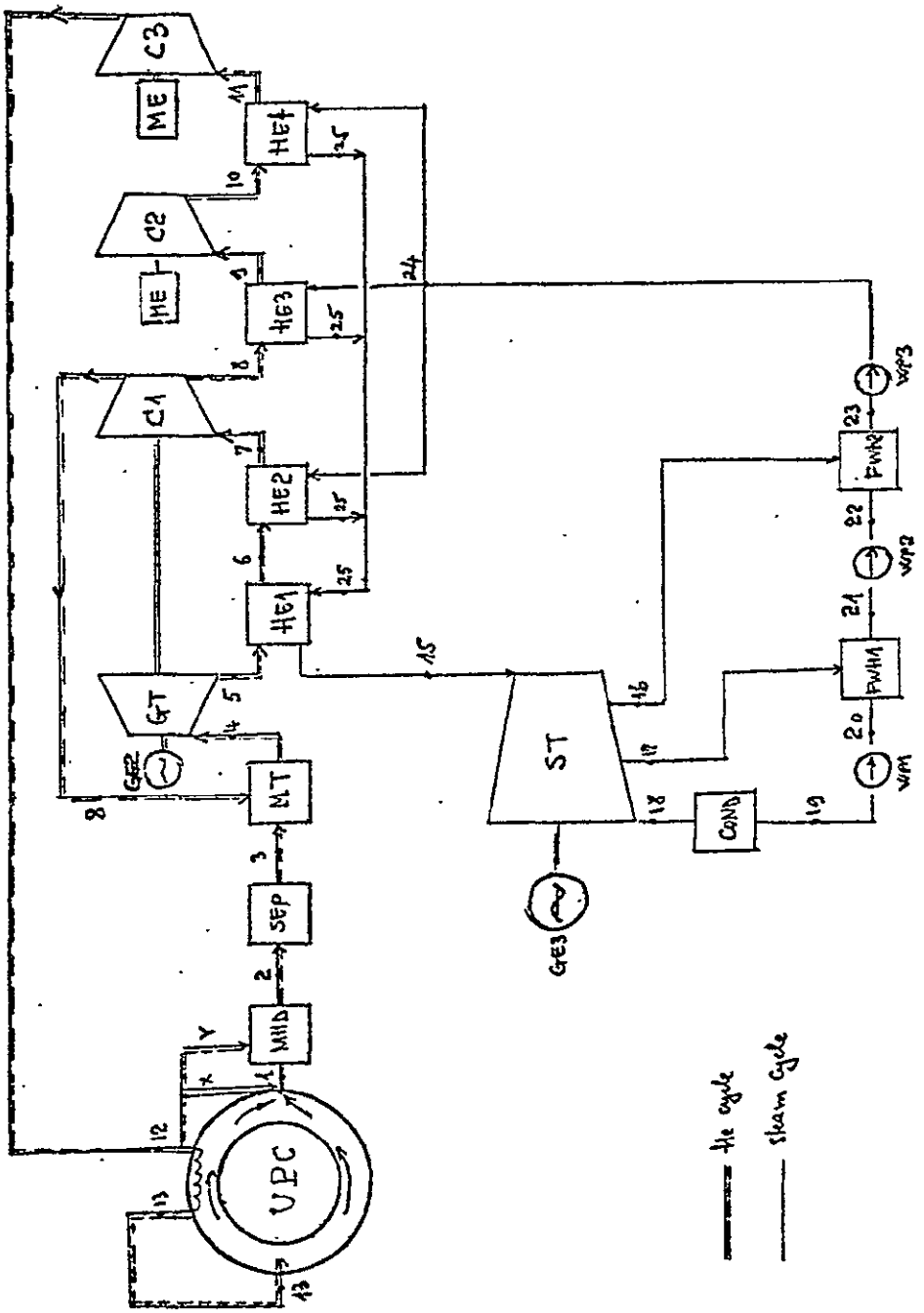

UPC - Uranium Plasma Core; MHD - MHD generator; SEP - Diffuser and Separator; MT - Mixing Tank; GE - Electric Generator; GT - Gas Turbine; C - Compressor; HE - Heat Exchanger; ME - Electric Motor; ST - Steam Turbine; COND - Condenser; WP - Water Pumps; FWH - Feed Water Heater.

Fig. 10.1 Nuclear MHD Power Plant Without Regeneration

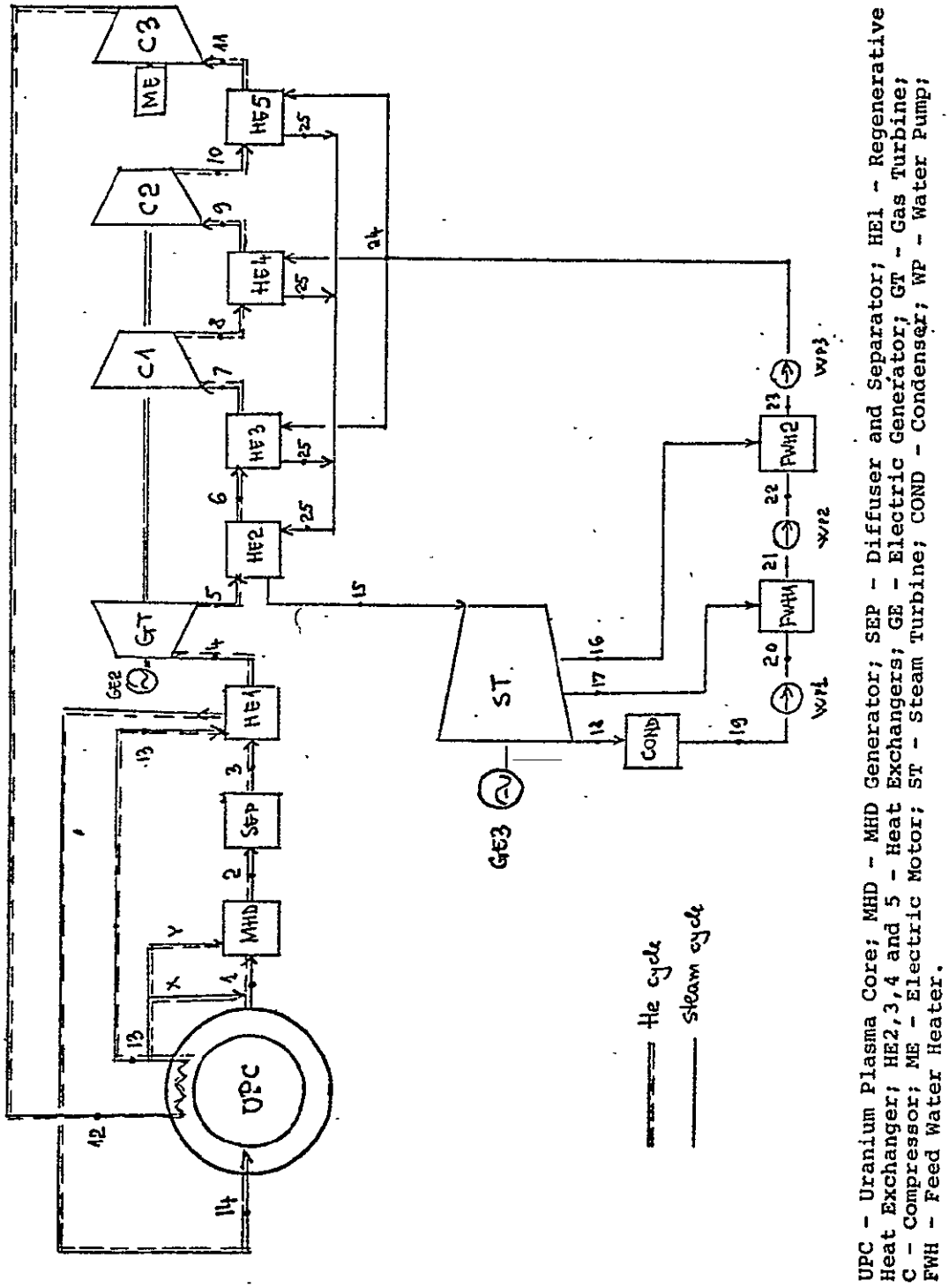

Fig. 10.2 Nuclear MHD Power Plant With Regeneration

then split into two loops. The inner loop is provided to feed the mixing tank. The outer loop is to cool the reactor and for this purpose the helium needs two more compression stages (C2 and C3). The intercoolers (HE3 and HE4) transfers heat to the steam cycle. Before entering the reactor, two fractions, x and y, are taken for cooling the nozzle and MHD duct. Since the MHD pressure ratio is greater than that of the gas turbine, and to maintain a functional unity for the components with the same mass flow rate of gas, compressor (C1) is on the same axis with the gas turbine and electric generator (GE2), while compressors (C2) and (C3) are powered by electric motors.

The nuclear MHD power plant with regeneration (Fig. 10.2) is similar to the previous system in the heat source region (reactor, MHD, and SEP). After the separator, helium passes through a regenerative heat enchanger (HE1) and enters the gas turbine. Between states 5 (exit GT) and 12 (inlet breeding zone of the reactor), helium is compressed in three stages and transfers a part of its heat to the steam cycle in heat exchangers HE2, HE3, HE4, and HE5. Unlike the previous system, helium passes through only one loop and transfers a major part of its heat through regeneration.

For both systems the steam cycle is the same. Water heated in one or two stages of feedwater heaters (or directly from the condenser) goes to a boiler. Superheated steam enters a steam turbine (ST) and then passes through a condenser (COND).

All studies used values for input data according to current commercial technology (i.e. efficiencies for steam cycle components, gas turbine, and compressors) or with current use in MHD research. For the

isentropic efficiency of the MHD generator we assumed values of 75% - 80%.[1,2] The electric efficiency of the MHD generator was provided by Fig. 10.3.

The modeling of the MHD cycle consisted of defining a pseudo - Brayton cycle and treating the expansion within the MHD generator in a similar manner as in a gas turbine. In order to analyze the two systems it was necessary to write two computer codes:

(1) NMHD-1 — code to analyze the nuclear MHD power plant without regeneration in the helium loop

(2) NMHD-2 — code to analyze the nuclear MHD power plant with regeneration in the helium loop.

The basic logic followed in the computer codes is presented in Fig. 10.4. Table 10.1 lists input parameters for each system.

The codes are general in that they permit any changes in input data. From the input data, using special subroutines (TSAT, SUPER and SATL), the program STEAM evaluates all necessary parameters for the steam cycle and calculates the net power produced within the cycle. In addition, the code prepares the enthalpy values for determining the mass flow rate ratio between the helium cycle and steam cycle. For evaluation of state parameters characteristic to the top cycles the codes have implemented a subprogram MHD (different for the two codes). Taking information from calculations done by STEAM and MHD the codes evaluate the power distribution for each energy conversion unit and calculates the plant overall efficiencies.

For a pair of selected parameters by the user, the codes permit a parametric study of the whole system yielding information for evaluating power distributions and overall efficiencies. The first parameter

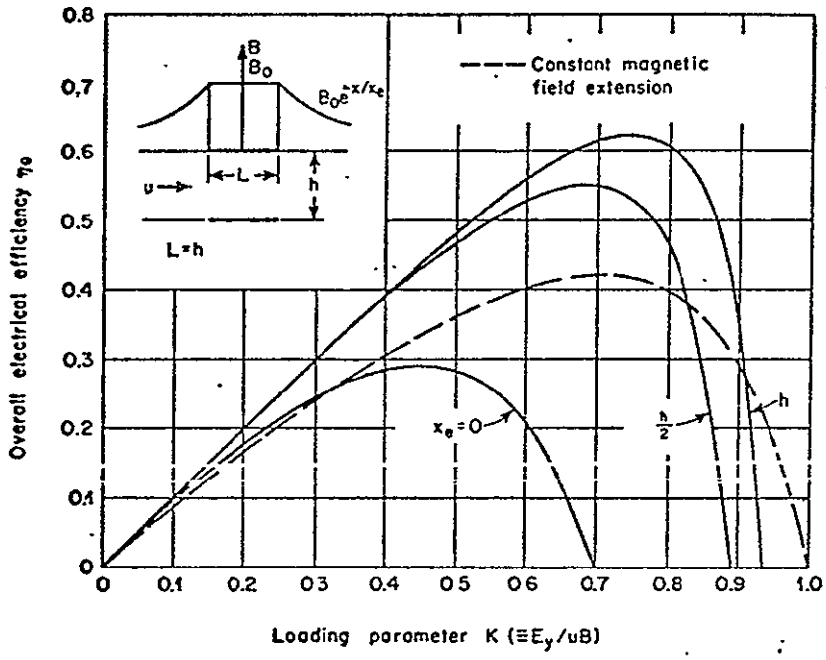

Fig. 10.3 Overall Electrical Efficiency Versus Load Parameter K for a Faraday MHD Generator(3).

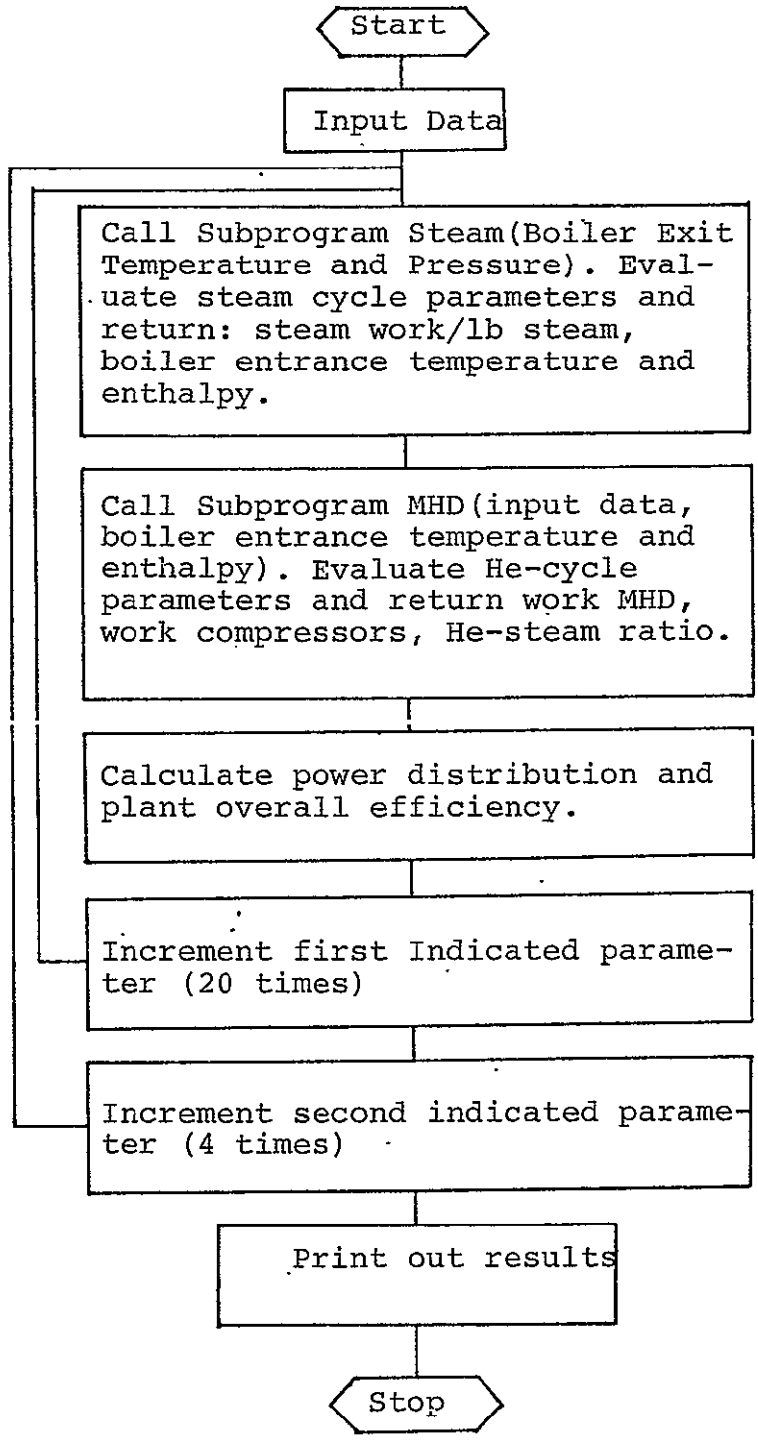

Fig. 10.4 NMHD Program Flow Chart

Table 10.1 Input Data for NMHD-1 and NMHD-2

Index	NMHD-1		NMHD-2	
1	Boiler Temperature ----	1000°F	Boiler Temperature ----	1000.°F
2	Boiler Pressure -------	1600 psia	Boiler Pressure -------	1600 psia
3	Condenser Pressure ----	1.0 psia	Condenser Pressure ----	1.0 psia
4	Steam Turbine Efficiency	81%	Steam Turbine Efficiency	81%
5	Pump Efficiency -------	80%	Number of Feed Heaters	0,1 or 2
6	Number of Feed Heaters	0,1 or 2	Reactor Temp Difference	200°K
7	Compressor Efficiency -	85%	Compressor Efficiency -	85%
8	MHD Inlet Temp --------	3000°K	MHD Inlet Temp --------	3000°K
9	MHD Inlet Press -------	200 bar	MHD Inlet Press -------	200 bar
10	MHD Pressure Ratio ----	5.0	MHD Pressure Ratio ----	3.0
11	Gas Turbine Pressure Ratio	2.0	Gas Turbine Press. ratio	3.0
12	Feed Heater 1 Pressure	12. psia	Feed Heater 1 press. --	12. psia
13	Feed Heater 2 Pressure -	4. psia	Feed Heater 2 press. --	4.0 psia
14	Bottom Temp Difference -	150°K	Bottom Temp Diff. ----	150°K
15	MHD Inlet Mach No. ----	0.5	MHD Inlet Mach No. ----	0.5
16	Sep Outlet Mach No. ----	0.1	Sep Outlet Mach No. ---	0.1
17	Gas Turbine Inlet Temp -	1500°K	Gas Turbine Inlet Temp	1500°K
18	MHD Efficiency ---------	49%	MHD Efficiency --------	49%
19	Gas Turbine Efficiency -	85%	Gas Turbine Efficiency	85%
20	Number of Compress Stages	3.0	Number of Compress Stages	3.0

is incremented twenty times; for each step of this variation, the second parameter is incremented four times.

The objectives of the parametric studies were to establish the influence of different parameters on overall efficiencies for each system and to determine power distribution. For a suitable comparison of the influence of each parameter on the overall efficiency, a new parameter called "sensitivity" was defined.

The sensitivity of the plant overall efficiency is defined as the ratio

$$\text{sensitivity (\%)} = \frac{\eta_i}{\eta_o} \times 100 \qquad (10.1)$$

where: η_o is the reference value efficiency obtained in the first step of calculation;

η_i is the efficiency obtained in the i^{th} step of the parametric study.

The results obtained in this study provide valuable information concerning the behaviour of overall efficiencies. Results are presented in Fig. 5. The most important parameters affecting overall efficiency are as follows:

1. MHD inlet temperature.
2. MHD pressure ratio.
3. Temperature drop across the regenerative heat exchanger (for NMHD2).
4. Gas turbine pressure ratio
5. MHD inlet pressure.
6. Boiler temperature
7. Boiler pressure

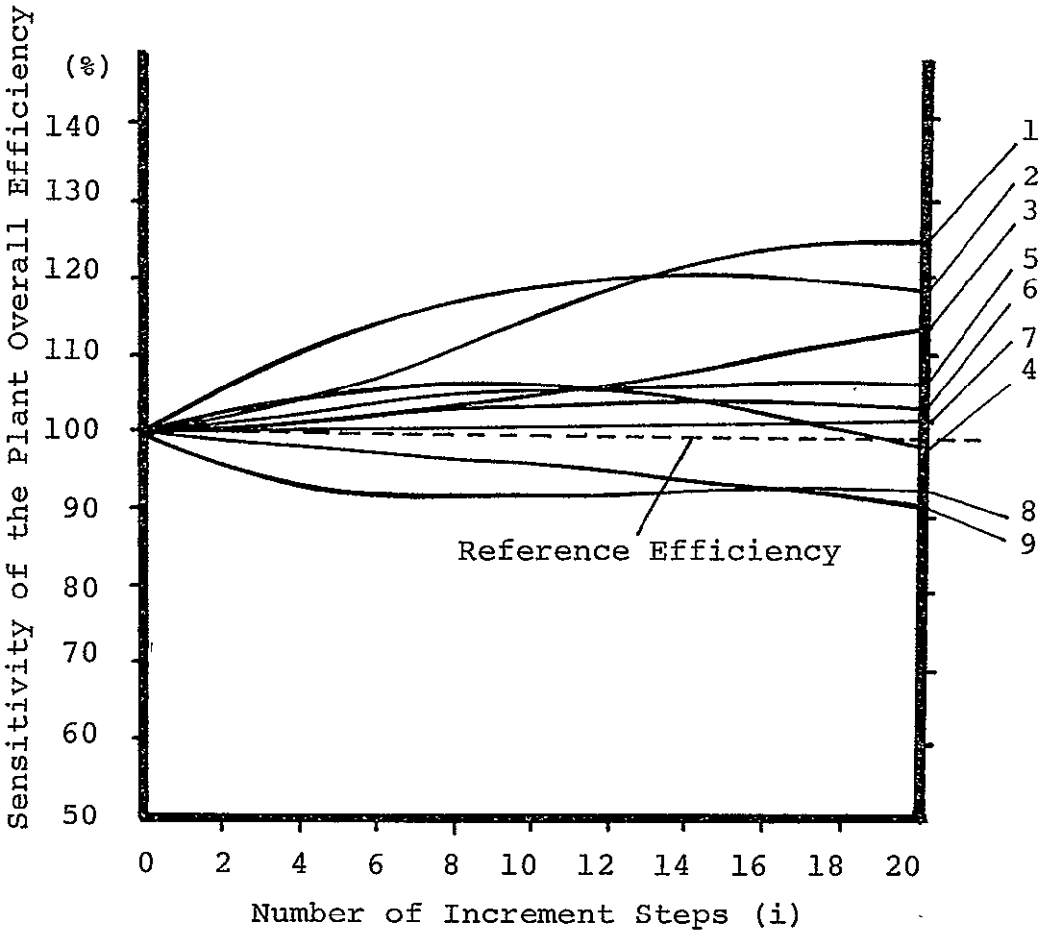

1 MHD Inlet Temperature (3000-5000°K, η_o=62.75%)
2 MHD Pressure Ratio (1.5-11.5, η_o=59.65%)
3 Temp Drop Regenerator (300-1000°K, η_o=60.13%)
4 Gas Turbine Press. Ratio(1.5-11.5, η_o=61.45%)
5 MHD Inlet Pressure (100-200bar, η_o=58.64%)
6 Boiler Temperature (1000-2000°F, η_o=62.75%)
7 Boiler Pressure (1000-2000psia, η_o=62.42%)
8 Number of Comp. Stages(1.0-10.0, η_o=67.5]%)
9 Bottom Temp. Difference(100-300°F, η_o=65.10%)

Fig. 10.5 Sensitivity of the Plant Net Overall Efficiency to the Variation of the Main Parameters

8. Number of compression stages

9. Bottom temperature difference.

Results from the sensitivity study are shown in Fig. 10.5.

After performing the sensitivity analysis a study was made of the effect on overall efficiency of varying the reactor coolant outlet temperature from 3000°K to 4000°K for the two systems. Tables 10.2 and 10.3 list the output works for each energy conversion device and plant overall efficiencies for systems without and with regeneration on the helium loop, respectively. The effect of reactor outlet temperature is more substantial on the system with regeneration. The effect of reactor outlet temperature on plant overall efficiency is shown graphically in Fig. 10.6.

For Nuclear MHD Power Plants without regeneration, the major contribution of electric power is due to the steam turbine subsystem (36.03% - 36.36% from 100 % heat produced by the reactor). Due to a significant fraction of the electric power being produced by the steam cycle with a low efficiency (40%), it is desirable to shift the power production toward the top of the cycle to improve the overall efficiency. This can be achieved by reducing the mass flow rate of helium within the inner loop and increasing the pressure ratio of the MHD generator. This system produced overall efficiencies that are 15-20% higher than actual power plants in use and that are 5-10% higher than the expected coal-fired MHD power plant. Due to the relatively low temperatures within the helium loop, this type of power plant could be considered as a first step in a national program of implementation of MHD power plants with a nuclear heat source.

Table 10.2 Plant Net Overall Efficiencies For MHD Inlet Temperature Variation

MHD Inlet Temperature	3000°K		3250°K		3500°K		3750°K		4000°K	
Gas Flow Rate Through the GT.	2.33 kg/sec		2.60 kg/sec		2.88 kg/sec		3.15 kg/sec		3.42 kg/sec	
Q_R	12265.71	100.0%	13563.96	100.0%	14862.21	100.0%	16160.46	100.0%	17458.71	100.0%
W_{MHD}	1777.71	14.49%	2077.87	15.32%	2378.55	16.0%	2679.22	16.58%	2929.90	17.07%
W_{GT}	456.46	3.72%	510.00	3.76%	563.54	3.79%	617.68	3.82%	670.62	3.84%
W_{ST}	4419.73	36.03%	4901.75	36.14%	5383.76	36.22%	5865.78	36.30%	6347.80	36.36%
η_{PLANT}	54.24%		55.22%		56.01%		56.70%		57.27%	

Q_R = REACTOR HEAT RATE

W_{MHD} = MHD NET ELECTRIC POWER : $W_{MHD} = W_{MHD}$ OUTPUT $- 2W_{COMPRESSOR}$

W_{GT} = GAS TURBINE ELECTRIC POWER : $W_{GT} = W_{GT}$ OUTPUT $- W_{COMPRESSOR}$

W_{ST} = STEAM TURBINE ELECTRIC POWER: $W_{ST} = W_{ST}$ OUTPUT $- W_{PUMP}$

$$\eta_{PLANT} = \left(\frac{W_{MHD}}{Q_R} + \frac{W_{GT}}{Q_R} + \frac{W_{ST}}{Q_R}\right) \times 100 = \left(\frac{W_{MHD}}{Q_R}\,100\right) + \left(\frac{W_{GT}}{Q_R}\,100\right) + \left(\frac{W_{ST}}{Q_R}\,100\right) \quad [\%]$$

Table 10.3 Plant Net Overall Efficiencies For MHD Inlet Temperature Variation

MHD Inlet Temperature	3000°K		3250°K		3500°K		3750°K		4000°K	
Q_R	4973.45	100.0%	5138.94	100.00%	5299.94	100.00%	5458.27	100.0%	5693.55	100.0%
W_{MHD}	1689.52	33.97%	1914.65	37.26%	2139.78	40.37%	2139.78	43.44%	2590.04	45.49%
W_{GT}	319.12	6.42%	319.12	6.21%	319.12	6.02%	319.12	5.85%	319.12	5.60%
W_{ST}	1112.20	22.36%	1112.20	21.64%	1112.20	20.99%	1112.20	20.38%	1112.20	19.53%
η_{PLANT}	62.75%		65.11%		67.38%		69.56%		70.62%	

Q_R = REACTOR HEAT RATE

W_{MHD} = MHD NET ELECTRIC POWER: $W_{MHD} = W_{MHD\ OUTPUT} - W_{COMPRESSOR}$

W_{GT} = GAS TURBINE ELECTRIC POWER: $W_{GT} = W_{GT\ OUTPUT} - 2 \times W_{COMPRESSOR}$

W_{ST} = STEAM TURBINE ELECTRIC POWER: $W_{ST} = W_{ST\ OUTPUT} - W_{PUMP}$

$$\eta_{PLANT} = \left(\frac{W_{MHD}}{Q_R} + \frac{W_{GT}}{G_R} + \frac{W_{ST}}{Q_R}\right) \times 100 = \left(\frac{W_{MHD}}{Q_R}\,100\right) + \left(\frac{W_{GT}}{Q_R}\,100\right) + \left(\frac{W_{ST}}{Q_R}\,100\right) \quad [\%]$$

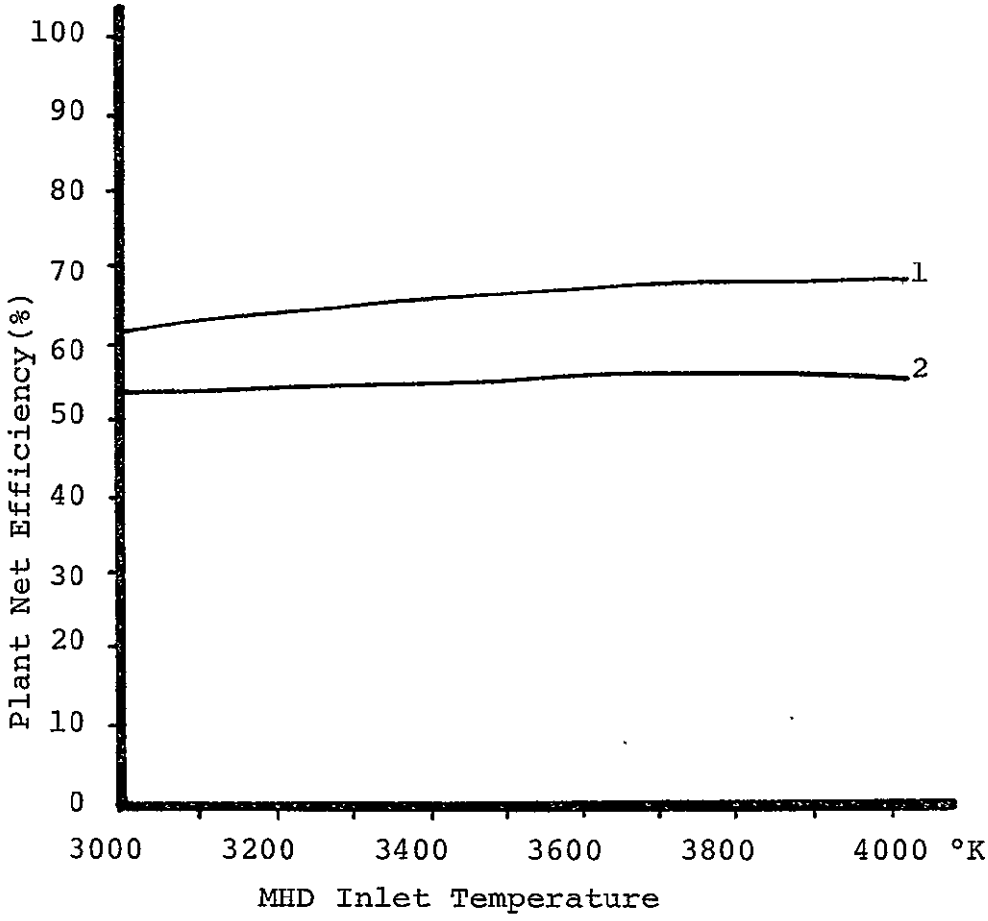

1 Nuclear MHD Power Plant - 1 (with Heat Exchanger)
2 Nuclear MHD Power Plant - 2 (with Mixing Tank)

Fig. 10.6 Plant Net Efficiencies vs MHD Inlet Temperature

For Nuclear MHD Power Plant with regeneration, the major contribution of the electric power is produced in the top of the power cycle by the MHD subsystem (33.97% - 45.49% from 100% heat produced by the reactor). The power production has been shifted toward the top of the ternary cycle with a positive effect on overall efficiency. This system produces overall efficiencies that are 25-35% higher than actual power plants in use and that are 15-20% higher than the expected coal-fired MHD power plants.

REFERENCES FOR CHAPTER 10

1. HOLMAN, R. R. and T. E. LIPPERT, "Liquid-Metal Magnetohydrodynamic System Evaluation," Eleventh Intersociety Energy Conversion Engineers Conference Proceedings, Nevada, Sept. 12-17 (1976).

2. ZAUDER, B., "System Studies for Coal Fired Closed-Cycle MHD for Central Station Power Plant," Eleventh Intersociety Energy Conversion Engineering Conference Proceedings, Nevada, Sept. 12-17 (1976).

3. ROSA, R. J., Magnetohydrodynamic Energy Conversion, McGraw-Hill (1968).